VILNIUS UNIVERSITY
CENTER FOR PHYSICAL SCIENCES AND TECHNOLOGY
INSTITUTE OF PHYSICS

Mikhail Grishin

DYNAMICS OF CONTINUOUSLY PUMPED REGENERATIVE LASER AMPLIFIERS

Doctoral dissertation

Physical sciences, physics (02 P)

Vilnius, 2011

The dissertation was prepared at Institute of Physics of Center for Physical Sciences and Technology in 2006-2010

Scientific supervisor:
Prof. Dr. Habil. Vidmantas Gulbinas (Institute of Physics of Center for Physical Sciences and Technology, physical sciences, physics – 02P)

Scientific advisor:
Dr. Andrejus Michailovas (Institute of Physics of Center for Physical Sciences and Technology, physical sciences, physics – 02P)

VILNIAUS UNIVERSITETAS
FIZINIŲ IR TECHNOLOGIJOS MOKSLŲ CENTRO
FIZIKOS INSTITUTAS

Mikhail Grishin

NUOLATINAI KAUPINAMŲ REGENERACINIŲ LAZERINIŲ STIPRINTUVŲ DINAMIKA

Daktaro disertacija

Fiziniai mokslai, fizika (02 P)

Vilnius, 2011

Disertacija rengta 2006-2010 metais Fizinių ir Technologijos Mokslų centro Fizikos institute

Mokslinis vadovas:
prof. habil. dr. Vidmantas Gulbinas (Fizinių ir Technologijos Mokslų centro Fizikos institutas, fiziniai mokslai, fizika – 02P)

Konsultantas:
dr. Andrejus Michailovas (Fizinių ir Technologijos Mokslų centro Fizikos institutas, fiziniai mokslai, fizika – 02P)

Contents

List of abbreviations and symbols

Abbreviations:

CW	continuous wave,
ISI	Institute for scientific information,
FWHM	full width at half maximum,
PRF	pulse repetition frequency,
Q	quality (of optical resonators).

Laser and electro-optic materials:

BBO	β-barium borate,
$GdVO_4$	gadolinium vanadate,
KD*P	deuterated potassium dihydrogen phosphate,
$LiNbO_3$	lithium niobate,
SFAP	barium substituted strontium fluorapatite,
YAG	yttrium aluminium garnet,
YLF	yttrium lithium fluoride,
YVO_4	yttrium vanadate.

Basic symbols:

A_a	effective mode area in the gain medium,
B	B integral,
E	total energy of intracavity photons or pulse energy,
F_{sat}	saturation fluence,
G	gain factor (proportional to population inversion),
G_0	steady-state gain per pass,
l	parasitic cavity losses per round trip,
N	population density,
P	power (usually average power),
R_{oc}	output coupler reflectivity,
T	pumping interval duration (pulse repetition period),
T_1	gain relaxation time,
T_{rt}	cavity round trip time,

σ emission (σ_{em}) and absorption (σ_{abs}) cross sections,

ϕ photon number.

Dimensionless normalized and effective terms:

g effective gain,

g_1 fixed point in terms of initial gain,

$\tilde{g}$ the term representing logarithmic pulse repetition period,

$\hat{F}$ map function designating the gain transformation rule,

k the cycle number in iterative formulating,

$\tilde{t}$ normalized time within the amplification interval,

β number of passes through the gain medium per round trip,

δ factor of cavity losses due to parasitic losses (δ_l) or output coupling (δ_{oc}),

ε dimensionless energy,

τ amplification interval duration (or effective round-trip number),

Notation for subscripts and superscripts:

cd cavity dumping, indicating the way of pulse output coupling;

i initial, as in initial gain g_i;

f final, as in dimensionless final energy ε_f or final gain g_f;

l loss, referring to parasitic cavity losses, as for energy losses ε_l;

oc output coupling, applying to parameters which describe a regime of stationary output coupling;

p pump, notation for pumping, as for the final gain of the pumping interval g_{pf};

s seed, as for the seed pulse energy ε_s.

It is also used through the manuscript: max ≡ maximum, *opt* ≡ optimum, *out* ≡ output, *peak* ≡ peak value, *th* ≡ threshold.

i. Introduction

The discovery of the solid-state, ruby laser by Theodore Maiman has initiated beginning of the laser era. Performance characteristics of solid-state lasers were improved drastically during five decades. Nowadays, solid-state lasers remain one of the most rapidly developing branches of laser science and become an increasingly important tool for the modern industry. In particular ultrafast laser systems, which are for the most part based on the solid-state laser technology, demonstrate amazing progress in recent years. Picosecond and femtosecond high average power lasers extended their share in a field of micro-fabrication and material processing including manufacture of solar cells and liquid crystal displays. Impressive achievements in amplification of femtosecond pulses to high energies allow development of coherent radiation sources, which produce extremely short wavelength (reaching soft X-rays domain) and simultaneously feature the attosecond pulse duration that in turn intensifies investigations in a scope of the high-field science.

Regenerative amplification is the important constituent part of that integrated technology, which makes possible to produce ultrashort pulses of outstanding specifications. Regenerative amplifiers are involved in both actively developing techniques: in direct amplification using laser media as a high-gain stage and in optical parametric chirped-pulse amplification as a part of pumping systems. High system efficiency and stable output parameters over a wide range of pulse repetition frequencies (PRF) are essential for these systems. Neodymium and ytterbium laser gain media are well suited for direct laser diode pumping, and therefore they have an advantage in power efficiency. Long lifetime of the upper laser level typical of both these ions supports accumulation of substantial population inversion even under continuous pumping. However, the long inversion lifetime may also cause stability problems at repetition frequencies exceeding the inverse excited state lifetime. The dynamics of such systems are subject to equilibrium between population inversion depletion caused by amplification and its restoring under

the pumping action. If this balance breaks then the regenerative amplifier produces periodically alternating energy pulses or even trains having chaotic energy distribution. This phenomenon requires understanding in order to use potential advantages of regenerative amplification and to avoid drawbacks by optimum means.

Initial tasks which initiated the present work were pretty utilitarian, namely, to create a numerical model of regenerative amplification for a picosecond Nd:YVO_4 system and to evaluate basic output parameters taking into account effects of complex dynamics. However, preliminary theoretical study has shown that attainment of a more ambitious aim might be feasible. The primary **goals of research** for this thesis then became the following:

- to develop a general pattern of system dynamics for continuously pumped regenerative amplifiers based on long lifetime solid-state laser media;
- to find a way to improve performance characteristics affected by instabilities.

This general goal consisted of several specific **tasks** which were formulated as follows:

- Creation of the proper model of regenerative amplification with reduced number of variables
- Analysis of repetitive steady-state operation analytically
- Comprehensive elaboration of complex system dynamics numerically
- Search for possibilities to eliminate negative effect of instabilities
- Experimental verification of the results

Both theoretical and experimental **methods and means** were used in order to succeed in solving the established tasks. Amplification modeling was based on the space independent rate equations formulated for quasi-three-level laser

system and some conventional complementary approximations. This simplified model is yet quite productive both to describe different fundamental aspects of amplifiers behavior and to adequately map practically important properties. Appropriate formulation of equations reduced a large number of system parameters to a few composite variables. This improvement along with the advantage of analytic formulation gain physical insight into patterns of regenerative amplification. The formalism of one-dimensional discrete-time dynamical systems turned to be a versatile tool to analyze the stability of obtained solutions. The initial results of research were applied to design the Nd:YVO_4 picosecond laser system. Such a system was then used as the experimental setup to verify more general theoretical inferences.

Scientific novelty

- Analytical expressions which describe stable operation of optimally coupled regenerative amplifiers are obtained.
- A comprehensive pattern of existing dynamic regimes (stable, quasi-periodic and chaotic) in space of controlling parameters is elaborated.
- A method of stability diagrams, which forms a systematic approach to the optimization of regenerative amplification dynamics, is developed.
- Performance characteristics are determined and experimentally verified in the critical PRF range, where analytical solutions are unavailable and instabilities are most crucially pronounced.
- The suppression of instabilities by using the seed pulse pre-amplifying was implemented for the Nd:YVO_4 regenerative amplifier.

The results of research represented in the thesis possess a definite **practical value**. This work not only forms general insight into physical aspects of regenerative amplification (that is important for practical purposes by itself) but also offers guidelines for design and manufacture of practical devices. The latter includes analytic description of the steady-state regime, thorough

specification of the range of controlling parameters which permits stable operation, and a set of diagrams, obtained by elaborating dynamic effects, which allows evaluation of real performance characteristics. Increase in the seed pulse energy as a means to eliminate stability problems and a way to achieve the required energy were patented. The picosecond system for industrial applications was created in UAB EKSPLA using ideas of this invention and other results of the research.

Statements to defend

1. Basic performance characteristics of the regenerative amplifier can be formulated analytically in terms of conventional controlling parameters for the practically important case when conditions of stable operation are satisfied and the round-trip number is set to provide the maximum output energy.

2. Dynamics of regenerative amplification are unambiguously determined by controlling parameters. Quasi-periodic and chaotic operation is inherent to the moderate level of round-trip numbers at repetition frequencies higher than the rate of population inversion relaxation. The space of unstable operation shrinks as the seed pulse energy increases.

3. Within the critical PRF range the maximum stable output energy is obtained at the round-trip number approaching the boundary of the stable operation zone. This leads to the specific V-shaped-form dependences of the average power on the repetition rate.

4. Increase in the seed pulse energy improves dynamics of the regenerative amplification. Addition of a preamplifier to the seed pulse formation chain is an effective way to achieve stable and power efficient operation of the Nd:YVO_4 regenerative amplifier.

Dissertation structure

The dissertation consists of introduction, six chapters, conclusions and a list of references. The manuscript begins with an overview of different types of high-gain laser amplifiers and on this background unique capabilities of regenerative amplifiers are emphasized. Chapter 2 is dedicated to description of the initial modeling equations and introduction of the basic terms. Then in Chapter 3, expressions for performance characteristics of the regenerative amplifier are derived in analytical form, using assumption of the steady-state repetitive operation. Causes and effects of steady state violation are examined in Chapter 4 with the aid of the discrete-time dynamical system theory. Chapter 5 describes specific performance limitations caused by instabilities and methods of system optimization. Picosecond Nd:YVO_4 laser system experiments illustrating specific functional features within both the instability space and the stability space are presented and discussed in Chapter 6. The manuscript is concluded by summarizing the presented results.

ii. Author's publications

The results presented in this thesis were published in peer-reviewed journals included in ISI list and having (good) impact factors [A1, A2, A3]. Also these results constituted a basis of the recently published book chapter [B1]. Two international patent applications were filed during and due to this research [P1, P2].

[A1]. M. Grishin, V. Gulbinas, and A. Michailovas, Dynamics of high repetition rate regenerative amplifiers, Optics Express **15** (15), 9434-9443 (2007).

[A2]. M. Grishin, V. Gulbinas, and A. Michailovas, Bifurcation suppression for stability improvement in Nd:YVO_4 regenerative amplifier, Optics Express **17** (18), 15700-15708 (2009).

[A3]. M. Grishin, Cavity dumping versus stationary output coupling in repetitively Q-switched solid-state laser, Journal of the Optical Society of America B - Optical Physics, **28** (3), 433-444 (2011).

[B1]. M. Grishin and A. Michailovas, Dynamics of Continuously Pumped Solid-State Regenerative Amplifiers, in *Advances in Solid State Lasers: Development and Applications*, M. Grishin (Ed.) (INTECH, Vukovar, 2010) ISBN: 978-953-7619-80-0.

[P1]. M. Grishin, A. Michailovas, Stable Picosecond Laser at High Repetition Rate, Patent Numbers: WO2008016287; EP2064784.

[P2]. M. Grishin, A. Michailovas, Multiple Output Repetitively Pulsed Laser, Patent Number: US2010135341

Results of the research were also reported at international scientific conferences:

1. M. Grishin, V. Gulbinas, A. Michailovas and J. Verseckas, Operation Features of Regenerative Amplifiers at High Repetition Rate, *Conference*

on Lasers and Electro-Optics, CLEO-08, San-Chose, CA, USA, May 4-9, 2008. Technical digest in CD, paper CFB7.

2. S. Balickas, M. Grishin, S. Jacinavičius, J. Kolenda, A. Michailovas, Picosecond lasers for science and industry, *International Conference "Laser Optics 2008", St. Petersburg, Russia, June 23-28, 2008*. Invited talk WeR1-27.
3. M. Grishin, J. Verseckas, Diode-pumped picosecond laser with 1 MHz electro-optical cavity dumping, International Conference "*Laser Optics 2008", St. Petersburg, Russia, June 23-28, 2008*. ThR1-p46.
4. M. Grishin, A. Michailovas, Inherent instabilities of Q-switched cavity-dumped solid-state lasers, *International Conference on Coherent and Nonlinear Optics (ICONO 2010) and International Conference on Lasers, Applications, and Technologies (LAT 2010),* Kazan, Russia, August 23-26, 2010. LTuL17.
5. M. Grishin, Operation Features of Q-switched Cavity Dumped Solid-State Lasers Caused by Inherent Instabilities, *4th EPS-QEOD Europhoton Conference on Solid-State Fiber and Waveguide Coherent Light Sources, Hamburg, Germany, 29 August – 3 September, 2010*. ThP20

iii. Author's contribution

All experimental and theoretical work described in the thesis has been performed by the author. The author was also responsible for preparation of the articles [A1-A3] and of the book chapter [B1]. Scientific supervisor V. Gulbinas and scientific advisor A. Michailovas participated in formulation of research tasks and goals, discussions and preparation of publications.

Chapter 1. Introduction to regenerative amplification

This chapter gives a short overview of primary solid-state laser techniques allowing high-gain operation and represents distinctive features of regenerative amplifiers as devices mainly used for amplification of ultra-short pulses. Typical performance characteristics are outlined for the systems based on the most widely used gain media. A state of the art of physical insight into regenerative amplification including issues related to the complex dynamic behavior is discussed.

1.1. High-gain systems

The most typical function of *regenerative amplifiers* is to produce optical pulses of relatively high energy (of order of millijoule) from weak input signal of nano- and even picojoule level. Such uniquely high gain (~10^6-10^9) is achieved due to multiple passes of the optical pulse through the gain medium. Furthermore, multiple passes allow efficient extraction of energy stored in the gain medium even when low emission cross section media are used. The regenerative feedback is organized by placing the gain media in an optical resonator. The resonator also determines spatial mode of the output beam. This allows good beam quality (TEM_{00} transverse mode) even for a very large number of round trips (passes through the gain media). The number of round trips is controlled by an intracavity optical switch which couples the input signal in and, after a given time period, releases the amplified pulse out of the cavity. The optical switch also realizes quality control of the optical cavity in order to suppress parasitic lasing and amplification of spontaneous emission during the time period when population inversion accumulates. Combination of these functional features substantially enhances the capability of regenerative amplification with respect to competitive techniques.

The *multi-pass amplifiers*, incorporating an angle multiplexing scheme, are the closest “relatives” of the regenerative amplifiers. The radiation is directed through the gain medium several times at slightly different angles

each pass by means of mirrors and/or prisms. This multi-pass configuration has certain advantages when: i) amplification is to be applied to long optical pulses (longer than several nanoseconds) or CW signal [1]; ii) optical switches are impossible or undesirable to incorporate; e.g. if the pulse repetition frequency (PRF) is extremely high (higher than megahertz level) or in order to reduce material dispersion, e.g. for Ti: sapphire systems while producing pulse duration of 20 fs or shorter [2]; iii) it is necessary to reduce the radiation intensity by using larger area gain media which is relevant to higher energy systems [3].

Generic disadvantages of the multi-pass amplifiers are complicated optical layout and bulky design. Lack of robustness may become unavoidable especially for low gain media requiring large number of passes. System flexibility is also a problematic point: the number of passes is determined by the system geometry and its adjustment requires intervention to the hardware. The spatial beam quality is subject to accumulation of optical imperfections, including thermo-induced aberrations of the gain medium, over multiple passes. The basic performance characteristics are substantially limited by parasitic amplification of the spontaneous emission or even by parasitic lasing. Amplification of spontaneous emission is the competing process which lasts during the entire time when the inversion population is accumulated and leads to parasitic depletion of population inversion if the useful signal is weak. This phenomenon actually limits the lower value of the input pulse energy. Relatively large net gain with magnitudes as high as 10^5-10^6 was achieved for Ti: sapphire systems [2, 4] due to quick population inversion accumulation resulted from short (nanosecond) pulse pumping. In case of flash lamp or laser diode pumping this time is an order of magnitude of the gain relaxation time. Therefore, the systems based on laser media with longer lifetime pumped by this means typically operate at far lower gain levels. Although the small signal gain of 57 dB was achieved in 6-pass Nd:YVO_4 amplifiers the resulting net gain was less than 18 dB [5, 6]. Some improvements can be obtained by using saturable absorbers [7] or other means hampering buildup of stimulated

emission. By using threshold nature of the phase-conjugate mirror based on stimulated Brillouin scattering the net gain of 10^3 was obtained for 16-pass Nd:YAG amplifier [8]. The phase-conjugate mirror also served to improve the beam quality. This approach however complicates the system and drastically limits the operation range. Optical pulses having a narrow spectral width and duration of several nanoseconds are the only suitable ones to be amplified.

Very high small-signal-gain (~10^3-10^4 per pass) was obtained by using *grazing-incidence configuration* [9, 10]. This is a side-pumped bounce amplifier featuring a very high inversion population density in a shallow absorption depth below the pump face. Laser radiation is amplified by taking a path that experiences total internal reflection at the pump face. Being compact robust and relatively simple this configuration yet suffers from problems similar to those for multi-pass amplifiers. The effect of amplified spontaneous emission is pronounced so much that only two passes through the Nd:YVO_4 structure were sufficient to get efficient "mirrorless lasing" [10, 11], that of course is not advantageous for amplification purposes. Intrinsic to bounce configuration asymmetric thermo-induced aberrations degrade the beam quality and quite sophisticated methods are required in order to preserve the spatial characteristics of the input signal. A phase conjugate mirror based on a photorefractive rhodium doped barium titanate (Rh:$BaTiO_3$) crystal [12] and an adaptive deformable membrane mirror [13] were offered to achieve a satisfactory-quality laser beam. High absorption and emission cross sections are substantially involved in the concept of bounce amplifiers so that the list of suitable laser media is virtually reduced to only neodymium doped vanadate crystals. Great number of applications, therefore, could not be covered with this technique particularly those to which large bandwidth of the gain spectrum is relevant.

With respect to the combination of performance characteristics, ytterbium doped *fiber amplifiers* compete with regenerative amplifiers in a number of applications [14, 15]. Fiber amplifiers as well as other laser systems based on optical fibers exhibit impressive progress over the recent 10-15 years. Main

advantages of this technique can hardly be overestimated. These are high average output power and high wall-plug efficiency, robustness and absence of misalignment problems, diffraction-limited output radiation along with relatively low demands for pump beam quality (for double-clad fibers) [16].

There are also a number of specific difficulties associated with high-gain and high-peak-power applications. In particular the amplified stimulated emission is a serious factor limiting performance of fiber based amplifiers especially when the low level of noises is in the list of system requirements [17, 18]. Resulting effective gain values rarely exceed three orders of magnitude for a single piece of fiber [19].

The extremely small mode diameter and large medium length intrinsic to optical fibers lead to significant influence of detrimental nonlinear effects. These distort the amplifying signal optical spectrum eventually resulting in substantial limitation of the peak power so that 0.7 MW before compression is among the typical top values for this technique [20]. The progress here is related to developing of large mode area fibers maintaining single mode propagation [21, 22, 23]. However, there is no chance to overcome quite fundamental self-focusing limit (~4-5 MW for the widest spread fused silica optical fibers [24]) at least within the known up to date types of fibers.

1.2. Basic characteristics and basic limitations

Regenerative amplifiers commonly do not use guided light propagation; they are designed with bulk materials allowing a larger mode area a and relatively short pass length within the volume of solid-state media. This moves the peak power limit well above tens of megawatts [25]. Regenerative amplifiers are therefore extensively used for amplification of ultra short laser pulses [26]. Regenerative amplification copes well with weak input signals generated by CW mode-locked oscillators and even by ultrafast laser diodes [27]. The output energy was independent of the input for *input energy* down to 10^{-15} J, as reported in [28]. It is quite reasonable to estimate the minimum input pulse energy to be just by one or two orders of magnitude higher than the competing

total energy of spontaneous photons at initial buildup stage (which, as commonly accepted, corresponds to a few photons per optical cavity mode). This is attainable level because the multi-pass amplification channel is blocked (with the intracavity optical switch) for spontaneous emission until the input pulse is injected.

The ultrafast laser systems, which incorporate regenerative amplifiers, can be conventionally classified either as scientific or as industrial. Output pulse energy and peak power are important performance characteristics for many scientific applications including ultra-fast phenomena and high-field science. The *output pulse energy* of the regenerative amplifier is essentially determined by the energy stored in the gain media and energy extraction conditions. The energy in general may substantially exceed the saturation fluence times the mode area. But the saturation usually cannot be achieved in case of ultra-short pulses and hence high intensities. High intensity of light degrades the spatial and spectral properties by self-focusing and self-phase-modulation (caused by the Kerr-effect which is unavoidable in optical media) and also may cause optical component damage.

Evident way to enhance the system performance when the intensity is the limiting factor is to increase the *mode area* in the active element. The properties of stable optical resonators are however such that the mode expanding without detriment to the beam quality is possible just to a certain extent. The resonator stability range in terms of dioptric power of the thermo-induced lens of the laser rod is inversely proportional to the stationary value of TEM_{00} mode area in the laser rod [29]. Moreover, the misalignment sensitivity rapidly increases if the mode area grows that may causes problems with the system robustness. These limitations are relevant to all kinds of devices which incorporate optical resonators including regenerative amplifiers. The TEM_{00} mode diameter usually cannot exceeds 2-3 mm in practical rod-type systems and the typical output pulse energy is about one millijoule at moderate thermal loads [30, 31, 32]. At low repetition rates and consequently for weak thermal lenses the output pulse energy may reach tens of millijoules as reported for

Nd:glass [33, 34] and Yb:SFAP systems [35]. High repetition rate simultaneously with high output energy is possible to achieve by using cryogenically cooled active media as a consequence of substantial improvement in thermal conductivity and thermo-optic constants. As much as 6.5 mJ from YAG/Yb:YAG composite ceramics [36] and 13.2 mJ from Yb:YAG crystal [37] were obtained at 1 kHz repetition rate. Promising functional properties have also a thin-disk configuration. This configuration is power scalable and features reduction in thermo-induced aberrations as the active area is expanded [38, 39]. Consequently a larger mode area allows higher energy extraction; as much as 25 mJ was obtained from the picosecond Yb:YAG disk amplifier at 3 kHz [40].

The vitally important technique which enables one to avoid too *high intensities* associated with femtosecond pulses is chirped-pulse amplification [41]. The essence of this technique is that the amplifier deals with the stretched pulse the duration of which may exceed hundreds of picoseconds. The amplified pulse is then compressed so that to the initial (femtosecond) duration is restored. The stretcher-compressor scheme reduces the light intensity for the amplifier by several orders of magnitude and thus eliminates nonlinear pulse distortions [42]. The well established architecture of the femtosecond laser systems represents the master oscillator, pulse stretcher, regenerative amplifier (possibly with subsequent high aperture booster-amplification) and then the compressor stage [43].

Although not of specific interest here, another way to build ultrafast amplifiers should be mentioned for completeness sake. The parametric chirped-pulse amplification was discovered in Vilnius University by Dubietis, Jonušauskas and Piskarskas in 1992 [44]. Nowadays this technique attracts a lot of attention as a promising route toward intensity scaling of extremely short pulses. Large single-pass gain (tens of decibels) along with very high power contrast in a very broad spectrum range and low heat generation allow high energy pulses with duration up to a few cycles [45]. The parametric interaction, in contrast to laser amplifiers, makes stringent demands for the pump source

which include matching of the pump pulse duration with the signal (typically stretched to hundred of picoseconds), precise synchronization and also near diffraction limited beam quality. The pumping source for the ultrafast parametric amplifier usually represents a picosecond laser system seeded by frequency-shifted and stretched small portion of the primary femtosecond pulse [46, 47]. The regenerative amplifier plays an important role in such a setup since it is able to amplify this extremely weak seed pulse to substantial magnitudes while keeping a low noise level.

The regenerative amplifier systems designed for scientific applications usually operate at low or moderate average power (in favor of higher pulse energy) and repetition rates not exceeding several kHz. Demands for high average power and *high repetition rates* have risen to satisfy specific requirements of industrial applications [48]. Moreover since the pulse energies suitable for micro-machining are usually limited from above by sub-millijoule level then increase in the repetition rate is the only way to increase the average power and thus to enhance throughput of material processing.

The fundamental PRF limitations are originated from the amplification dynamics and this is one of the subjects of the present manuscript. The limitations of technical nature are essentially associated with the optical switch. The intracavity optical switch controls both the resonator quality and the number of round trips which the amplified pulse undergoes before being released. Good extinction ratio (~10^3) and fast rise time (better than ten nanoseconds) are the primary requirements on regenerative amplifier switches. By satisfying them in general, the electro-optic switches over a long period of time were regarded as having doubtful potential for the high PRF operation. The main reason is that the most of traditional electro-optic crystals (KD*P, $LiNbO_3$ and their isomorphs) exhibit severe piezo-electric ringing which affects the extinction ratio and thus complicates their use at high switching frequencies. Typical situation is reflected in [49]; $LiNbO_3$ electro-optics limits the contrast ratio to 20:1 already at 1 kHz repetition rate. By using acoustic damping and special means of pulse operation the pulse-to-leakage ratio was

enhanced to 40:1 at 10kHz [30]. Apart from that, the traditional electro-optic crystals have poor power handling capability. The only opportunity to reach higher PRF was associated with acousto-optic modulators (as e.g. 250 kHz in [50]), although slow switching edges (~100 ns) substantially hamper the control of regenerative amplification.

The situation has radically changed after β-barium borate (BBO) started to be employed as an electro-optic crystal. BBO Pockels cells feature weak piezoelectric effect, and possibility to maintain good switching properties while withstanding the average optical power up to hundred watts [51]. The obtained repetition rate of 6 kHz was actually limited by high-voltage Pockels cell drivers available at that time (in 1995). A new generation of fast high-voltage electronics appeared in the middle 2000s and PRF's of 100-200 kHz became quite routine for several research groups [52, 53, 54, 55]. The state of the art in this area is 1 MHz for 2-3 kV drivers and up to 4 MHz for 1 kV drivers which are designed to operate in conjunction with BBO Pockels cells of 3-4 mm and 1 mm apertures, respectively [56, 57].

1.3. Gain materials

Regenerative amplification is conceptually insensitive to choice of laser materials and a great number of different materials are used to build regenerative amplifiers. We review much fewer laser systems which however are commercially important and widely used in the practical design. *Titanium doped sapphire* is most frequently used for amplification of femtosecond pulses and thoroughly dominates for durations below hundred of femtoseconds. Broad gain bandwidth, exceptionally good lasing properties and opto-mechanical characteristics place this medium in such a special position [58]. High pulse energy and high average output power have been achieved by using Ti:saphire amplifiers [59, 60]. The disadvantages of this laser material are related to possible means of pumping. First, the absorption lines are located in the green spectrum range, where suitable laser diodes with reasonable power are not available. Second, the short gain relaxation time (3.2 μs) requires

pulsed pumping with high pulse energy (usually with Q-switched frequency-doubled neodymium lasers) in order to store substantial population inversion and consequently to obtain high output energy. The issues developed in the present manuscript are not valid for Ti:saphire systems regenerative amplifiers since we will use approximations which are suitable only for long lifetime media. From the other hand due to very short lifetime the Ti:saphire amplifiers do not exhibit extraordinary dynamic properties, which is not of interest of our study.

Another family of popular laser materials is *ytterbium* doped crystals and glasses. They have wide enough spectrum to support amplification of ultrashort pulses (however not as short as Ti:sapphire supports). Moreover ytterbium materials allow direct laser diode pumping with intrinsically small quantum defect (typically 10% or even less). The latter enhances the overall power efficiency and reduces the heat generation in active elements, that in turn alleviates thermal effects which inhibit average power increase. Long upper-level lifetime of ytterbium ions virtually in all the crystals and glasses allows good capacity of stored energy under convenient continuous laser diode pumping. What somewhat challenges operation with ytterbium materials is relatively low gain (typically less than 30% per pass) which originated from small stimulated emission cross section peculiar to this materials. On the other hand regenerative amplification is indeed a way of efficient energy extraction at low gain; just intracavity losses have to be reduced as much as possible [61]. Cryogenic cooling of active elements is an efficient way to improve stimulated emission related characteristics [62; 37]. At the same time, this method is bulky, and as a rule, it narrows the gain bandwidth [63]. Then special attention should be paid to host crystal selection not to limit development towards shorter pulses, as features e.g. CaF_2 co-doped with Na and Yb [64].

Ytterbium doped media are able to withstand very intense optical pumping without detriment to excited-state population which in other materials can be limited by quenching effects (e.g. excited state absorption or up-conversion) [65]. This favorable property permits use of active elements in thin

disk geometry. In particular, Yb:YAG thin disk lasers are scalable to very high average power and to high pulse energies [66]. Extremely short optical pass within the thin disk reduces nonlinear effects (in essence the Kerr effect) allowing high peak power pulses even without using stretcher-compressor scheme [25].

On the other hand, regenerative amplification is quite important technique for thin disk lasers. A drawback of the short optical pass is low round-trip gain and indeed regenerative feedback may allow efficient energy extraction in this case. Intrinsically low gain and long optical cavities are also not favorable for Q-switched lasers, especially when a short pulse length is required. As the result thin disk regenerative amplifiers serve not only in ultra-short domain but also in order to produce pulses of about 10 nanosecond duration [67]. The techniques of regenerative amplification and thin disk power scalability thus successfully supplement each other allowing pulse durations from sub-picoseconds to nanoseconds, average powers to hundred watts and pulse energy to tens of millijoules [40, 67, 68, 69].

The amplifiers based on *neodymium* gain media have their specific advantages. High stimulated emission cross section and rod-type geometry lead to high single pass gain which in turn simplifies system design and reduces requirements for optical components. Four-level atomic energy system and pumping wavelengths appropriate for laser diodes allow reliable and power efficient operation. Neodymium laser materials are well suited for picosecond pulse durations and are competitive for moderate average power. Systems based on Nd:YVO_4 and Nd:$GdVO_4$ crystals routinely produce more than 10 W of output power [70, 71]. They are successfully used for micro-machining and in other high-PRF applications [55, 70].

Long lifetime crystals, Nd:YAG and Nd:YLF (230 µs and 520 µs, respectively), have good energy storage capabilities, and therefore they are important for high-energy applications. Joul-class Nd:YAG picosecond systems, in which regenerative amplifiers play an important role, are widely

used as pump sources for optical parametric chirped pulse amplification [72, 73, 74].

1.4. Theoretical development

The term “regenerative amplification” has come from electronics and corresponds to strong gain enhancement originated from the positive feedback action. The feedback factor is usually controlled so that the threshold of the self-excitation (i.e. oscillation) is not reached. By using an optical resonator as the feedback mechanism one can organize this kind of regenerative amplification in the optical domain. The theory of regenerative laser amplification below the threshold is a part of classical laser physics and it is particularly useful in understanding dynamics of free-running laser oscillators [75]. Its application to practical laser devices is however quite limited. Although the effective gain approaches infinity when the laser amplifier approaches the oscillation threshold, the attainable gain-bandwidth product is too small to be useful [75].

Much more conventionally the term regenerative amplification applies to the regime in which the threshold is exceeded (the round-trip gain is larger than the round-trip loss) but in a manner that the laser action has no time to take place. The amplification time window is set so short (by the Q-switch) that spontaneous emission noise (which amplification eventually results in lasing) cannot compete with the useful signal. The useful signal being substantially more powerful builds up quicker and finally consumes the stored energy. Regenerative amplification indeed in this sense is the subject of the present manuscript.

Theoretical basis of regenerative amplification was created by Lowdermilk and Murray and reported in two classical papers [28, 76]. The Frantz and Nodvik equation [77] describing energy fluence increase and gain reduction for a separate pass was used recurrently in order to determine efficiency, peak fluence, and amplification time in the multi-pass situation. This approach does not allow analytical solution in general case but it gives the

straightforward algorithm for numerical procedure. The analytic results presented in the present manuscript were verified numerically by using this iterative method.

One of important inferences obtained by Lowdermilk and Murray is that the rate equations governing the intracavity pulse energy and the gain evolution in regenerative amplifiers have the same form as the equations describing the photon number and the population inversion density in actively Q-switched oscillators. Despite the fact that formally amplifiers and oscillators correspond to different classes of laser devices, there are a lot of similarities in operation and in the dynamic pattern. Q-switched lasers are in many respects equivalent to regenerative amplifiers seeded with the extremely low signal (of spontaneous emission level) [28]. Although, being the workhorse of modern ultrafast photonics, regenerative amplifiers were not favored with adequate attention from the scientific society. We need to have a look through the Q-switching theory since physical insight created here can be applied to regenerative process.

There are two versions of the actively Q-switched lasers which differ in output coupling mechanisms. The radiation output is organized via the partially transmitting cavity mirror (output coupler) in a more conventional version, usually referred to simply as the Q-switched laser. However, the intracavity optical switch may serve not only to control the resonator quality but also for dumping the radiation out of the optical cavity in controllable manner when the required intensity is reached. This is an alternative way to release circulating inside the cavity energy as the output pulse in Q-switched lasers. The cavity dumping is less common technique but it has advantage when the peak power enhancement is required at high pulse repetition frequency (PRF). This coupling method provides constant pulse duration, whereas in case of ordinary Q-switching the pulse duration grows inevitably as the repetition rate increases [78].

Regenerative amplifiers can also be separated into two types according to a way of output coupling. Here, in contrast to Q-switched lasers, the most

commonly used version is dumping of the amplified pulse. Really the separate high energy pulse is the most obvious and expected result of the amplifier's action. However, there are applications for which batches of ultrashort pulses are preferable to have (e.g. as the pump source for synchronously pumped parametric oscillators [79]). Then output coupling via the end mirror is also used for regenerative amplifiers. Such a device produces the train of pulses with the period equal to the cavity roun-dtrip time; the pulse train envelope has the shape of a Q-switched pulse.

Q-switching with radiation output via the end mirror was extensively studied, so that this type of lasers became the classical example, the theory and important practical aspects of which are summarized in laser textbooks [26, 75]. A considerable contribution to the theory has been made by Degnan [80]. The fruitful idea was to reduce intrinsically transcendental Q-switching equations to analytical formulas by treating a special point corresponding to the optimally coupled laser (in a sense of the maximum output energy). The resulting expressions became simple and useful guidelines for the practical laser design. This concept was later extended to the maximum peak power and the minimum pulse duration [81]. An alternative way to formulate the basic output parameters analytically has been offered in [82]. The general Q-switching equation was converted to another transcendental equation whose solution in terms of Lambert W-function is included in the most of mathematical computer programs and therefore is easily computable.

The results mentioned above are based on the model of a single Q-switching event, which omits important aspects of repetitive operation. Features of periodic Q-switching were initially described for CW pumped Nd:YAG lasers Q-switched by the acoustooptic modulator [83]. The presented model included the assumption that the population inversion returns to its original value after each Q-switching cycle. This concept of steady-state iteration of functional cycles has since become the integral part of high-PRF system analysis [84]. However, in order to calculate the basic performance characteristics a numerical treatment is still required. As far as I know, no

convenient analytic formulas have been demonstrated so far, despite the fact that continuously pumped high PRF lasers become increasingly involved in modern photonics and industrial applications.

1.5. Manifestations of complex dynamics

Cavity dumping and regenerative amplification have been studied not so extensively as ordinary Q-switching, although a number of specific properties require understanding in order to use potential advantages and to avoid drawbacks by optimum means [26, 85]. In particular, these systems have peculiar pulse formation dynamics in the high PRF range. Output pulse instabilities may appear when the repetition rate exceeds the inverse excited state lifetime. This can reduce the obtained performance characteristics almost twice relative to expectations.

Complex dynamic behavior is a well known phenomenon in laser physics [86]. Generally, the coupled differential equations governing nonlinear system tend to have unstable solutions containing multi-stabilities and bifurcations when a number of independent variables representing system states are equal or more than three [87]. By no means a complete list of laser systems satisfying this condition, and therefore exhibiting complicated dynamics includes Q-switched gas lasers [88], passively Q-switched solid state lasers [89, 90, 91], optically injected solid state lasers [92], CW lasers in the presence of the resonant reabsorption losses [93].

Operation of regenerative amplifiers can be described with two differential equations [28, 94] and its state space is two-dimensional, but periodic disturbance caused by amplified pulse dumping complicates the system behavior. Actually, the pattern of dynamic behavior is determined by the coupling mechanism. As we will see below, indeed cavity dumping regime features complex dynamics, whereas the output coupling constant in time gives inherently stable solutions. This is irrespective of what type of devices is considered either a regenerative amplifier or a Q-switched laser. At higher repetition rates, when the pump stage is comparable or shorter than the gain

relaxation time, the operation cycles become interdependent. The equilibrium between population inversion depletion caused by amplification and inversion restoring caused by pumping may become unstable. This leads to violation of the single-energy regime and to generation of periodically alternating (high/low energy) pulses, or more complicated instability patterns [94].

Unlike many lasers which have been created specially to study dynamic phenomena and chaotic behavior, dynamics of regenerative amplifiers needs to be understood from a more utilitarian position in order to comprehensively optimize real systems. To date, only a few articles have been dedicated to this phenomenon despite its critical influence on the performance of regenerative amplifiers. Peculiar pulse amplification dynamics when the pulse repetition period approaches the gain relaxation time was first observed by Müller et al. [95] for the picosecond thin disk Yb:YAG system. A little later a period doubling regime passing to chaotic operation has been observed for a system based on ytterbium doped glass and the role of bifurcations has been investigated both theoretically and experimentally [94]. However, the experiments were confined to studying cavity dumping of the Q-switched laser that corresponds to amplifier seeded by extremely low pulse energy. One of the important parameters, the seed pulse energy, thus was left beyond the scope. Consequently, the applicability of obtained results turned out to be limited. On the other hand, utilization of later obtained, more comprehensive theoretical results (included to this thesis) promoted top performance from the multi-kilohertz Yb:YAG disk amplifier [40] and aided authors of [37] in understanding the luck of instabilities in the cryogenic amplifier.

The bifurcations induced by the complex dynamics were reported to limit performance of powerful picoseconds Nd:YVO_4 amplifier at the level of 25.5 W at 200 kHz [71]. However, there are still some disagreements in estimations of sensitivity to bifurcations even for similar crystals (Yb:KGW and YbKLuW) in the same setup, as reported by [96] and [68], respectively. There is even less information which is dedicated to instability phenomenon in Q-switched lasers, moreover the available articles have certain disagreements. On

the one hand, good stability in the repetition rate range 20-100 kHz is demonstrated for the powerful Q-switched cavity-dumped laser [78]. On the other hand, inherent instabilities (period doubling up to PRF halving) have been reported to limit ability of intracavity pulse-clipping to control the pulse duration [97]. Pulse-clipping is essentially the hybrid regime: the output radiation comes out via the partially transmitting mirror while the trailing edge of the optical pulse is clipped by cavity dumping.

Since instabilities are the substantial factor limiting performance characteristics, there is a demand to create methods of system stabilization. Probably, because the phenomenon itself is studied not comprehensively enough there were very few disclosed suggestions how to eliminate or at least to reduce instability effects. Authors of [97] succeeded in substantial reducing this problem for the just mentioned pulse-clipped laser by running the system in a regime of intracavity frequency doubling. The key to this solution is nonlinear output coupling the level of which (essentially the level of conversion to the second harmonic) can be adjusted so that pulse-to-pulse energy fluctuations settle down. Obviously, this method is impossible to adapt for regenerative amplifiers unless the output as batches of frequency doubled pulses is desirable. More universal solution could be a feedback control, which modulates the pump diode current as a function of the detected output pulse energy. This idea was suggested by Dörring et al. in [94], however, as far as I know, neither practical realization nor theoretical modeling has been reported so far.

Chapter 2. Premises of modeling

A physical model which adequately describes all the relevant processes and does not suffer from redundant detailing is the perfect tool to study complex systems. In this chapter the principle of operation of regenerative amplifiers is represented to ground a simplified but still quite realistic model based on rate-equation approximation. Basic assumptions and validity conditions for this model are comprehended. Theoretical analysis of intracavity energy and system gain evolution is implemented. A dimensionless form of the output pulse energy as a function of initial and final gains is derived to be extensively used in successive chapters.

2.1. Distinctive intervals of operation

Operation of a regenerative amplifier consists of two functionally different processes: the population inversion accumulation and the amplification itself. Inversion accumulation can be organized in essence by two different methods. Pulsed laser pumping with nanosecond pulses is a way to create a required inversion population density virtually instantaneously. Pulse pumping is the only way to store up a substantial amount of energy for laser media having short relaxation time. The most important representative of the short relaxation time media is a titanium doped sapphire crystal. The most conventional type of pump sources for this crystal is the frequency doubled Q-switched Nd:YAG laser. The pumping process occurs so rapidly that both multi-pass amplification of spontaneous emission and parasitic lasing do not arise due to buildup time shortage.

Short-pulse “instantaneous” pumping is suitable for long lifetime media also, but “slow” pump sources such as flash lamps or laser diodes are a lot more practical here. Long-lasting inversion accumulation is however unfeasible in the high quality optical resonator due to parasitic lasing. Quality control of the optical cavity can prevent the system from oscillating and thus allows energy stored in the laser medium to grow during pumping process. The

optical modulator (Q-switch) is commonly used to hold cavity losses high until amplification process begins.

The present study is adapted to long-lifetime media such as neodymium and ytterbium doped media since power-efficient diode-pumped systems can be built on this basis. Inversion population storage in which Q-switching is involved is consequently the only variant we will consider. Moreover, we consider continuous (CW) pumping as the basic model, and the system PRF is determined by the repetition frequency of Q-switching. This assumption does not restrict generality of the regenerative amplifier model. CW pumping is the most rational way of pumping for the high PRF systems. Results obtained under this assumption, as we will see later, can be easily extended to pulsed pumping for the low PRF case.

Another useful modeling assumption is that processes of pumping and amplification are separated in time. In reality these processes take place simultaneously. CW pumping does not interrupt; however its contribution during amplification stage is usually negligible since the duration of this stage is insignificant (~0.1 μs) compared to the entire operation period. Consequently, the basic functional processes are assumed to take place in turn: pumping and then amplification which correspond to low-Q and high-Q state of resonator quality respectively.

The amplification process starts when the modulator losses are reduced to minimum and the seed pulse is coupled into the cavity. The stored energy in essence turns into energy of the optical pulse circulating inside the cavity. The intracavity pulse energy grows while the population inversion decreases. This evolution continues until the round-trip losses exceed the round-trip gain and then the energy starts decaying. If this process is not intentionally interrupted, it ends by itself when few photons remain inside the cavity and the inversion population virtually stops changing.

The output coupling can be organized by two different means (and also by combination of them). First, the output signal can be formed by leaking of the intracavity radiation through the partially transmitting mirror (output coupler)

during the entire amplification process. In fact, this is not to be necessarily a mirror, but e.g. a variable beamsplitter or other optical components whose distinct property is that the coupling rate remains constant in time. Output radiation then represents a train of equidistant pulses with the bell-shaped envelope. A demand for producing separate pulses is evidently far stronger than for pulse trains in the most of applications. To produce a single pulse the output coupling is organized in transient manner. The optical modulator is used to quickly (less than for the cavity roun-dtrip time) dump the circulating energy out of the cavity. The intracavity modulator then acts both to trigger amplification process at switching to the high-Q state and to extract the amplified pulse off the cavity at switching to the low-Q state. We will consider the cavity dumping regime in greater detail in the present thesis, whereas the stationary coupling will be described just as complementary results in the initial analytical part.

2.2. Structure of regenerative amplifiers

A schematic diagram of a conventional solid-state diode-pumped regenerative amplifier is depicted in Figure 2.1. Optical resonator provides multiple passes of optical pulse through the gain medium by reproducing spatial structure every pass. The number of round trips is controlled by an intracavity optical modulator. This imposes high requirements on the modulator's switching speed. The leading edge is to "lock" the seed pulse within the cavity for amplification. The trailing edge should be fast for clean cavity dumping; the modulator should fully switch from the high-loss-state to the low-loss-state during less than the cavity round-trip time. For distinctness sake, we will consider the system with the electro-optic switch as an intracavity optical modulator. Acousto-optic modulators are quite occasionally used in regenerative amplifiers because of poor switching speed.

The electro-optic switch consists of a Pockels cell, a quarter-wave plate and a polarizing beamsplitter. When the voltage is not applied to the Pockels cell, the wave plate along with the polarizer provides high intracavity losses

(low-Q state of the resonator). Laser action is suppressed, and the gain medium, being under continuous pumping, accumulates population inversion. The voltage is still not applied when the seed pulse enters into the resonator via the polarizer. After passing the retardation plate twice and consequently changing polarization to the orthogonal state the seed pulse propagates towards the laser rod. Indeed at this moment the quarter-wave voltage is applied to the Pockels cell and the seed pulse is turned out to be “locked” within the resonator. At the same time, since the voltage is applied, the intracavity losses become minimal and the high-Q state of the resonator sets in. This state is maintained for some pre-set time while the optical pulse circulating in the resonator is amplified. As soon as the intracavity energy reaches a desired level the Pockels cell voltage is switched off. This extracts the amplified pulse out of the cavity (by exactly opposite to seeding sequence), thus creating the output pulse. The system returns to the initial low-Q state. In periodic repetitive operation the depleted part of the inversion population is restored by uninterrupted pumping and the cycles iterate.

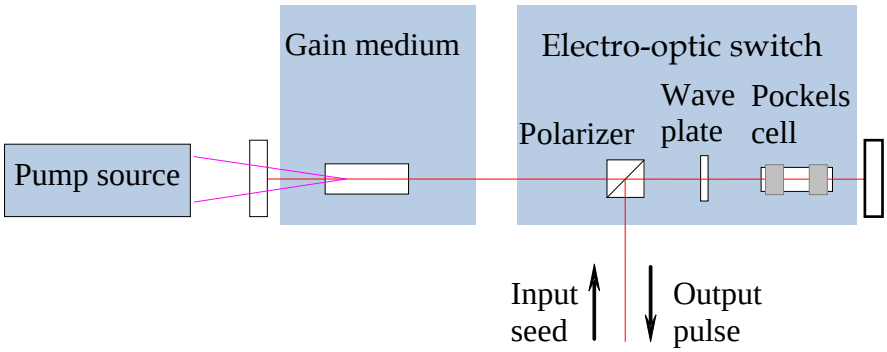

Figure 2.1. Schematic layout of typical solid-state diode pumped regenerative amplifier.

A regenerative amplifier thus can be regarded as a system in which an optical resonator provides multiple passes, the gain medium excited by pumping is responsible for amplification and an electro-optic switch serves as a valve in-turn admitting a weak input pulse and releasing an amplified pulse. Evidently, spatial properties of the amplified radiation are primarily determined by the

optical resonator; the output energy mostly depends on the population inversion stored in the gain medium whereas the amplified pulse duration is imposed by the input seed pulse.

The optical layout of the regenerative amplifier (Figure 2.1) differs from that for a common Q-switched laser only by input-output means and consequently there are certain similarities in operation [28]. Q-switched lasers are in some sense the limiting case of regenerative amplifiers. The output pulse is in both cases a result of amplification of some initial signal. This signal is the either spontaneous emission noise or the external seed pulse. The spontaneous emission is extremely weak and its level is hardly controllable whereas the seed pulse energy can be by many magnitudes higher. The results presented in this manuscript are in many respects valid for Q-switched lasers; just different initial energy should be taken into account.

2.3. Rate equations

The process of regenerative amplification is essentially determined by the interaction of the intracavity radiation with the laser medium excited by pumping. The rules of this interaction can be established by using a simple phenomenological notion of a dynamic balance between basic processes: pumping and relaxation, amplification and extinction. We use the space independent rate equations formulated for the idealized quasi-three-level laser medium with a homogenously broadened line [98]. The idealized four-level system is included in this approach as a limiting case and thus actually all the practically important laser systems are taken into consideration.

The schematic diagram of the quasi-three-level system is depicted in Figure 2.2. We should note that all the laser levels in reality may represent sets of sublevels between which we assume rapid relaxation towards thermal equilibrium. The three-levelness of this model is related to the fact that we assume separation between the ground and lower laser levels so that thermal populating of the lower laser level in general may be substantial. The total population of the two lower levels N_1 is then split so that $N_1\sigma_{abs}/\sigma_{em}$ is

population of the laser level and $(1-\sigma_{abs}/\sigma_{em})N_1$ is the ground state population, where the terms σ_{abs} and σ_{em} represent effective absorption cross section and effective emission cross section, respectively.

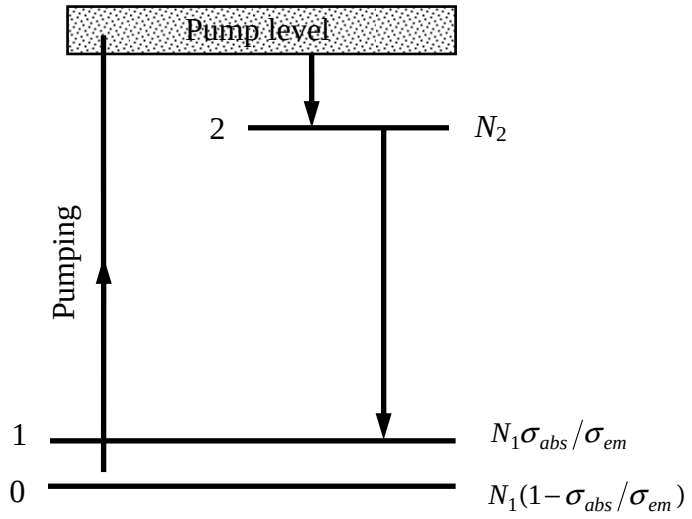

Figure 2.2. Schematic diagram of the quasi-three-level system.

We also assume rapid relaxation from the pump level to the upper laser level that creates population N_2. The overall population N_t therefore can be evaluated as $N_t=N_1+N_2$. The physically quasi-three-level laser system thus reduces to the equivalent two-level situation. The difference in populations for these levels corresponds to the most relevant variable, the population inversion density: $N=N_2-N_1\sigma_a/\sigma_e$. The system evolution can be eventually described by coupled differential equations for the population inversion density and the photon number ϕ:

$$\frac{dN}{dt} = R_P\left(1+\frac{\sigma_{abs}}{\sigma_{em}}\right) - \frac{(\sigma_{em}+\sigma_{abs})c\phi N}{V} - \frac{\sigma_{abs}}{\sigma_{em}}\frac{N_t}{T_1} - \frac{N}{T_1}, \qquad (2.1)$$

$$\frac{d\phi}{dt} = \left(\frac{\sigma_{em}c\,L_a A_a N}{V} - \frac{1}{T_c}\right)\phi. \qquad (2.2)$$

The density of population inversion grows due to pumping (proportionally to the pumping rate R_p) and decays with the constant rate inversely proportional

to the upper laser level lifetime T_1. The second equation establishes a rule of stimulated photon multiplication. The photon number increases proportionally to the population inversion and at the same time it decreases by dissipating through the intracavity losses. The losses here are defined in terms of the photon lifetime T_c which determines the rate of decay for the light field in the optical resonator. Geometry of the amplifier is accounted for in terms of the mode volume within the optical resonator V, the active medium length L_a and the beam area in the active medium A_a. The velocity of light c is a constant which couples temporal and spatial terms of the equations.

The first equation establishing the population inversion is convenient to represent in terms of steady state inversion density N_{ss}. The steady-state density of inversion population appears as a result of the equilibrium ($dN/dt = 0$) between constant pumping ($dR_p/dt = 0$) and the relaxation process in the absence of stimulated photons, $\phi = 0$: $N_{ss} = T_1 R_P (1 + \sigma_a/\sigma_e) - \sigma_a/\sigma_e N_t$. Then Eq. (2.1) becomes:

$$\frac{dN}{dt} = -\frac{(\sigma_e + \sigma_a) c \phi N}{V} - \frac{N - N_{ss}}{T_1}. \tag{2.3}$$

By moving towards macroscopic variables we can replace the population inversion density with the system gain $G = N\sigma_e L_A$ and the total energy of photons within the resonator $E = \phi\hbar\omega$ can be used instead of the total photon number. These transformations yield coupled differential equations for macroscopic variables:

$$\frac{dG(t)}{dt} = -\frac{E(t)G(t)}{A_a T_{rt} F_{sat}} + \frac{G_0 - G(t)}{T_1}, \tag{2.4}$$

$$\frac{dE(t)}{dt} = \frac{E(t)G(t)}{T_{rt}} - \frac{E(t)}{T_C}. \tag{2.5}$$

Consequently, the steady-state gain per pass $G_0 = N_{ss}\sigma_e L_A$ becomes the only term which ultimately, via steady state inversion N_{ss}, depends on pumping

conditions. This term has simple physical meaning: $\exp(G_0)$ is the power amplification factor obtained under continuous pumping and in absence of stimulated emission. The round-trip time T_{rt}, the ratio of the cavity round-trip length to the speed of light has appeared as a composition of the system geometry terms: $T_{rt} = V/(cA_a)$. The saturation fluence $F_{sat} = \hbar\omega/(\sigma_{em} + \sigma_{abs})$ is the laser medium characteristic which in case of a quasi-three-level system contains both the effective emission cross section σ_{em} and the effective absorption cross section σ_{abs}. This term looks more known for four-level lasers where zero ground-state absorption is a certainty, $F_{sat} = \hbar\omega/\sigma_{em}$.

2.4. Decoupling of pumping and amplification

At this stage we can further simplify the situation by splitting the equations according to functional destinations: pumping and amplification. A possibility to treat these processes separately gives a quick result for the pumping process. Really, there are no stimulated photons in the resonator during low-Q interval (E=0), therefore, a set of Eqs. (2.4) and (2.5) transforms into a single equation:

$$\frac{dG(t)}{dt} = \frac{G_0 - G(t)}{T_1}. \tag{2.6}$$

The solution represents a system gain evolution in time:

$$G(t) = G_0 - [G_0 - G(t_0)]\exp\left(-\frac{t - t_0}{T_1}\right), \tag{2.7}$$

where the system gain at the beginning of the process t=t_0 defines initial conditions $G(t_0)$. As it should be for three-level systems, negative gain obtained at the earlier stage of pumping, implies absorption instead of amplification. For instance at t=t_0, we evidently have a familiar law of absorption: $G(t_0) = -N_t\sigma_{abs}L_A$.

In a contrast to the pumping period, only stimulated processes are relevant during amplification. At the high-Q interval the population inversion change due to pumping and relaxation processes is assumed to be negligible compared to the inversion depletion caused by amplification. This approximation is appropriate for laser media having a long excited state lifetime such as neodymium or ytterbium doped media, the most frequently used in diode pumped systems. The relations given by Eqs. (2.4) and (2.5) then reduce to the following coupled equations:

$$\frac{dG(t)}{dt} = -\frac{E(t)G(t)}{A_a T_{rt} F_{sat}} \tag{2.8}$$

$$\frac{dE(t)}{dt} = \frac{E(t)}{T_{rt}}[G(t) - G_{th}], \tag{2.9}$$

where $G_{th} = T_{rt}/T_C$ represents the threshold gain. Obvious property of the threshold gain is that the intracavity energy grows when the current gain exceeds the threshold ($dE/dt > 0$), otherwise it decays.

2.5. Dimensionless form

The rate equations are usually formulated in terms of photon number and population inversion [80] or in terms of intracavity energy and system gain [94]. It is convenient to modify such equations to a form containing normalized and effective dimensionless variables. This reduces a large number of separate system parameters to a few composite variables and thus enables one to obtain a more generalized picture of the system behavior. A primary normalization coefficient is the steady-state small signal gain per pass G_0 (dependent on the pumping intensity). The time scale was modified by introducing the dimensionless time $\tilde{t} = t\beta G_0/T_{rt}$, a product of the round-trip number t/T_{rt} and the steady state gain per round trip βG_0. The factor β represents here the number of passes through the laser medium per round trip. This factor has been introduced in order to account for a type of laser cavity. Ring cavity and linear

cavity imply $\beta = 1$ or $\beta = 2$, respectively. The system evolution during the high-Q interval is thus described by two coupled differential equations:

$$\frac{d\varepsilon(\tilde{t})}{d\tilde{t}} = \varepsilon(\tilde{t})[g(\tilde{t}) - g_t], \tag{2.10}$$

$$\frac{dg(\tilde{t})}{d\tilde{t}} = -\varepsilon(\tilde{t})g(\tilde{t}), \tag{2.11}$$

in which the basic variables are the normalized gain $g = G/G_0$ and the normalized energy ε. Here G is the conventional logarithmic single pass small signal gain, the term proportional to the population inversion per unit area. The normalized energy $\varepsilon = E/(A_a F_{sat} G_0)$ is a macroscopic parameter proportional to the ratio of the total energy of cavity photons E to the mode area in the active medium A_a.

The optical cavity losses are represented in terms of the normalized threshold gain g_{th}. The total losses are conventionally divided into useful losses, associated with the output coupler (of R_{oc} reflectivity), and unavoidable parasitic losses, determined by the loss factor l. By using the regular oscillation threshold criterion we can express the normalized threshold gain in terms of effective coupling losses δ_{oc}, and effective dissipative losses δ_l as:

$$g_{th} = \delta_{oc} + \delta_l, \tag{2.12}$$

where

$$\delta_{oc} = (\beta G_0)^{-1} \ln(1/R_{oc}) \text{ and } \delta_l = (\beta G_0)^{-1} \ln[1/(1-l)]. \tag{2.13}$$

Note that equations formulated in terms of these new variables do not contain pumping characteristics in explicit form. Parameter G_0, depending on the pumping rate, is hidden in the composition of basic variables. The pump effect (as well as other control parameter effects) is easy to restore when applying

modeling results by performing reciprocal transformation from normalized to real parameters. Moreover, further in the theoretical part we often omit the words “effective” and “normalized” just for shortening.

2.6. Remarks on validity

Since our modeling of regenerative amplification is based on simplified rate equations, the range of the model validity is established by the approximations involved in writing of these equations. The equations which we use as a starting point of the study [Eqs. (2.1) and (2.2)] are derived by Svelto and a comprehensive analysis of initial assumptions is represented in [98]. General analysis of conditions for validity of the rate-equation model is also presented in Siegman’s book [75]. Typical mistakes resulting from improper understanding of laser modeling limitations are investigated in the reference [99]. Nothing particular new is added to this subject in the present manuscript. Here we consider just a few but the most important points related to some peculiarities in application of rate equations to regenerative amplification.

The approximation of “space-independence” in particular implies that the amplifying mode energy density is uniform within the laser material both transversely and longitudinally. The latter condition passes over effects of the spatial hole burning caused by the standing wave nature of cavity modes. This may bring substantial mistakes in laser dynamics evolution, e.g. for single longitudinal mode in linear resonators. In case of regenerative amplification the amplified pulse duration is typically so short relative to the round-trip time that the gain media positioning far enough from the end mirror virtually eliminates the spatial hole burning effect. Therefore, in contrast to ordinary lasers, extending of regenerative amplification formulation from the ring cavity to the linear cavity does not bring specific complication. Factor β, introduced in previous section as the number of passes through the gain media per cavity round trip, is a sufficient attribute to account for linear and ring resonator difference.

The condition on the longitudinal uniformity of the energy density establishes the requirement that the system gain and cavity losses should not exceed some moderate levels (G_0~1). The limitation on cavity losses are not so relevant to the systems with cavity dumping simply because the total cavity losses consist of only (usually weak) parasitic losses, whereas much more substantial output coupler losses are absent. This feature widens the model validity range for regenerative amplifiers whose ordinary output coupling method is cavity dumping.

One of the most important points among the assumptions is reduction in number of considered laser levels. The only population related variable, inversion population density, is eventually left in equations. Such a situation is pretty universal and such kind of simplified rate equations is very popular for (e.g.) Q-switched laser analysis. However different authors were guided by somewhat different physical suppositions while deriving their equations. The fact that laser levels may be either degenerate or consist of many strongly coupled sublevels was taken into account for “idealized” four-level or quasi-three-level systems [98]. Additionally, the thermal equilibrium was assumed to set instantaneously within the levels. Such a simplification implies using effective values of emission and absorption cross sections which can be derived from spectroscopic cross section data. In order to account for finite relaxation time of the lower laser level the dimensionless population saturation factor (or “bottleneck” parameter) 2* was introduced by Siegman [75]. The parameter called an “inversion reduction factor” γ was introduced by Degnan [80]. The value of this parameter depends on the degeneracy level, upper and low laser level thermalization times, and the low laser level relaxation speed. A similar factor, called a “degeneracy factor” was also described by Koechner [26].

Although these methods account for somewhat different “non-idealities” of laser systems, the corresponding rate equations can be modified to have identical form. The dimensionless equations which we use here, Eqs. (2.10) and (2.11), can be also derived e.g. from Degnan’s equations by replacing the

inversion reduction factor in accordance with the expression: $\gamma = 1 + \sigma_{abs}/\sigma_{em}$. However, actual values of the correcting factors are determined by the interplay between various relaxation speeds of the laser medium and the rate of the population inversion evolution. This rate corresponds to the inverse pulse duration in case of Q-switched lasers. In regenerative amplifiers the situation is more complicated. We have multiple passes of a short pulse rather than continuous change of the intracavity energy. There are at least two characteristic time parameters which substantially take place in this interplay, the pulse duration and the cavity round-trip time. A single phenomenological factor is, strictly speaking, not sufficient degree of freedom to correct for both time scales. Fortunately, the lack of accuracy in this aspect does not bring substantial deviations to practically useful results, as will be shown in Section 5.6 where the terminal level lifetime effects will be elaborated numerically. The method of simplified rate equations, being a conventional way of the laser dynamics study, gives sufficiently accurate results also for regenerative amplification in the great majority of practically important cases. After stating this we may proceed to analysis of the rate equation solutions.

2.7. Output pulse energy

Our examination will be performed for both cavity dumping and stationary output coupling. We choose the steady-state gain as the primary normalizing factor instead of more commonly used threshold gain (or threshold population inversion). This way turns out to be convenient to study both coupling mechanisms. The initial stage is yet similar to the conventional approach of Q-switched laser analysis [75, 80]. Dividing Eq. (2.10) by Eq. (2.11) makes the time variable implicit,

$$\frac{d\varepsilon}{dg} = \frac{g_{oc} + g_l}{g} - 1, \tag{2.14}$$

and the solution of the resulting differential equation represents the total energy of circulating photons versus instantaneous system gain:

$$\varepsilon(g) = \varepsilon_s + g_i - g - (\delta_{oc} + \delta_l) \ln\left(\frac{g_i}{g}\right). \qquad (2.15)$$

The initial gain g_i and the initial energy $\varepsilon_s = \varepsilon(g_i)$ establish conditions at the beginning of the amplification process. The initial energy, essentially the seed pulse energy, is typically small and often can be neglected.

The system gain decreases to its final level g_f on the amplification completion. The gain difference $(g_i - g_f)$ represents (in dimensionless terms) a part of the stored energy which is converted to the intracavity radiation. The dumped pulse energy ε_f is the energy remaining in the cavity by the high-Q termination moment [$\varepsilon_f = \varepsilon(g_f)$]. The total energy transmitted through the output mirror ε_{oc} and the energy dissipated in parasitic losses ε_l accumulate over the entire amplification process: $\varepsilon_{oc} = \delta_{oc} \int \varepsilon(\tilde{t}) d\tilde{t}$ and $\varepsilon_l = \delta_l \int \varepsilon(\tilde{t}) d\tilde{t}$. The integral belonging to these expressions can be determined by manipulating Eq. (2.10) that yields: $\varepsilon_{oc} = \delta_{oc} \ln(g_i / g_f)$ and $\varepsilon_l = \delta_l \ln(g_i / g_f)$. Equation (2.15) thus reduces to a rational conservation equation, $\varepsilon_f + \varepsilon_{oc} = g_i - g_f - \varepsilon_l$, the left-hand part of which represents the total output energy potentially available from the system. This energy is all delivered to the useful output in case of pure form of both cavity dumping ($\varepsilon_{out} = \varepsilon_f$, $\varepsilon_{oc} = 0$) and stationary coupling ($\varepsilon_{out} = \varepsilon_{oc}$, $\varepsilon_f \approx 0$), and generally for the combined regimes in which $\varepsilon_{out} = \varepsilon_f + \varepsilon_{oc}$ holds. The resulting output pulse energy ε_{out} is therefore independent of the coupling method and can be explicitly expressed as:

$$\varepsilon_{out} = g_i - g_f - \delta_l \ln\left(\frac{g_i}{g_f}\right). \qquad (2.16)$$

Of course the appearance of the output radiation is completely different: either a single pulse or a train of pulses. Relations between the basic system variables are also dependent on the coupling method. We have a pure form of stationary

coupling (as for ordinary Q-switch laser) when no substantial energy remains inside the cavity by the high-Q ending, $\varepsilon_f \approx 0$. Under this condition Eq. (2.15) reduces to the relation between the oscillation threshold $(\delta_{oc} + \delta_l)$ and the gains:

$$g_i - g_f = (\delta_{oc} + \delta_l) \ln\left(\frac{g_i}{g_f}\right). \qquad (2.17)$$

This relation is well recognizable from the Q-switched laser theory and furthermore it is originated from the same condition, $\varepsilon_f \approx 0$. Evidently, such a constraint is improper for the cavity dumping whose distinctive feature is forced termination of the amplification process when the intracavity energy is high.

Chapter 3. Periodic steady-state operation

In this chapter a theoretical analysis of regenerative amplification is presented for two basic methods of pulse extraction: for commonly used cavity dumping and for less common, output coupling via the partially transmitting mirror. Basic performance characteristics for periodic steady-state operation of the optimally coupled regenerative amplifier are expressed analytically. These parameters are represented as a dimensionless function of the normalized pulse repetition rate and the effective loss factor times the composite coefficient containing conventional characteristics of the optical cavity, gain medium, and pumping.

3.1. Assumption of steady-state operation

Expressions of the output energy presented in a previous chapter are obtained for a single amplification cycle at the given initial gain. We will consider periodic repetitive operation of the continuously pumped regenerative amplifier. Periodic single energy operation implies that the system evolution represents a regular in time sequence of identical cycles. Each cycle consists of two intervals: a low-Q interval covering the pumping process and a high-Q interval during which amplification takes place. Consequently the initial and final gains of any functional interval also represent sequences regular in time. In equilibrium the gain depletion caused by amplification is compensated by restoring the population inversion during a subsequent pumping interval and this situation iterates each cycle. This leads to interdependence between end-point gains which in case of periodic steady-state operation reduce to specific constraint on the initial gain magnitude.

By using relation for the gain evolution under continuous pumping and suppressed laser action [from Eq. (2.7)], we can relate the normalized gains at the beginning and at the end of the low-Q interval (denoted as g_{pi} and g_{pf}, respectively):

$$g_{pf} = 1 - (1 - g_{pi}) \exp(-T/T_1), \tag{3.1}$$

where T is the low-Q interval duration. Since the amplification buildup is typically short, the low-Q duration T is approximately equal to the pulse repetition period. The normalized pulse repetition rate is consequently defined as $(T/T_1)^{-1}$.

Obviously, the end of the pumping interval is the same time point as the beginning of the amplification interval. The corresponding gains are equal, $g_{pf} = g_i$, and similarly at the opposite end point we have: $g_{pi} = g_f$. We can then express the steady-state condition in terms of the normalized gains at the beginning and at the end of the high-Q interval:

$$g_i = 1 - (1 - g_f) \exp(-T/T_1), \tag{3.2}$$

For more compact subsequent formulation the just given relation is presented as:

$$g_i = \tilde{g} + g_f (1 - \tilde{g}), \tag{3.3}$$

where

$$\tilde{g} = 1 - \exp(-T/T_1). \tag{3.4}$$

Physically the term $\tilde{g}$ corresponds to the smallest value of the initial gain for the given repetition rate (which is realized at $g_f = 0$) and also to the maximum steady-state energy available for extraction, since $g_i - g_f = \tilde{g}(1 - g_f)$. The whole repetition rate range is thus covered within a range of $1 \le \tilde{g} < 0$. At high PRF $\tilde{g}$ approaches the dimensionless pulse repetition period: $\tilde{g} \approx T/T_1$. Note that the stationary behavior, which implies regular in time sequence of gains $...g_f; g_i; g_f; g_i...$, coupled in accordance with Eq. (3.3), is just an assumption. This assumption affords a ground for further development in Chapter 3, whereas its range of validity and consequences of the violation will be discussed in Chapters 4 and 5.

3.2. Optimum final and initial gains

By using the steady-state condition on the initial gain, Eq. (3.3), we can modify Eq. (2.14) so that the output pulse energy becomes a function of the primary parameters governing the system: the repetition rate and parasitic losses represented in terms of $\tilde{g}$ and δ_l, respectively,

$$\varepsilon_{out} = \tilde{g}(1-g_f) - \delta_l \ln\left(1+\frac{\tilde{g}}{g_f}-\tilde{g}\right). \tag{3.5}$$

The final gain g_f is the mediate parameter which itself is governed either by the output coupler transmission or by the round-trip number. In both cases this is a degree of freedom which is ultimately employed to maximize the output energy. The desired optimum value of the final gain g_f^{opt} can be derived using a function extremum condition for Eq. (3.5), $\partial\varepsilon_{out}/\partial g_f = 0$. This equation has the analytical solution:

$$g_f^{opt} = \frac{\sqrt{\tilde{g}^2 + 4\delta_l(1-\tilde{g})} - \tilde{g}}{2(1-\tilde{g})}. \tag{3.6}$$

The optimum initial gain g_i^{opt} is then found out by applying Eq. (3.3):

$$g_i^{opt} = \frac{\sqrt{\tilde{g}^2 + 4\delta_l(1-\tilde{g})} + \tilde{g}}{2}. \tag{3.7}$$

Equations (3.5), (3.6), and (3.7) apply universally to both versions of regenerative amplifiers which we consider. The optimal g_f and g_i magnitudes are achieved by output coupling adjustment, therefore, Eqs. (3.6) and (3.7) are in essence the condition on optimum coupling in terms of gains. The diagrams of g_f^{opt} and g_i^{opt} versus pulse repetition rate are presented in Figure 3.1. The optimum initial gain tends to unity and behaves virtually insensitively to parasitic losses at low PRF, whereas the final gain approaches the loss factor δ_l:

$$g_i^{opt} \approx \tilde{g} + \delta_l(1-\tilde{g}), \quad \tilde{g} \sim 1; \tag{3.8}$$

$$g_f^{opt} \approx \frac{\delta_l}{\tilde{g}}, \ \tilde{g} \sim 1. \tag{3.9}$$

Equation (3.9), in the simplest limiting case of $\tilde{g} = 1$, is a well recognizable rule stating that the dumping moment is optimum when the threshold gain is reached ($\delta_{oc} = 0$, consequently $g_{th} = \delta_l$, then $g_f^{opt} \approx g_t$). Really, the optical energy inside the resonator always culminates at threshold, but dumping at the threshold is optimum only when initial gain g_i is an independent, fixed parameter. Interdependence of the operation cycles [g_i versus g_f given by Eq. (3.3)] is so relevant at higher PRF that dumping well before reaching the threshold becomes more power-efficient.

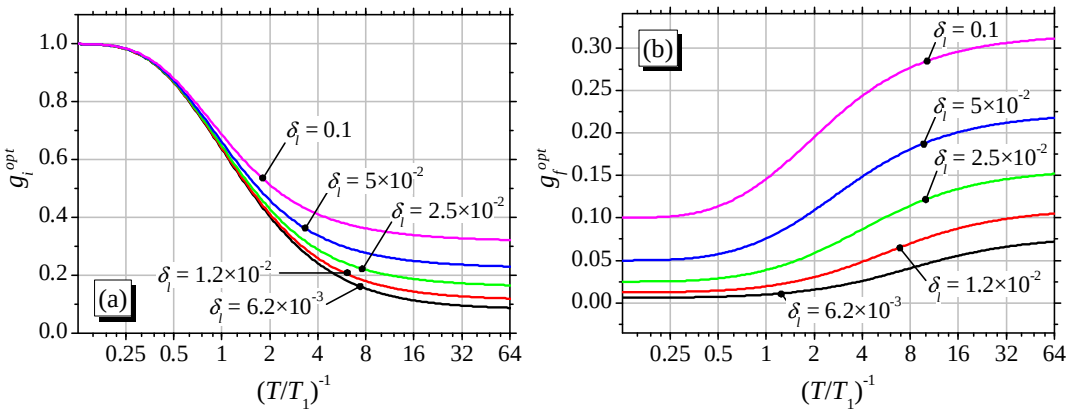

Figure 3.1. Optimum initial gain (a) and optimum final gain (b) versus normalized repetition rate at different parasitic losses.

As the pulse repetition rate becomes higher, the initial gain and the final gain approach a square root of the loss factor $\sqrt{\delta_l}$ from above and from below, respectively:

$$g_i^{opt} \approx \sqrt{\delta_l} + \frac{\tilde{g}}{2}\left(1-\sqrt{\delta_l}\right), \quad \tilde{g} \sim 0; \tag{3.10}$$

$$g_f^{opt} \approx \sqrt{\delta_l} - \frac{\tilde{g}}{2}\left(1-\sqrt{\delta_l}\right), \quad \tilde{g} \sim 0. \tag{3.11}$$

3.3. Maximum output energy

Since the gains g_i^{opt} and g_f^{opt} are determined, the maximum output energy $\varepsilon_{out}^{\max}$ and the corresponding complementary parameters, which the regenerative amplifier produces when this energy is obtained, can be expressed analytically. Notations for the parameters of the amplifier optimized in this sense will contain the superscript "*opt*" (except $\varepsilon_{out}^{\max}$ itself). These characteristics are particularly important as corresponding to the highest attainable amplification performance. Obviously, the maximum output energy is reached simultaneously with the maximum average power at given PRF and with the maximum power efficiency at a given pumping rate and losses. Substitution of the optimum final gain into Eq. (3.5) yields the desired value as a function of parasitic losses (given by δ_l) and the repetition rate (presented in terms of $\tilde{g}$):

$$\varepsilon_{out}^{\max} = \frac{\tilde{g}\left[2-\sqrt{\tilde{g}^2+4\delta_l(1-\tilde{g})}+\tilde{g}\right]}{2(1-\tilde{g})} - \delta_l \ln\left[(1-\tilde{g})\left(1+\frac{2\tilde{g}}{\sqrt{\tilde{g}^2+4\delta_l(1-\tilde{g})}-\tilde{g}}\right)\right]. \tag{3.12}$$

The output energy attainable at given system parameters is the universal value, even though the amplification process has different temporal pattern and results in either a single pulse or a batch of pulses depending on output coupling version. Diagrams of the maximum output energy versus the repetition rate for different parasitic losses are depicted in Figure 3.2. As the repetition rate decreases, the energy approaches the constant determined only by the losses. A simple formula, obtained from Eq. (3.12), describes this quantitatively:

$$\varepsilon_{out}^{\max} \approx \tilde{g} - \delta_l\left[1+\ln\left(\frac{\tilde{g}^2}{\delta_l}\right)\right], \quad \tilde{g} \sim 1. \tag{3.13}$$

In the opposite limiting case the output pulse energy decreases linearly with PRF increasing. Consequently, the product of the output energy and the repetition rate (essentially the dimensionless average power), as expected, approaches the constant value:

$$\varepsilon_{out}^{\max}\left(\frac{T}{T_1}\right)^{-1} \approx \left(1-\sqrt{\delta_l}\right)^2, \quad \tilde{g} \sim 0. \tag{3.14}$$

It is also important to evaluate the amount of energy dissipated inside the optical cavity. A quite definite (absorbed) part of this energy generates heat which may affect operation of components susceptible to heating (the Pockels cell crystal is usually the most critical one). Resulting reduction in performance may become significant especially for high power systems.

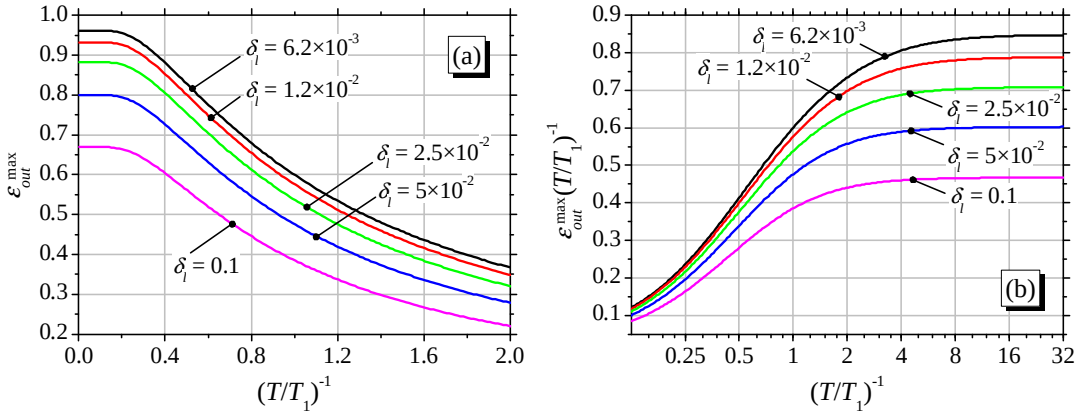

Figure 3.2. Amplification performance for optimum output coupling. Low-PRF dimensionless output pulse energy (a) and dimensionless output power (b) versus normalized repetition rate at different losses.

By comparing Eq. (2.16) with Eq. (3.12) we can deduce that the item proportional to δ_l in Eq. (3.12) represents the energy dissipated via parasitic losses:

$$\varepsilon_l^{opt} = \delta_l \ln\left[(1-\tilde{g})\left(1+\frac{2\tilde{g}}{\sqrt{\tilde{g}^2+4\delta_l(1-\tilde{g})}-\tilde{g}}\right)\right]. \tag{3.15}$$

The real physical form of the energy based parameters can be reproduced from dimensionless formulas by using variable definitions presented in describing Eqs. (2.10) and (2.11). These conversion expressions, and also the others

whose origin will be described in successive sections, are submitted in Table 3.1. Note that the term $\varepsilon_{out}^{\max}(T/T_1)^{-1}$, deliberately introduced as dimensionless output power, is also equivalent to the power-extraction efficiency (the ratio of extracted power to available power).

Table 3.1. Expressions for laser parameters

Laser parameter	Expression
Pulse energy	$\varepsilon \times G_0 F_{sat} A_a$
Average power	$\varepsilon\left(\frac{T}{T_1}\right)^{-1} \times \frac{G_0 F_{sat} A_a}{T_1}$
Time terms of the amplification interval	$\tau \times \frac{T_{rt}}{\beta G_0}$
Peak energy of the train	$\varepsilon_{peak}\delta_{oc} \times G_0 F_{sat} A_a$
Number of pulses in the train at FWHM level	$\frac{\varepsilon_{out}}{\varepsilon_{peak}\delta_{oc}}$
Train envelope duration FWHM	$\frac{\varepsilon_{out}}{\varepsilon_{peak}\delta_{oc}} \times \frac{T_{rt}}{\beta G_0}$
Output mirror reflectivity	$[\exp(-\delta_{oc})]^{\beta G_0}$

3.4. Optimum stationary coupling

The final gain in regenerative amplifiers with stationary coupling is controlled by the output mirror reflectivity, as well as in ordinary Q-switched lasers. The corresponding relation results from the gain constraining equation [Eq. (2.17)] and the condition of repumping in steady-state [Eq. (3.3)]. The desired coupling factor δ_{oc} can be written as:

$$\delta_{oc} = \frac{\tilde{g}(1-g_f)}{\ln(1-\tilde{g}+\tilde{g}/g_f)} - \delta_l \,. \tag{3.16}$$

Then, by replacing the final gain with its optimum value (from Eq. 13), we can determine the optimum (providing the maximum pulse energy) output coupling:

$$\delta_{oc}^{opt} = \frac{\tilde{g}\left[2-\sqrt{\tilde{g}^2+4\delta_l(1-\tilde{g})}+\tilde{g}\right]}{2(1-\tilde{g})\ln\left[(1-\tilde{g})\left(1+\frac{2\tilde{g}}{\sqrt{\tilde{g}^2+4\delta_l(1-\tilde{g})}-\tilde{g}}\right)\right]}-\delta_l. \qquad 3.17)$$

The diagrams of δ_{oc}^{opt} versus pulse repetition rate for different optical losses are depicted in Figure 3.3. We can see that δ_{oc}^{opt} gradually decreases in the low-PRF range,

$$\delta_{oc}^{opt} \approx \frac{\tilde{g}-\delta_l}{\ln\left(\tilde{g}^2/\delta_l\right)}-\delta_l, \quad \tilde{g}\sim 1; \qquad (3.18)$$

and then at high PRF it approaches the constant level:

$$\delta_{oc}^{opt} \approx \sqrt{\delta_l}\left(1-\sqrt{\delta_l}\right), \quad \tilde{g}\sim 0. \qquad (3.19)$$

The optimum reflectivity of the output mirror can be obtained by raising the normalized term $\exp\left(-\delta_{oc}^{opt}\right)$ to βG_0 power (Tab. 3.1).

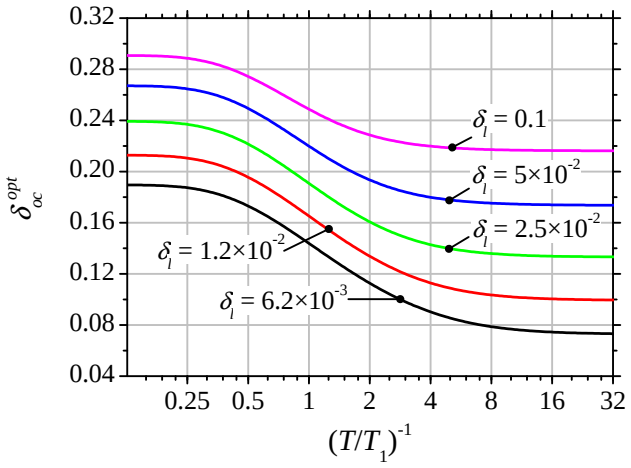

Figure 3.3. Optimum output coupling versus normalized repetition rate at different parasitic losses.

3.5. Time domain parameters

Temporal characteristics of the amplification process can be evaluated by integrating Eq. (1) in which the energy multiplier is expanded according to Eq. (3):

$$\tilde{t} = -\int \frac{dg}{g[\varepsilon_s + g_i - g - (\delta_{oc} + \delta_l)\ln(g_i/g)]}. \qquad (3.20)$$

The ranges of integration from g_i to g_{th} and from g_{th} to g_f give the buildup time and the decay time, respectively. The time intervals given in terms of dimensionless time $\tilde{t}$ (defined in Section 2.4 as a product of the round-trip number t/T_{rt} and the steady state gain per round trip βG_0) will also be further called the effective round-trip number.

Analytic expression for the integral of Eq. (3.20) is unknown and for correct numerical integration certain aspects should be taken into account. First, this is the case where the seed pulse item ε_s cannot be neglected even if its value is extremely low. The opposite leads to infinite time resulting from physically unfeasible situation of absence of initiating radiation. In reality, even if the seed pulse is blocked, spontaneously emitted photons always exist and take a role of seeding radiation. Second, presence of integrand singularities close to the domain of integration complicates numerical integration. This is a consequence of low energy magnitude at the oscillation beginning, $\varepsilon(g_i) = \varepsilon_s \sim 0$, and also by oscillation ending, when, as for stationary coupling, $\varepsilon(g_f) \sim 0$ holds.

It is possible to avoid the integration difficulties by using approximate evaluation. The pulse amplification process is then regarded as consisting of three stages. The initial stage, lasting while the inversion stays depleted insignificantly ($g \approx g_i$), is the exponential buildup stage, approximated as $\varepsilon = \varepsilon_s \exp[\tilde{t}\,(g_i - g_{th})]$. Similarly, the final stage (if the process is not interrupted and $g \approx g_f$ at $\varepsilon(g_f) \sim 0$) is the exponential decay with the decay rate of ($g_{th} - g_f$). The non-exponential energy evolution occurs transiently in between when the pulse amplified to substantial magnitude appears and the gain substantially drops. This stage is typically short compared to exponential wings, and therefore the entire time, necessary for completing the pulse generation process, can be evaluated as:

$$\tau_{cd} \approx \frac{\ln(\tilde{g}/\varepsilon_s)}{g_i - \delta_l}, \tag{3.21}$$

$$\tau_{oc} \approx \frac{\ln(\tilde{g}/\varepsilon_s)}{g_i - \delta_{oc} - \delta_l} + \frac{\ln(\tilde{g}/\varepsilon_f)}{\delta_{oc} + \delta_l - g_f} \tag{3.22}$$

for ordinary cavity dumping and rarely used stationary coupling, respectively. The term $\tilde{g}$ appears here as a roughly estimated PRF-dependent peak value of the exponential evolution (yet, being under logarithm, not requiring better accuracy).

By using the optimum values for the gains and for the useful output losses [Eqs. (3.6), (3.7) and (18)] we can find out the temporal characteristics for the optimally coupled regenerative amplifier. The characteristic notified as τ_{oc}^{opt}, stationary coupling attribute, represents the entire amplification time (pulse buildup plus decay within high-Q interval) which comes out when output coupling is set optimum. The term τ_{cd}^{opt} is the effective round-trip number (high-Q interval duration) which should be set in order to provide the best output coupling rate in case of cavity dumping.

The high-Q state duration is particularly important to estimate for high repetition rates. The long-lasting amplification interval may limit the system performance because of time shortage for the population inversion accumulation. By replacing terms in the denominators of Eq. (3.22) with their high-PRF values [Eqs. (3.10), (3.11) and (3.19)] we can determine the high-Q interval duration for the regenerative amplifier with the optimized output mirror:

$$\tau_{oc}^{opt} \approx 2\left(\frac{T}{T_1}\right)^{-1} \frac{\ln(\tilde{g}/\varepsilon_s) + \ln(\tilde{g}/\varepsilon_f)}{1 - \sqrt{\delta_l}}, \quad \tilde{g} \sim 0. \tag{3.23}$$

Note that the time constants for decay and growth in this case are equal so that the exponential wings of the pulse envelope are symmetric. However, a trailing edge of the pulse envelope can be intentionally clipped in order to reduce the high-Q interval in favour of the pumping interval. Switching to the low-Q state

at high PRF is useful to perform well before the complete tail fading out. If one cuts off a small fraction (~1%) of the total pulse energy, then the high-Q interval shortens almost twice (approaching the buildup time) without improper consequences. Stronger clipping gives no considerable advantages but may bring about specific stability problems (this topic will be discussed in Chapter 4).

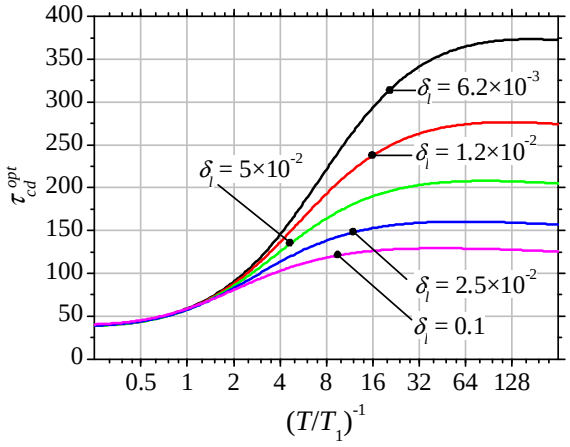

Figure 3.4. Optimum effective round-trip number versus normalized repetition rate at different losses and fixed seed pulse energy, $\varepsilon_s = 3\times10^{-15}$.

For cavity-dumped amplifiers the coupling rate is a function of the effective round-trip number and the highest value of the output energy is achieved by setting this number optimum, τ_{cd}^{opt}. By substituting explicit g_f^{opt} into Eq. (3.21) we can calculate the desired value:

$$\tau_{cd}^{opt} \approx 2\frac{\ln(\tilde{g}/\varepsilon_s)}{\sqrt{\tilde{g}^2 + 4\delta_l(1-\tilde{g})} + \tilde{g} - 2\delta_l}. \qquad (3.24)$$

This formula gives just a slightly underestimated result compared with exact numerical solutions and well reveals all the important dependences. Starting with a gradual increase, virtually independently of the optical losses, at low PRF,

$$\tau_{cd}^{opt} \approx \frac{\ln(1/\varepsilon_s)}{\tilde{g}(1-\delta_l)}, \quad \tilde{g} \sim 1; \qquad (3.25)$$

the τ_{cd}^{opt} then approaches the virtually constant level at high PRF:

$$\tau_{cd}^{opt} \approx \frac{\ln(\tilde{g}/\varepsilon_s)}{\sqrt{\delta_l}\left(1-\sqrt{\delta_l}\right)}, \quad \tilde{g} \sim 0. \tag{3.26}$$

The finite duration of high-Q interval is the relevant feature of cavity dumping. Numerical integration, giving more precision data, confirms that τ_{cd}^{opt} does not just stop growing but faintly decays after certain PRF, Figure 3.4. This behavior totally differs from a linear growth peculiar to systems with stationary output coupling [Eq. (3.23)]. Such a property of cavity dumping gives potential possibility to expand operation of regenerative amplifiers to very high repetition rates.

3.6. Train envelope duration

Specific characteristics of output pulse trains are needed to be determined for a regenerative amplifier with the output mirror. First, we will determine the peak energy value ε_{peak} which the amplifying pulse reaches while circulating inside the cavity. The intracavity energy stops growing and starts decaying when the current system gain becomes equal to the threshold gain. Direct substitution of the threshold gain $g = \delta_{oc} + \delta_l$ into Eq. (3) yields:

$$\varepsilon_{peak} = g_i - (\delta_{oc} + \delta_l)\left[1 + \ln\left(\frac{g_i}{\delta_{oc} + \delta_l}\right)\right]. \tag{3.27}$$

Obviously, this formulation is correct only if the threshold is passed during the amplification process. This always occurs for stationary coupling. Cavity dumping, however, quite typically can be performed “on rise,” before the threshold gain is reached. The energy inside the cavity thus amounts to the highest magnitude right before dumping. This value therefore equals to the output pulse energy and reaches $\varepsilon_{out}^{\max}$ given by Eq. (3.12) for the optimum coupling rate.

The output pulse train envelope behind the output mirror is simply a "reduced copy" of the intracavity energy evolution. The reduction factor is in essence determined by the output coupling factor. The energy of the highest energy pulse in this train is thus defined as $\varepsilon_{peak}\delta_{oc}$, which in case of the optimally coupled amplifier corresponds to $\varepsilon_{peak}^{opt}\delta_{oc}^{opt}$, where δ_{oc}^{opt} is given by Eq. (3.17). The analytical expression of ε_{peak}^{opt} results from Eq. (3.27) by replacing g_i and δ_{oc} with their optimal values:

$$\varepsilon_{peak}^{opt} = g_i^{opt} - \left(\delta_{oc}^{opt} + \delta_l\right)\left[1 + \ln\left(\frac{g_i^{opt}}{\delta_{oc}^{opt} + \delta_l}\right)\right]. \qquad (3.28)$$

In low-PRF and high-PRF approximations Eq. (3.28) is compact enough to write explicitly:

$$\varepsilon_{peak}^{opt} = \tilde{g} - \frac{\tilde{g} - \delta_l}{\ln(\tilde{g}/\delta_l)}\left\{1 - \ln\left[\frac{\tilde{g} - \delta_l}{\tilde{g}\ln(\tilde{g}/\delta_l)}\right]\right\}, \quad \tilde{g} \sim 1; \qquad (3.29)$$

$$\varepsilon_{peak}^{opt}\delta_{oc}^{opt} \approx \left(\frac{T}{T_1}\right)^2 \frac{\left(1 - \sqrt{\delta_l}\right)^3}{8}, \quad \tilde{g} \sim 0. \qquad (3.30)$$

As soon as the peak point of the train is determined, the pulse envelope duration can be estimated by conventional means as the ratio of the total pulse energy to the peak pulse energy (Tab. 3.1). This duration in dimensionless form approximately corresponds to the number of pulses in the output train at the FWHM level. In case of the optimally coupled amplifier the number of pulses reduces to a combination of the analytically represented components, $\varepsilon_{out}^{\max} \Big/ \left(\varepsilon_{peak}^{opt}\delta_{oc}^{opt}\right)$. At high PRF the peak energy decreases as the repetition rate square [Eq. (3.30)], the total energy of pulses decreases linearly [Eq. (3.14)]. Consequently, the number of pulses in the train linearly increases approaching the value equal to $8\left[\left(1 - \sqrt{\delta_l}\right)T/T_1\right]^{-1}$. The ratio of the train envelope duration to the buildup time [Eq. (3.23)] in high-PRF approximation is virtually a

constant. This value, $4[\ln(T/\varepsilon_s T_1)]^{-1}$, is independent of losses and logarithmically weakly dependent on both PRF and the seed pulse energy.

3.7. Multi-pass *B* integral

Usual occupation of regenerative amplifiers is amplification of ultra-short optical pulses that naturally implies high optical intensity. High intensities influence the system operation mainly by means of the optical Kerr effect. The conventional quantitative gauge of the Kerr effect is the *B* integral, nonlinear on-axis phase shift which light waves with the wavelength λ undergo while propagating through the media:

$$B_{sp} = \frac{2\pi}{\lambda}\int n_2(z)I(z)dz\,. \tag{3.40}$$

The terms $I(z)$ and $n_2(z)$ are distributions of on-axis intensity and nonlinear refractive index along current coordinate z. The *B* integral for regenerative amplifiers implies multi-pass integration over the entire propagation length. The integration length is consequently a product of the optical cavity pass length and the round-trip number. In an approximation of relatively low single pass gain (the integral within the gain medium can be replaced with the average) and also for moderate Kerr effect influence (iteration of the intensity profile in the optical resonator is not disturbed too much by self-focusing) we can replace the overall integral with a sum of single pass integrals:

$$B \approx \frac{2\pi}{\lambda}\sum_{NRT}\int n_2(z)I_{NRT}(z)dz\,, \tag{3.41}$$

where index *NRT* implies summation over round trips. The sum of integrals is equal to the integral of the sum and also $n_2(z)$ is independent of the round-trip number function. These yield:

$$B \approx \frac{2\pi}{\lambda}\int n_2(z)\sum_{NRT} I_{NRT}(z)dz\,. \tag{3.42}$$

In an assumption of Gaussian beam shape for which the peak intensity is equal to $2P/A(z)$ (the term P is the optical power, the term $A(z)$ is a function of the Gaussian beam area on longitudinal coordinate) we can calculate the intensity for the optical pulse of duration Δt in terms of the pulse energy:

$$\sum_{NRT} I_{NRT}(z) \approx \frac{2}{A(z)\Delta t} \sum_{NRT} E_{NRT} \,. \tag{3.43}$$

Summation of energies can be rewritten as the integral over time which in turn can be expressed in dimensionless terms:

$$\sum_{NRT} E_{NRT} \approx A_a F_{sat} \int_0^{\tau} \varepsilon(\tilde{t}) d\tilde{t} \,. \tag{3.44}$$

The beam area in the active medium obviously can be expressed through the Gaussian beam radius: $A_a = \pi w_a^2$. The time integral of dimensionless intracavity energy can be derived similarly as for Eq. 2.16 in Section 2.7:

$$\int_0^{\tau} \varepsilon(\tilde{t}) d\tilde{t} = \ln\left(\frac{g_i}{g_f}\right). \tag{3.45}$$

Finally, by combining Eqs. (3.42-3.45) we can derive explicit multi-pass B integral in a form which is convenient for evaluation of the Kerr effect in regenerative amplifiers:

$$B = B_1 \ln\left(\frac{g_i}{g_f}\right), \tag{3.46}$$

where

$$B_1 = \frac{4\pi}{\lambda} \frac{F_{sat}}{\Delta t} \int n_2(z) \frac{A_a}{A(z)} dz \,. \tag{3.47}$$

The functional physical contributions are separated in this formula. The first multiplier, B_1 , represents attributes of the system geometry, material parameters and optical pulse duration. Essentially, this term is a single-pass B integral calculated for the Gaussian beam in given optical cavity and for the pulse energy fluence equal to the gain medium saturation fluence. The second

multiplier is effective multiplication factor for the single pass *B* integral which in essence is responsible for accumulation of the Kerr effect due to multiple passes. This is a function of regenerative amplifier dynamics represented in terms of normalized initial and final gains.

The multiplication factor is possible to represent analytically for the optimally coupled amplifier:

$$\ln\left(\frac{g_i^{opt}}{g_f^{opt}}\right)=\ln\left[(1-\tilde{g})\left(1+\frac{2\tilde{g}}{\sqrt{\tilde{g}^2+4\delta_l(1-\tilde{g})}-\tilde{g}}\right)\right]. \qquad (3.48)$$

It is logical that the same factor but under the single pass cavity loss δ_l is involved in the expression for dissipated energy [see Eq. (3.15)]. Intuitively a less logical result is that the multi-pass B-integral is independent of the coupling mechanism parameter. Really, the energy available from the cavity dumping scheme as a single pulse is distributed over the burst of pulses in case of stationary coupling. The reason for *B* integral equality is that the pulse energy difference inside the cavity is not as high as outside and the residual difference is compensated by the larger pulse round-trip number.

Much simpler formulas, convenient for the Kerr effect evaluation, can be obtained for marginal repetition rates. The multiplication factor at low PRF reduces to the slowly varying, logarithmic function of PRF which, at approaching the single-shot operation, approaches the value dependent only on the parasitic losses:

$$\ln\left(\frac{g_i^{opt}}{g_f^{opt}}\right)\approx\ln\left(\frac{\tilde{g}^2}{\delta_l}\right)\sim\ln\left(\frac{1}{\delta_l}\right),\quad \tilde{g}\sim 1. \qquad (3.49)$$

The multiplication factor decreases linearly with the repetition rate at high PRF so that at high-PRF-operation the Kerr effect relevance is substantially reduced:

$$\ln\left(\frac{g_i^{opt}}{g_f^{opt}}\right)\approx\frac{T}{T_1}\frac{1}{\sqrt{\delta_l}},\quad \tilde{g}\sim 0. \qquad (3.50)$$

3.8. Remarks on steady-state results

The simplified low-PRF formulas presented in previous sections are appropriate for normalized repetition rates below $(T/T_1)^{-1} = 1$. In case of single-shot regime ($T >> T_1$), the expressions for basic characteristics simplify still further by setting $\tilde{g}$ equaled to unity. In this case the pumping method (CW or pulsed) becomes insignificant in formulation. The important factor is the resulting gain level at the beginning of the high-Q stage. In order to get dimensional results, the same formulas from Table 3.1 can be used; just the term G_0 takes a role of the initial gain factor. In this marginal case the expressions for the maximum pulse energy, peak energy, pulse train envelope duration, and optimal output mirror reflectivity reduce to Degnan's formulas for the optimally coupled Q-switched laser [80]. Also the optimum output pulse energy is the same as formulated by Murray and Loudermilk in [28]. Regenerative amplification at high PRF in some sense approaches the CW laser regime. The amplifier parameters such as the average power, the optimum output mirror reflectivity and the optimum cavity gain expressed in the high-PRF approximation are identical to CW laser parameters.

Important characteristics such as optimum end-point gains and output pulse energy are expressed by equal formulas for both considered coupling versions cavity dumping and output coupling mirror. This identity in formulation however should not create the illusion of excessive similarity. In repetitive amplification process the instantaneous system gain oscillates in time within the bounds of g_i and g_f. If PRF increases, then these gains approach each other and converge to $\sqrt{\delta_l}$ [see Eqs. (3.10) and (3.11)]. It is evident from Eq. (3.19) that $\sqrt{\delta_l}$ is equal to the threshold gain in case of a stationary coupling scheme. Being close to the oscillation threshold incurs challenges to robust operation in real systems (pulse drop-out and related effects may appear). This causes considerable limitation of high-PRF capabilities. The cavity dumping situation is quite different. The threshold gain is significantly

reduced: $\delta_{oc} = 0$ and then $g_{th} = \delta_l < \sqrt{\delta_l}$. The optimum gain substantially exceeds the threshold irrespective of PRF.

Due to already mentioned similarity, the results derived for regenerative amplifiers apply to Q-switched lasers. Obviously the cavity dumping results are suitable for cavity dumped Q-switched lasers whereas stationary output coupling formulas correspond to ordinary Q-switching.

Chapter 4. Pattern of inherent instabilities

In this chapter theoretical analysis of complex dynamics of regenerative amplifiers is presented. The causes and effects of the steady-state regime violation are illustrated in the space of system states using a discrete-time dynamical system approach. Regular single-energy operation, quasi-periodic pulsing and chaotic behavior regions are distinguished in space of controlling parameters. Influences of cavity losses and seed pulse energy on the amplification stability are described quantitatively. The seed pulse energy is shown to be an important parameter determining the stability space at high repetition rates.

4.1. Coupling of successive cycles

The formulas for the optimally coupled regenerative amplifier are derived using the assumption that the system exhibits periodic stationary response to repetitive Q-switching. This implies that inversion consumption caused by amplification is precisely restored during pumping stage. Such a steady-state balance obviously exists on average over a great number of operation cycles, but the condition of the consumption-restoring equilibrium for every individual period is needed to be analyzed. We can consider the system evolution as the sequence of stages alternating in time (… high-Q, low-Q, high-Q, …). Each functional interval in this sequence is fully specified by the gain magnitude on its opening boundary. The boundary gain thus serves as a variable defining the system state. The term $g_i(1)$ is introduced as the initial gain of the amplification phase for the first cycle of operation. This stage finishes with the final gain denoted as $g_f(1)$. The subsequent pump phase of the current cycle obviously begins with the same gain value, $g_{pi}(1)=g_f(1)$. Similarly, the gain evolution continuity should be taken into account for coupling of all operation cycles: $g_f(k)=g_{pi}(k)$ within the cycle number k and $g_{pf}(k)=g_i(k+1)$ for neighboring cycles. The legend of the gain evolution can thus be presented as follows:

$$... g_i(k) \rightarrow g_f(k) = g_{pi}(k) \rightarrow g_{pf}(k) = g_i(k+1) \rightarrow g_f(k+1)... \qquad (4.1)$$

The evolution of boundary gains occurs on a discrete time scale. The corresponding system states are separated in time by periodically iterating high-Q and low-Q intervals. Analogous transition to the discrete time scale can be applied to energy evolution. However, unlike continuity of the gain evolution, the build-up of intra-cavity energy $\varepsilon_s \rightarrow \varepsilon_f(k)$ interrupts at the end of the amplification phase of each cycle at the moment of pulse dumping and then it begins again from the constant level which corresponds to the seed pulse energy ε_s. Hence the term $\varepsilon_f(k)$, determining the output energy, does not depend on its own pre-history. Therefore, the gain becomes the only independent variable that needs to be analyzed in order to understand regenerative amplification dynamics.

The immediate operational process takes the current state as input and updates it by producing a new state. For the cycle number k, the oscillation process takes the initial gain $g_i(k)$ and produces the final gain $g_f(k)$. This new output state becomes the input for the repumping process which produces the initial state for the next $(k+1)$-cycle, $g_i(k+1)$. The rule establishing transformation of $g_i(k)$-state to $g_i(k+1)$-state is the property of the dynamic system which eventually determines the entire stability pattern.

The gain transformation rule for the regenerative amplifier with coupling via cavity dumping can be obtained by manipulating the expression for the high-Q window duration [Eq. (3.20) at $\delta_{oc} = 0$]:

$$\tau_{cd} = -\int_{g_i}^{g_f} \frac{dg}{g[\varepsilon_s + g_i - g - \delta_l \ln(g_i/g)]}. \qquad (4.2)$$

The term τ_{cd} here is the effective number of cavity round trips. Numerical treatment then gives the final gain as a function of the initial gain and also of parameters controlling the laser action, $\tau_{cd}, \delta_l, \varepsilon_s$. We can formulate this

solution as: $g_f = \hat{F}_{cd}(g_i)$, where $\hat{F}_{cd}$ designates the gain transformation rule for the high-Q interval in the operating point $(\tau_{cd}, \delta_l, \varepsilon_s)$. Analogous function for stationary coupling, implying $\varepsilon_f \sim 0$, results from Eq. (2.17). This equation is transcendental and the numerically obtained gain transformation rule is also convenient to represent implicitly as $g_f = \hat{F}_{oc}(g_i)$, having in mind that in this case the operating point is given by (δ_{oc}, δ_l).

During the low-Q interval the gain magnitude grows under continuous pumping so that the subsequent oscillation process begins with $g_i = 1 - (1 - g_f)\exp(-T/T_1)$ [see Eq. (3.2)]. In such a context this simple linear dependence essentially serves as the gain transformation rule for the repumping process. Then it is possible to combine amplification and pumping intervals within a certain operation cycle and to form a joint gain transformation rule. The composite function $\hat{F}_\Sigma$ either

$$\hat{F}_\Sigma = 1 - (1 - \hat{F}_{cd})\exp(-T/T_1) \text{ or } \hat{F}_\Sigma = 1 - (1 - \hat{F}_{oc})\exp(-T/T_1) \qquad (4.3)$$

(depending on a coupling mechanism) describes the gain transformation for the complete operation cycle.

4.2. Discrete-time dynamical system approach

Thus, we have reduced the regenerative amplification dynamics to the evolution of a single variable (system state, g_i) on a discrete time scale; and also we have found a rule of this variable updating. The basic properties of this updating function fit to the mathematical definition usually referred to as maps [functions whose domain (input) space and range (output) space are the same]. Then the regenerative amplification can be described by using the theory of one-dimensional discrete-time dynamical systems (one-dimensional maps) [100]. The sequence of the system states $g_i(1)$, $g_i(2)$, … $g_i(k)$ … is called an orbit in terms of this theory. The orbits can be calculated by using a recurrent

formula determining the subsequent state of the system in terms of the present state: $g_i(k+1) = \hat{F}_\Sigma[g_i(k)]$.

It is obvious that in a regular single-energy regime the gain depletion during the amplification interval should be compensated by restoring the population inversion by repumping. In terms of states evolution, the initial gain of the amplification stage eventually should iterate, i.e. there is a certain gain value (designated as g_1) such that the subsequent gains stabilize upon reaching that value, $g_i(k+1)=g_i(k)=g_1$. Consequently, the system eigenstate satisfying the condition $g_1 = \hat{F}_\Sigma(g_1)$ should exist. The solution of this equation is known as a fixed point in the discrete-time dynamical system theory. The fixed point state is such that the system reproduces this state in every cycle and therefore operates in a regular manner. However, requirement of technical feasibility of such a regime establishes a more strict condition to be fulfilled. The system should return to the fixed point after some perturbation has occurred, in other terms, more common for theory of dynamical systems, the fixed point should be attracting. Thus, the study of regenerative amplification is reduced to the analysis of conditions of the fixed point existence and its stability characterization.

4.3. System evolution in the state space

Cavity dumping becomes the main version of output coupling to consider in the remaining part of the manuscript. This technique is not only more important for practical applications but also more sophisticated. As we will see below, the complex system dynamics is the relevant property of the cavity dumping regime. The only exception is Section 4.7 where inherent stability of stationary output coupling will be proved.

Effects of parasitic cavity losses on amplification dynamics will be considered in Section 4.6. At the initial stage of the dynamics study the patterns of the regenerative amplifier behavior will be represented under the assumption of negligible losses ($\delta_l \to 0$). This approximation substantially

simplifies the description of the method which will be used. The simplification appears not only due to existence of the analytical solution for the rate equations but also, more importantly, because of the reduced number of parameters governing the system. Equation 4.2 can be integrated analytically in case of zero parasitic losses. In case of the fixed round-trip number, τ_{cd}, we obtain the gain transformation rule for the high-Q interval $g_f = \hat{F}_{cd}(g_i)$, where $\hat{F}_{cd}$ is represented analytically:

$$\hat{F}_{cd}(g_i) = \frac{g_i}{1 + \frac{\varepsilon_s}{g_i}\exp(g_i \tau_{cd})} \tag{4.4}$$

The composite function $\hat{F}_\Sigma$ responsible for the gain transformation for the complete cycle (see Eq. 4.3) can also be written in closed form:

$$\hat{F}_\Sigma(g_i) = 1 - \left[1 - \frac{g_i}{1 + \frac{\varepsilon_s}{g_i}\exp(g_i \tau_{cd})}\right] \exp\left(-\frac{T}{T_1}\right). \tag{4.5}$$

The equation determining the fixed points $g_1 = \hat{F}_\Sigma(g_1)$ is thus can be expressed in closed form. However, this equation is transcendental and we start analysis of the system state evolution with the graphical illustration. For this purpose it is convenient to rearrange the fixed point existence condition [$g_1 = \hat{F}_\Sigma(g_1)$ with the explicit form of $\hat{F}_\Sigma$ given by Eq. (4.5)] to the form:

$$1 - (1 - g_1)\exp\left(\frac{T}{T_1}\right) = \frac{g_1}{1 + \frac{\varepsilon_s}{g_1}\exp(g_1 \tau)}. \tag{4.6}$$

The right-hand part of this expression represents the gain transformation function during amplification, $\hat{F}_{cd}$ [see Eq. (4.4)]. The left-hand part may be regarded as an inverse function of the gain recovery during the pump phase.

Since gain continuity implies equality of the boundary states ($g_i=g_{pf}$ and $g_f=g_{pi}$) we can combine both curves g_f versus g_i and g_{pi} versus g_{pf} in a common diagram (Figure 4.1). A space of system states, defined by this means, can give an intuitively simple but strict and fruitful picture of the system state evolution. The intersection of those curves, having clear physical meaning, gives solution of Eq. (4.6), i.e. it determines the fixed point of the system. It is important that the intersection of these curves always exists and it is always single for any set of controlling parameters. Really, the amplification stage curve is single-peaked, it begins with zero and always lies under the state space diagonal ($g_f=g_i$). The latter is natural because during the amplification (with, as we assumed, negligible pumping contribution) the population inversion is depleting by transforming to the intracavity pulse energy and respectively the gain can only decrease, $g_f<g_i$. The pump stage curve is a straight line whose slope depends on the repetition rate. This curve begins in the right upper corner of the state space [(1, 1) point] and also always locates under the state space diagonal. Note that the state space, due to proper normalizing, has dimensions of (0-1)×(0-1). Thus, these curves cannot help intersecting and they intersect only once. Moreover, since the basic properties of the curves are universal, a fixed point existence and uniqueness are not only the result of mathematical speculations obtained under certain approximations but also the consequence of inherent physical properties of regenerative amplification.

One of two necessary requirements for existence of a stable single-energy regime, namely the fixed point uniqueness, is fulfilled and then the main concern is the fixed point stability study. Figure 4.1 represents diagrams of system state evolution for two typical cases. Figure 4.1(a) presents the orbit converging into an attracting fixed point. Such a convergence means that the regenerative amplifier eventually (after sufficient number of reiterations when initial value of the orbit is “forgotten”) starts producing regular pulsing. It is intuitively seen that the behavior of the resulting orbit (convergent or non-convergent) depends on the slope of the “amplification” curve in the fixed point with respect to the slope of the “pump” curve. Strictly speaking, the fixed

point becomes attracting if the derivative of $\hat{F}_\Sigma$ function at this point satisfies the requirement $\left|\hat{F}_\Sigma'(g_1)\right|<1$ [100]. The condition $\left|\hat{F}_\Sigma'(g_1)\right|=1$ represents the transition point between stable and unstable operation. In case of $\left|\hat{F}_\Sigma'(g_1)\right|>1$ the fixed point is repelling, and consequently stable operation becomes unfeasible.

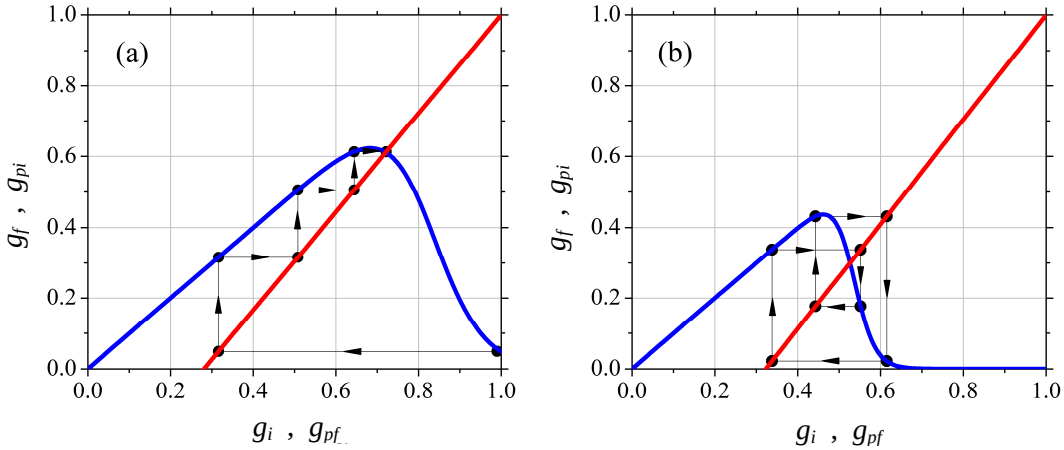

Figure 4.1. Graphical presentation of orbits in state space. The fixed point is the intersection of the "amplification" (g_f versus g_i) and "pumping" (g_{pi} versus g_{pf}) curves (blue and red lines respectively). Transition to the stable (attracting) fixed point (a) at ε_s=3×10^{-7}; τ_{cd}=18.0; T_1/T=3.0. Period-4T orbit (b) at ε_s=10^{-10}; τ_{cd}=42.0; T_1/T=2.56.

It becomes apparent that in the latter case the system is unable to reproduce its own state after one cycle of operation. However, such iteration may occur after two or several cycles. The corresponding set of system states is called a periodic orbit. An example of the periodic orbit is depicted in Figure 4.1(b). The condition for existence of the orbit with the period $2T$ can be written by introducing an appropriate composite function. Define $\hat{F}_\Sigma^2=\hat{F}_\Sigma(\hat{F}_\Sigma)$ to be the result of applying the map-function $\hat{F}_\Sigma$ to the system state two times. The system state g_2, such that $g_2=\hat{F}_\Sigma^2(g_2)$, is the fixed point analogue but suited for two successive operation cycles. Generally the orbit with the period mT

exists if there is a system eigenstate g_m satisfying the equation: $g_m = \hat{F}_\Sigma^m(g_m)$. Here the term m is an integer number exhibiting a factor of output pulse repeatability for the corresponding multi-energy regime. If such a regime is realized, the system produces a quasi-periodic sequence of the output pulses. The pulses of identical magnitude in this sequence appear each time in a multiplied period equaled to mT. In much the same way as the existence of a fixed point does not ensure stable operation, the existence of a periodic orbit itself does not mean that the corresponding regime is realizable. Additional analysis of the orbit stability is required, that, similar to the fixed point case, reduces to evaluation of the corresponding map-function derivative. The orbit $g_i(k)$ of period-m is stable provided that $\left|(\hat{F}_\Sigma^m)'(g_m)\right| < 1$. Computation of the derivative for this composite function is feasible since its value eventually (at $k \to \infty$) tends to the product of its inner function derivatives at points along the orbit: $(\hat{F}_\Sigma^m)'(g_m) = \hat{F}_\Sigma'[g_i(1)]\hat{F}_\Sigma'[g_i(2)]\cdots\hat{F}_\Sigma'[g_i(k)]$. If the absolute value of the product of the derivatives is larger than one, then periodicity of the orbit becomes unfeasible meaning that the system exhibits a chaotic behavior. This is the Lyapunov number criterion of deterministic chaos [100].

The map-function $\hat{F}_\Sigma$ itself is a function of system parameters (τ, ε_s, T/T_1). As one of the governing parameters is varied the corresponding fixed point passes through different states of stability. A pass through the position $\left|(\hat{F}_\Sigma^m)'[g_i(k)]\right| = 1$ causes a qualitative change of the system operation. Such transitions (e.g. transition from stable to unstable regime at m=1) are usually called a bifurcation. A set of control parameters (operation point) at which the bifurcation occurs is referred to as the bifurcation point. Correspondingly, the diagram of the output parameter versus one of the control parameters for the system exhibiting bifurcations is often called a bifurcation diagram. Among many possible types of bifurcations, known for dynamical systems, we have met here the bifurcation of period doubling. This relatively simple type of dynamic behavior is one of the consequences of the fixed point

uniqueness. This attribute also gives primary uniqueness of the system behavior. The dynamics of regenerative amplification and output characteristics of the system are determined by the set of control parameters alone in contrast to e.g. bi-stability effects where the initial value of the orbit, $g_i(1)$, may also influence the operation. One can imagine the latter as a qualitative change of system behavior caused by a way of switching it on (e.g. in practice either one has the pumping source enabled first and then seeding or other way around). The unambiguous relation between control parameters and operation regimes is quite an important property of regenerative amplifiers and our further analysis always implies this property without necessarily mentioning it.

4.4. Dynamic regimes in the parameter space

Simplifying assumptions and non-dimensional effective parameters, introduced for the basic rate equation model, reduce the number of independent control parameters of the system to the set of three. These are the normalized repetition rate, T_1/T, amplification phase duration expressed in terms of the effective round-trip number τ and normalized seed energy ε_s. Analysis of stability for orbits of the initial gain of amplification phase [$g_i(k)$] at each given control parameter provides a thorough picture of the regenerative amplifier behavior. The orbits were calculated by iterating Eq. (4.5) in the range of control parameters wide enough to comprehend all the relevant dynamics features: $0.2<(T_1/T)<20$; $10<\tau<110$; $10^{-11}<\varepsilon_s<10^{-3}$. As much as 3000 iterations were implemented, the sufficient number to be confident that the results are independent of the system state at the beginning of iterating. The orbits were analyzed in two stages. At first, the minimal number of cycles between repeating system states was revealed for each orbit in parameter space. It was performed by direct comparison of the system state sequences with themselves but shifted by a certain cycle number, $g_i(k)$ versus $g_i(k+m)$. In that way the periodic orbits up to m=32, including regular ones (m=1), were identified. Then

the Lyapunov number criterion was applied to the residual unidentified orbits. They were separated into two fundamentally different bunches: chaotic and eventually periodic.

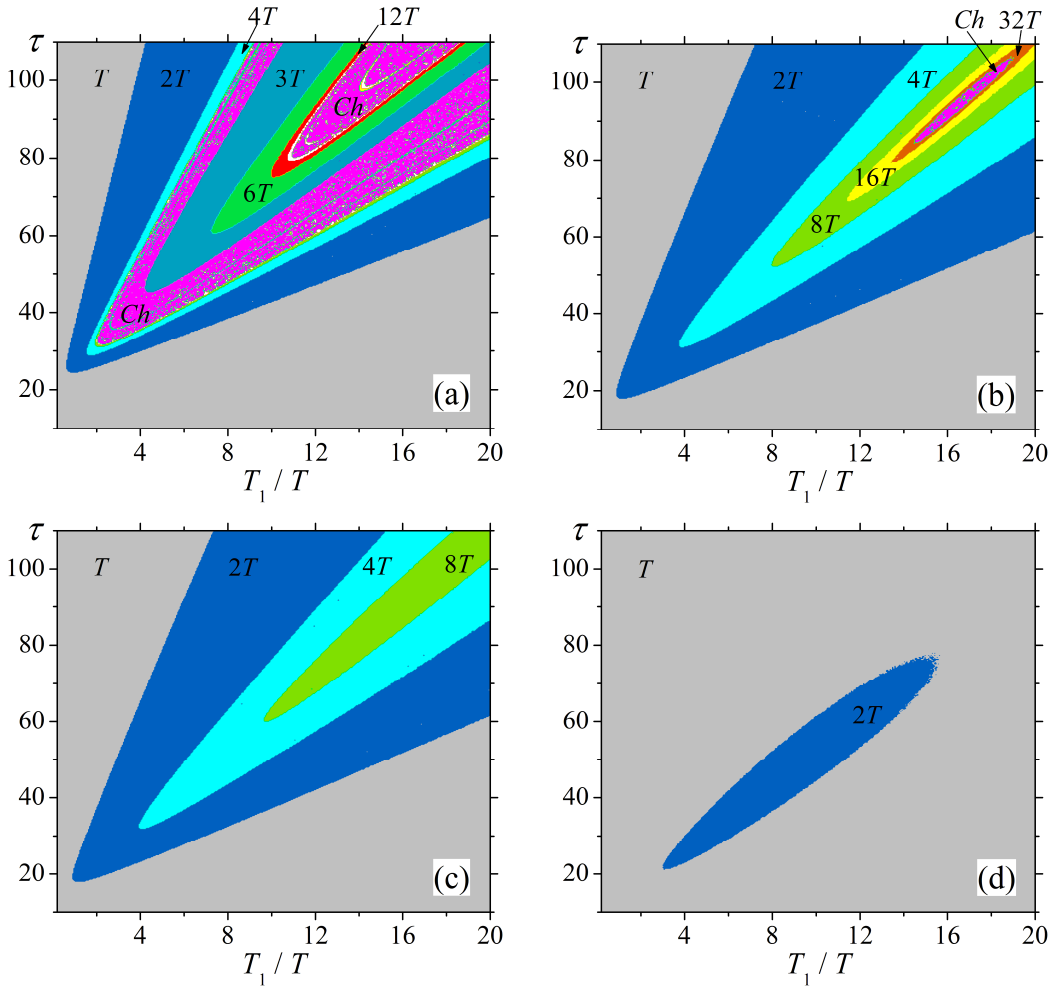

Figure 4.2. Diagrams of amplification dynamics in the parameter space (round-trip number – PRF) for different seed energies: $\varepsilon_s=10^{-10}$ (a); $\varepsilon_s=2.5\times10^{-7}$ (b); $\varepsilon_s=3\times10^{-7}$ (c); $\varepsilon_s=1.3\times10^{-4}$ (d).

Thus, the following dynamic regimes were distinguished in three-dimensional space of control parameters in accordance with the orbits properties: (1) The orbits evolving into stable fixed points (m=1) corresponding to the regular system behavior (single pulse energy output, i.e. 1T-regime). (2) Periodic orbits corresponding to multi-energy regimes with repeatability coefficients in the range of $2\leq m\leq32$. (3) Eventually periodic orbits having a larger repeatability factor (m>32), for which the m-number itself is not identified. (4)

Regime of deterministic chaos in accordance with the Lyapunov number criterion. The regions of different dynamics are mapped in space of the repetition rate – round-trip number (Figure 4.2). The major part of the parameter space is occupied by the regions corresponding to the following regimes: single-energy (1*T*); quasi-periodic with fundamental period of two (2*T*, 4*T*, 8*T*, 16*T*, and 32*T*); quasi-periodic with fundamental period of three (3*T*, 6*T*, and 12*T*); and chaotic behavior. These domains are marked with different colors, whereas the rest of the space containing the remaining zones of eventually periodic orbits is left unfilled. The boundaries between adjacent colors (i.e. between different regimes) represent manifolds of bifurcation points in parameter space.

As it is seen, the dynamics turned out to be multifarious. Chaotic regime ordinarily comes out from the chain of successive period doubling bifurcations: *T*-2*T*-4*T*-8*T*-16*T*-32*T*… The chaotic zone itself has fine structure. Quasi-periodic "windows" with various periods are disseminated in it. The dynamics of regenerative amplification strongly depends on the seed value. The pattern is complex for the low seed level ($\varepsilon_s<10^{-9}$), the parameter space contains more than one clearly distinguishable chaotic regions [Figure 4.2(a)]. Quasi-periodic regimes with a fundamental period of three are observed between zones of chaotic dynamics. The higher the seed energy, the simpler the instability pattern becomes. Initially, chaotic domain shrinks to ellipse [Figure 4.2(b)] and then disappears from the parameter space. Furthermore, period doubling bifurcations with fundamental period of two only remain for $\varepsilon_s>2.52\times10^{-7}$. Then the maximum order of bifurcations decreases [Figures 4.2(c) and 4.2(d)] and finally, at $\varepsilon_s>1.9\times10^{-4}$, the system becomes stable in the whole range of control parameters.

4.5. Seed pulse energy effect

The obtained results, demonstrating dependence of the operation on the seed pulse energy, are not quite trivial. This phenomenon is in controversy with

intuitive comprehension of regenerative amplification. The following speculations seem to demonstrate the negligible extent of the seed influence or at least to evidence much simpler looking relations. Imagine that the initially low seed pulse energy ε_{s1} after certain number of round trips is amplified to energy ε_{s2} of several orders of magnitude larger but still much less than the energy stored in the gain media, $g_i >> \varepsilon_{s2} >> \varepsilon_{s1}$. Then further amplification should give the same output as if the amplification had initially started with seed energy ε_{s2} because the previous stage ($\varepsilon_{s1} \rightarrow \varepsilon_{s2}$) virtually had not changed the stored energy and, as a consequence, the system gain. This logic leads to an inference that a lack of seed energy can be compensated with additional round trips. Consequently, the operation diagrams have to look identical but shifted in the coordinate of the round-trip number for different seed values. However, this logic is accurate only when we are considering amplification process as "isolated" with given initial gain that works only for low repetition rates. Accurate computations for the wider PRF range give absolutely different results, Figure 4.2.

Previously it has been commonly accepted that regenerative amplification is virtually independent of the seed energy because only low repetition rates were under consideration. In reality, even for low repetition rate systems the seed energy value should not be too low. However, the reason for that is rather different from that we are describing. Simply, competing parasitic processes of amplification of spontaneous emission always exist in regenerative amplifiers. Thus, the seed energy should be well above the spontaneous emission level in order to get the amplified seed pulse at the output instead of amplified spontaneous emission. At low repetition rates the sufficient seed energy is extremely small, e.g. down to 10^{-15} J in accordance with the experiments presented in the classical paper [28]. Some infrequent exceptions include very special applications requiring extremely clean, high contrast optical pulses and consequently higher seed energies (e.g. the parametric chirped pulse amplification [101]).

It becomes apparent that at high repetition rates the initial gain depends on preceding operation cycles and can be determined indeed by taking them into account. This procedure is in fact nothing else but the fixed point determination. Let us return to geometric presentation of fixed points in state space. Figure 4.3(a) represents diagrams of the final gain against the initial gain for three seed energy values. Corresponding numbers of round trips were selected so that the fixed points at certain repetition rate were identical. All the curves intersect in a single point which corresponds to the fixed point for the repetition rate T_1/T=8.0 This means that decrease in seed energy is compensated by increasing of round trips but only in a sense of equal position of the fixed points. However, the shapes of curves g_f versus g_i are different and their derivatives at the intersection point are dependent on the seed energy [Figure 4.3(b)]. Such derivatives indeed determine the regenerative amplification stability as we have described in Section 4.3 by referring to the theory of discrete-time dynamical systems.

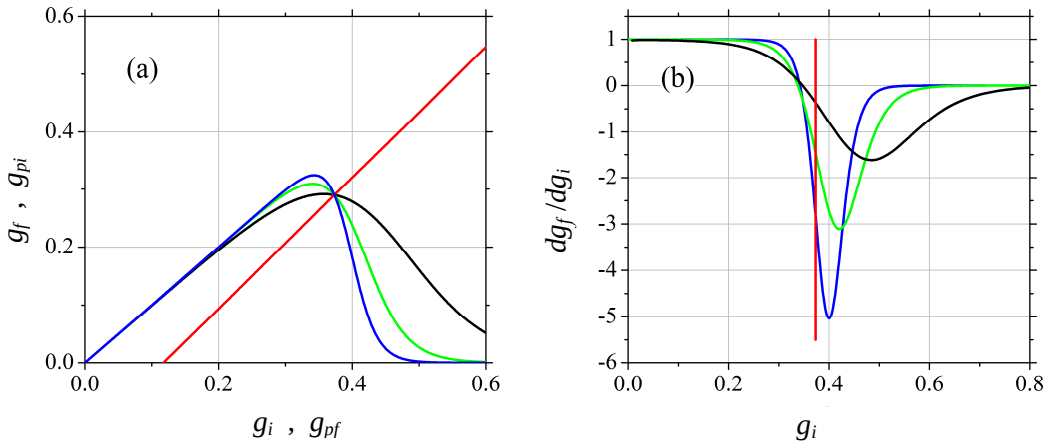

Figure 4.3. Typical state space diagrams of regimes having equal fixed points at different seed energies (black, green and blue lines correspond to ε_s=1.3×10^{-4}, 2.5×10^{-7} and 10^{-10} respectively). (a) Dependencies g_f versus g_i (black, green and blue lines) and g_{pi} versus g_{pf} (the red line). (b) Corresponding derivatives of the „amplification" (g_f versus g_i) curves.

The identity of the fixed points can be realized by compensation of the seed energy difference by appropriate selection of the round-trip number. Output

energies corresponding to those fixed points are equal too. However, the peculiarity of operation at high repetition rates is such that dynamical system behavior is absolutely different. At high repetition rates the seed pulse energy thus becomes one of those critical parameters which determine the operation regime of the regenerative amplifier. The specific operation points, which have been analyzed here, can also be found in the diagrams of dynamic regimes (Figure 4.2). With regard to stability, they were classified as stable, 2*T*-periodic and chaotic for seed values of 1.3×10^{-4}, 2.5×10^{-7} and 10^{-10}, respectively. The dynamic regimes which are in general possible to obtain (by changing the round-trip number) within a certain range of seed values are summarized in Table 4.1.

Table 4.1. Possible regimes versus seed pulse energy range.

Existing regimes	Seed value range	
	δ_l=0	δ_l=0.028
Chaos and "all" periods	$<2.52\times10^{-7}$	$<1.4\times10^{-5}$
T, 2*T*, 4*T*, 8*T*, 16*T*, 32*T*…	2.52×10^{-7}-2.56×10^{-7}	1.4×10^{-5}-1.5×10^{-5}
T, 2*T*, 4*T*, 8*T*, 16*T*	2.56×10^{-7}-2.72×10^{-7}	1.5×10^{-5}-1.74×10^{-5}
T, 2*T*, 4*T*, 8*T*	2.72×10^{-7}-3.56×10^{-7}	1.74×10^{-5}-2.5×10^{-5}
T, 2*T*, 4*T*	3.56×10^{-7}-1.39×10^{-6}	2.5×10^{-5}-4.1×10^{-5}
T, 2*T*	1.39×10^{-6}-1.90×10^{-4}	4.1×10^{-5}-3.5×10^{-3}
T (stable)	$>1.90\times10^{-4}$	$>3.5\times10^{-3}$

4.6. Influence of parasitic losses

The approximation of negligible losses is a good way to present the main ideas for application of the discrete-time dynamics method for regenerative amplification and to understand the dynamic patterns most relevant at high repetition rates. However, this approximation has limited application in practice. The output pulse energy grows in the lossless system monotonically together with amplification phase duration and reaches saturation at the level of $\tilde{g} = 1 - \exp(-T/T_1)$ that corresponds to full conversion of stored energy (population inversion) to the output pulse energy. Consequently, the number of

round trips can be increased, without detriment to output energy, to the values high enough for operation behind the bifurcation zone that in turn assures stable operation. Actually, the system is always (i.e. irrespective of losses) stable provided that the population inversion is well depleted during the amplification phase. In this case the initial gain tends to the constant, determined only by the repetition rate, [as results from Eq. 3.3: $g_f \to 0 \Rightarrow g_i \to 1-\exp(-T/T_1)$]. Consequently, the interdependence of operation cycles vanishes which leads to eliminating of immediate cause of unstable behavior. In reality, parasitic losses prevent utilization of this property, since because of losses the mode of complete gain depletion becomes inefficient.

A well known efficiency criterion, to dump optical pulse off the resonator at the moment when the current gain has dropped down to the threshold gain ($g_f=g_{th}=\delta_l$), is not applicable to repetitive operation as relating to only "isolated" operation cycles. Power efficiency enhancement takes place at high repetition rates when stored energy is left partially under-depleted ($g_f>>g_{th}$) forming a substantial gain background after several operation cycles. The proportion of gain to losses, which eventually determines extraction efficiency of the stored energy, can be substantially improved by this means. However, incomplete depletion is an origin of operation cycles interdependence, therefore, in the presence of losses the system efficiency in some sense collides with the system stability.

Parasitic losses in laser systems are given by optical component imperfections and diffraction losses of the optical resonator. The latter are objects of resonator geometry optimization. In case of solid-state lasers pumped longitudinally (virtual absence of hard apertures) high order optical aberrations (spherical e.g.) may become the main origin of diffraction losses, especially at high pumping intensities [102, 103]. Among optical components, the electro-optic switch is usually the most critical part; contributions of the Pockels cell and the polarizer to the loss factor surpass the remaining components [95]. Practically, the level of total parasitic losses can vary in quite a wide range, but the typical value should not exceed a few percent per round

trip for high-quality, well optimized systems. The losses, inherent for quasi three-level gain media and related to partially populated ground state, are not dissipative and they do not belong to the parasitic losses which we are considering.

By accounting for intracavity losses, a general, qualitative pattern of amplification dynamics (fixed point uniqueness, variety of orbits for the repulsive fixed points, significance of the seed pulse energy) remains the same, but naturally the quantitative difference factors in. The intracavity losses of the regenerative amplifier not only reduce efficiency (that is natural for lasers), but also substantially interfere in total system stability.

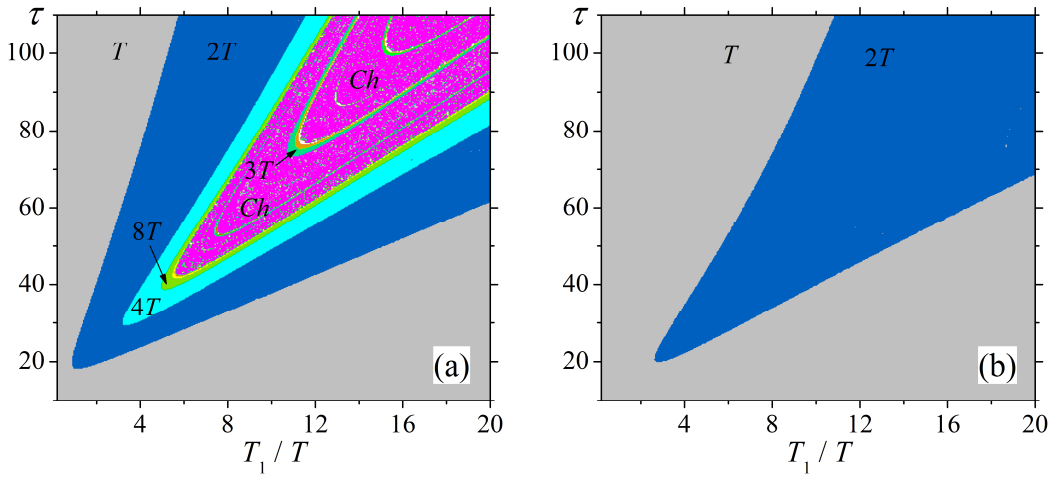

Figure 4.4. Diagrams of amplification dynamics in the parameter space (round-trip number – PRF) for cavity losses δ_l=0.028 and the seed pulse energies ε_s=3×10^{-7} (a); ε_s=1.90×10^{-4} (b).

The diagrams of regenerative amplification dynamics in parameter space (repetition rate – round trips) for intracavity losses δ_l=0.028 are presented in Figure 4.4. Fixed point calculation and their stability evaluation were performed in an analogous manner as described in Section 4.4. The only difference is function $\hat{F}_{cd}$, relating final and initial gains, has been calculated numerically since analytical solution is unknown in case of nonzero losses. The diagram presented in Figure 4.4(a) can be compared with that given for the same seed pulse energy ε_s=3×10^{-7} but for zero losses [Figure 4.2(c)]. The

influence of losses results in a more complicated dynamic pattern; the zone of chaotic dynamics evolves and the high order bifurcations shift closer to the tip of the instability zone (towards lower repetition rate and lower round-trip number). The second diagram [Figure 4.4(b)] was calculated for the seed energy ε_s=1.90×10^{-7}, which at zero losses provided stable operation in the whole range of control parameters. Now a period doubling zone (2*T*) has occupied a certain part of the parameter space and noticeably narrowed the range of stable operation.

A more cumulative picture of dynamical regimes is presented in Table 4.1. One can see some general change for the worse the system stability with respect to the zero-loss case. The decrease in stability caused by losses is not an obvious phenomenon (why not increase?). The reason for that bears similarity to the seed energy effect. The losses decrease pulse energy addition per round trip that can be compensated by increasing of round-trip number, but only in a sense of fixed point identity. The derivative magnitude of the gain transformation function, $\left|\hat{F}_\Sigma^{'}(g_1)\right|$, at this point has changed so that the system stability becomes worse as the losses increase. This phenomenon is not obvious but the conclusion is straightforward – the parasitic losses should be minimized as much as technically possible not only for efficiency but also for better stability.

4.7. Stationary output coupling

Here we shortly return to the variant of regenerative amplification in which the energy extraction is organized through a partially transmitting cavity mirror (output coupler). As was revealed in Section 4.1 (see Eq. 4.3), the composite function $\hat{F}_\Sigma = 1-\left(1-\hat{F}_{oc}\right)\exp(-T/T_1)$, where $\hat{F}_{oc}$ is the implicitly expressed solution of the equation relating initial and final gains [Eq. (2.17)], represents the gain transformation rule for stationary coupling. The derivative of $\hat{F}_\Sigma$ function determines the system stability. Implicit differentiation yields the

desired derivative in terms of the just mentioned solution of transcendental equation for the inner function, $\hat{F}_{oc}(g_1)$:

$$\hat{F}'_{\Sigma}(g_1) = \frac{1 - g_t / g_1}{1 - g_t / \hat{F}_{oc}(g_1)} \exp(-T/T_1). \qquad (4.7)$$

Then one can prove the inequality statement $-1 < \hat{F}'_{\Sigma}(g_1) < 0$ for any PRF in the functional case of exceeding the oscillation threshold at the given fixed point, $g_1 > g_{th}$.

The stability criterion, $\left|\hat{F}'_{\Sigma}(g_1)\right| < 1$, is ultimately met, meaning that the regenerative amplifier with stationary output coupling is the inherently stable system. Hence the assumption of steady-state behavior is valid and the steady-state formulas derived in Chapter 3 apply properly in the entire range of parameters. Note that in this inference the uninterrupted intracavity evolution is considerably involved [Eq. (2.17) results from $\varepsilon_f \sim 0$ condition]. The opposite (significant output pulse clipping e.g. in order to control the pulse train envelope shape) may lead to generating sequence of irregular magnitude pulses as we observed for cavity dumping.

Chapter 5. System optimization in the vicinity of bifurcations

In this chapter we will proceed from proper unstable behavior to specific limitations of the regular amplifier performance caused by the instabilities. The bifurcation diagrams created in the previous chapter will be extended with the output pulse energy data. This provides the foundation for a method of stability diagrams which serves to comprehensively optimize operation of regenerative amplifiers. A set of numerically obtained diagrams for dimensionless parameters enables one to determine the main amplifier characteristics for operation regimes in which instabilities substantially manifest themselves.

5.1. Output pulse energy versus round-trip number

For understanding regenerative amplifier capabilities, not only dynamical regimes but also the output pulse energy should be represented in relation to the parameters governing the system. The method of fixed points and related orbits determination was in detail described in previous sections. The orbit of the output energy comes out as alternate solutions of Eqs. (3.2) and (2.16) for the given initial gain orbit $g_i(k)$. If the system parameters are such that operation is unstable, then the initial gain varies from cycle to cycle by specific means and consequently the output energy becomes a multi-valued function of system parameters. Typical dependences of output energy versus round-trip number (bifurcation diagrams) at several repetition rates for the fixed loss factor, δ_l=0.028 and seed pulse energy ε_s=7.7×10^{-7} , are represented in Figure 5.1. The selected seed pulse energy belongs to the same range that is typical of functionally important class of seed lasers operating in CW mode-locking regime with the moderate average power (around several hundred of milliwatts). The repetition rates are chosen according to the diagram of dynamic regimes [Figure 5.1(a)] so that typical bifurcation diagrams up to 16*T*-regime are demonstrated.

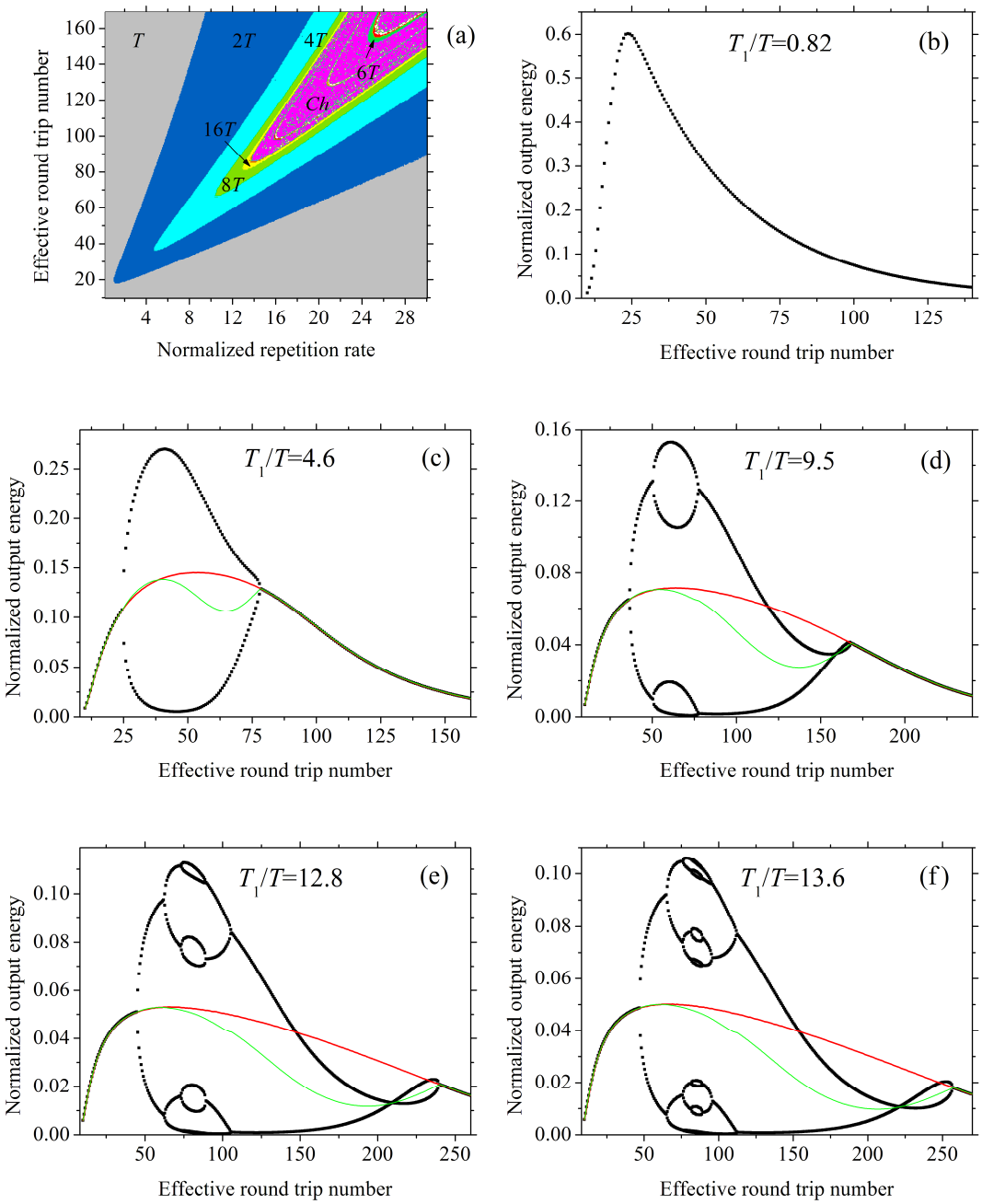

Figure 5.1. Diagram of dynamic regimes (a) and corresponding bifurcation diagrams for different repetition rates (b–f) at ε_s=7.7×10^{-7} and δ_l=0.028. Pulse energy, averaged pulse energy and steady-state energy correspond to black, green and red lines respectively.

It is seen that the output energy variation in the presence of period doubling is so high that it virtually leaves no opportunity to use such a regime in practical applications. For example, at repetition rate T_1/T=4.6 and within the round trips

range of 30-60 the output energy alternates between high and low value so badly that the output pulse train looks almost as at twice less repetition rate [Figure 5.1(c)]. It is even more regretful that such bad stability often appears in regimes which are potentially capable of providing the highest performance characteristics.

The reference output of the system, corresponding to operating at the fixed point, can be determined by calculating the steady-state pulse energy using Eqs. (2.16) and (3.5) at $g_i=g_1$. This energy is obviously a single-valued function of the governing parameters regardless of whether the fixed point is attracting or repulsing. In case of a repulsive fixed point (i.e. unstable operation), the corresponding output pulse energy becomes an artificial parameter but it can serve as a convenient reference level for evaluating the power efficiency reduction caused by instability effects.

By accounting for multi-energy nature, we can also determine "real" output energy averaged over a large number of operation cycles $\langle \varepsilon_f(k) \rangle$ (Figure 5.1). Interestingly, the real averaged energy is considerably lower than the reference steady-state energy in regimes exhibiting pronounced period doubling. One can suppose that in a multi-energy regime a relatively larger part of the resonator energy circulating is redistributed to the channel of parasitic losses. The evidence for this explanation is that the same curves calculated in case of zero losses coincide in spite of bifurcations. The only alternative is stored energy depletion through spontaneous emission during the pump phase. However, the latter effect becomes dominant when the population inversion is on average high, which is not the case at a large number of round trips.

5.2. Energy extraction efficiency in stable and unstable regions

The averaged output energy, being a single-valued characteristic, allows presentation of an informative picture of the system performance in 2*D* form. Even more conveniently, the extraction efficiency of the stored population

inversion may be used for this purpose. The extraction efficiency is defined as the averaged output energy divided by the maximum steady-state energy available for extraction at a given repetition rate, $\langle \varepsilon_f(k) \rangle / \tilde{g}$, where (see Section 3.1) $\tilde{g} = 1 - \exp(-T/T_1)$. Typical diagrams of this parameter in the space of repetition rate versus round-trip number are presented in Figure 5.2. In order to give a complete pattern of the system capabilities, stability data should be added to this diagram.

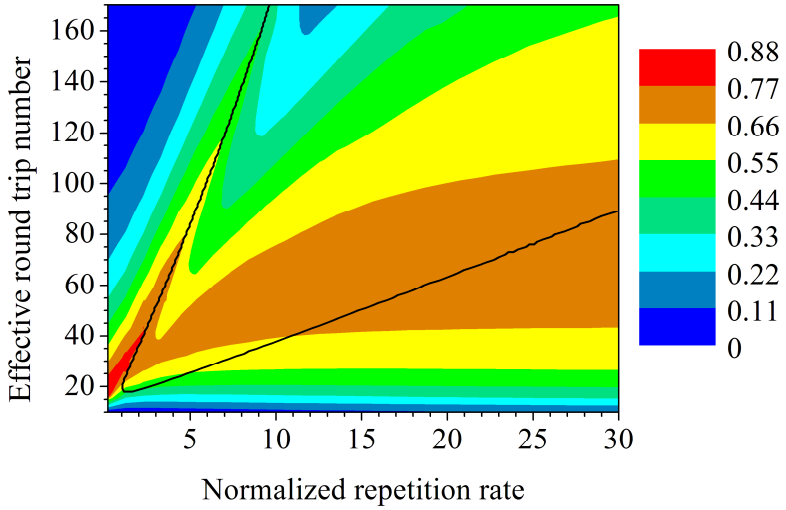

Figure 5.2. The stability zone boundary (the solid line) against the background of the energy extraction efficiency at ε_s=7.7×10^{-7} and δ_l=0.028.

Apparently, stable single-energy operation is the only suitable regime for routine use of regenerative amplifiers. For completeness sake we can note that one may successfully use certain unstable regimes for specific applications provided that there is comprehensive understanding of the essence of period doubling [40]. However, this is rather an exception than a common rule. By proceeding towards more pragmatic considerations we will thus focus on stable and unstable behavior zones in the parameter space and omit a detailed picture of the unstable operation itself.

The stability criterion $\left|\hat{F}'_{\Sigma}(g_1)\right| < 1$ is formulated in terms of the map-function which itself is dependent on controlling parameters. This set of

parameters (in other words, the operating point in parameter space) includes four dimensionless variables: $T/T_1, \tau_{cd}, \delta_l, \varepsilon_s$, responsible for the repetition rate, cavity dumping moment, parasitic losses, and initial energy, respectively. The fixed point g_1, being a solution of the equation $g_1 = \hat{F}_\Sigma(g_1)$, is also a function of the same set of variables. The surface $\left|\hat{F}'_\Sigma(g_1)\right| = 1$ thus separates a zone of stable operation from the instability zone in the four-dimensional parameter space. This surface reduces to the stability boundary curve in the $T/T_1, \tau_{cd}$ plane, provided that the remaining parameters are fixed. This curve is essentially a manifold of the first order bifurcation points (1*T*-2*T* boundary) which separates zones of stable and unstable operation.

The instability zone occupies the upper-right corner in the diagram of Figure 5.2. A substantial drop of the averaged energy is observed just below the upper branch of the boundary curve. The cross-sections of this feature are observed in Figure 5.1 at several repetition rates and it has been concluded that this “valley” originates from enhanced influence of parasitic loses in the period doubling regime.

For system optimization it is important to find operation points which provide maximum performance at each given repetition rate. At low repetition rates the operation is stable for any roun-dtrip number. The stable attainable energy is therefore equal to the steady-state pulse energy $\varepsilon_{out}^{\max}$ and the optimum round-trip number is equal to the corresponding steady-state term, τ_{cd}^{opt}, both determined analytically in Chapter 3. Within the PRF range where instabilities are considerable, there are two possible positions of the operating point which may provide maximum output in the stable regime – the points along the lower and upper branch of the stability boundary. According to the diagram of Figure 5.2, at lower repetition rates the upper branch has an advantage from the efficiency point of view. Operation at lesser round-trip number (lower branch) becomes preferable at higher repetition rates.

Thus optimization of the regenerative amplifier is actually reduced to selection of the round-trip number which provides the maximum output pulse energy and at the same time allows stable operation for the required repetition rate range (imposed by the system specifications). All the issues described in this and previous sections are regarded to a certain value of the seed pulse energy, ε_s=7.7×10^{-7}. The corresponding diagrams give a typical but single plane of multidimensional space of control parameters. However, as we have already seen from amplification dynamics data presented in Chapter 4, the space of stable operation depends on the seed pulse energy. Thus, the picture of regenerative amplification is still incomplete and it is time to proceed to consideration of system optimization taking into account influence of the seed pulse energy.

5.3. Stability diagrams

It is possible to present data which allow evaluation of regenerative amplification of different seed pulse energies by considering a single diagram. The necessary premises for doing that have been formulated in the previous sections. The condition where bifurcations are absent in the whole parameter space (Table 4.1) gives general understanding of the seed energy influence; however, this condition is too strong from a practical point of view. In order to thoroughly utilize power capabilities of the regenerative amplifier at a certain repetition rate, the round-trip number should be set equal to τ_{cd}^{opt}. The laser performance deteriorates when the operating point which potentially provides the highest output is located in the instability zone. In other words, the energy magnitude of $\varepsilon_{out}^{\max}$ is not attainable as the train of regular pulses because the corresponding τ_{cd}^{opt} point is in the unstable zone. These characteristics do not exhibit the optimum coupling if the situation differs from steady state, but they nevertheless remain important as the reference characteristics. The location of τ_{cd}^{opt} curve with respect to the instability region allows one to evaluate the

limitations caused by deviations from the stationary behavior. The pulse energy is reduced in the PRF range in which τ_{cd}^{opt} curve is located inside the instability zone (call this range "critical"). Within the critical range, the highest "stable" output energy is achieved either in the upper branch or in the lower branch of the stability boundary, where the τ_{cd} position is in some sense closer to the reference τ_{cd}^{opt} curve (see Figure 5.2). The diagrams consisting of τ_{cd}^{opt} curves and stability boundary curves (further referred to as stability diagrams) for selected seed pulse energies are presented in Figure 5.3.

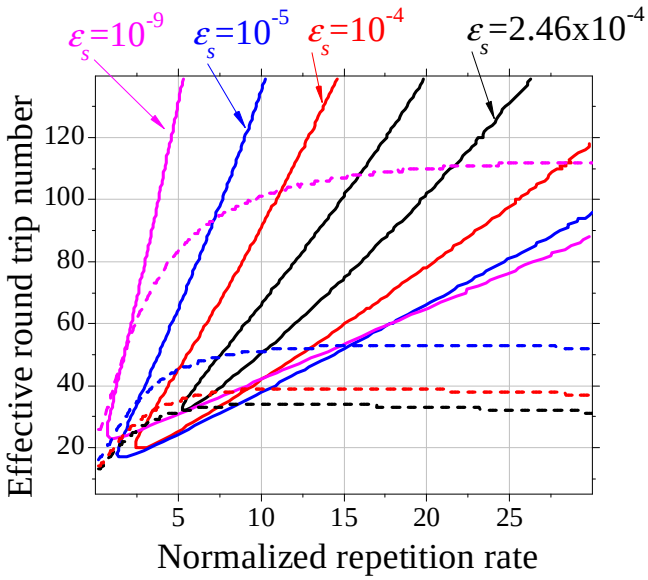

Figure 5.3. Typical stability diagrams. Stability zone boundaries (solid lines) and τ_{cd}^{opt}-curves (dashed lines) for the parasitic losses δ_l=0.028. Curve pairs of the same color correspond to equal seed energies.

The approach of stability diagrams forms a more systematic concept of the system behavior and specifically allows estimation of the seed level which may enable one to avoid instability effects at the required pulse repetition rate. We can also see that the critical range shrinks as the seed energy is increasing. The most critical repetition rate is T/T_1=5.5, the point of the "worst stability", requiring the highest seed energy for optimal operation. Finally one can determine the seed pulse energy at which τ_{cd}^{opt} curve does not pass the

instability zone at all. For the specific parasitic losses that we consider (δ_l=0.028) this energy is equal to 2.46×10^{-4}. Consequently, a regenerative amplifier seeded with pulse energy higher than that value (further referred to as "ample") allows theoretically attainable average power and stable operation over the whole repetition rate range.

5.4. Power curves

It is possible to use the approach of stability diagrams in order to understand the power curve shape providing the maximum output at stable operation. A typical stability diagram (just on the logarithmic scale) is depicted in Figure 5.4(a). The filled area corresponds to the instability zone. As expected at low PRF, where interdependence of Q-switching cycles is weak, the system is stable independently of what the round-trip number is set. However, a "prohibited" range of τ_{cd} magnitudes appears starting with $(T/T_1)^{-1} \approx 0.5$, gradually expands and occupies a substantial space at high PRF.

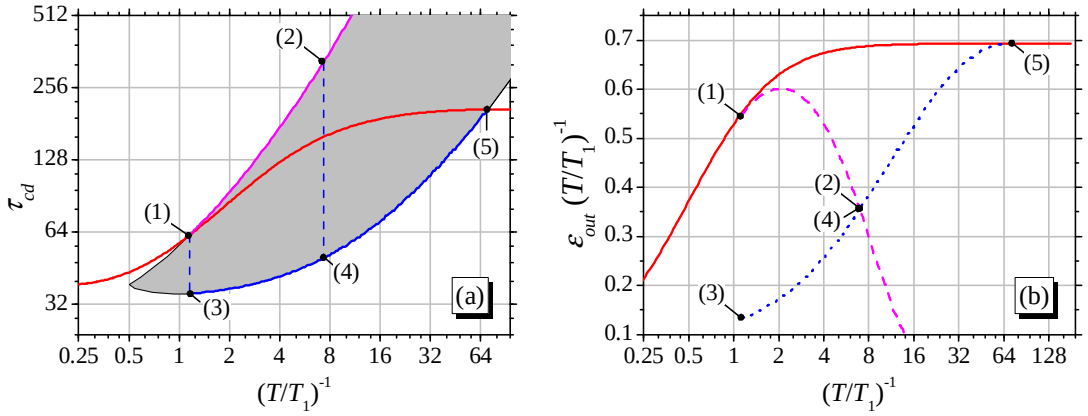

Figure 5.4. (a) Steady-state optimum round-trip number (τ_{cd}^{opt}) versus PRF (solid line) with respect to instability zone (filled area). (b) Output power versus PRF: the steady-state optimum (solid line), upper-branch output (dash line), lower-branch output (dot line). Both diagrams are presented for δ_l=0.025 and ε_s=3×10^{-15}.

The average power curves corresponding to both branches of the instability zone boundary and also the reference power curve $\varepsilon_{out}^{\max}(T/T_1)^{-1}$ are depicted in Figure 5.4(b). The upper-branch power [from point (1) towards point (2)] exhibits a slight rising followed by a steady drop, which can be explained by increasingly inefficient operation at late (with respect to τ_{cd}^{opt} moment) dumping. The lower-branch curve gradually grows from point (3) towards point (5) approaching the steady-state limit as PRF increases. When instability effects are taken into account, the pattern of the optimized regenerative amplifier looks as follows. The average power attainable in stable regime versus PRF represents a V-shape curve [connecting points (1), (2) and (5) in Figure 5.4(b)]. The corresponding round-trip number curve [τ_{cd} versus $(T/T_1)^{-1}$] also consists of two segments: the upper branch of the stability boundary in the low-frequency half of the critical range and the lower branch in the high-frequency half [from (1) to (2) and from (4) to (5), respectively, in Figure 5.4(a)].

The highest average power attainable in stable regime coincides with the analytically obtained value, $\varepsilon_{out}^{\max}(T/T_1)^{-1}$, at low and very high PRF and exhibits significant shortage at medium frequencies. The typical power curve has a ν-shape dip (Figure 5.5), whose characteristics depend on parasitic losses and also on the initial energy. Influence of the initial energy, even being weak, may nevertheless become an important factor under certain conditions. Really, to reduce the shortfall in the output power approximately twice, an increase in the initial energy by eight orders of magnitude (from 10^{-16} to 10^{-8}) is required. The effect of parasitic losses is more straightforward. Reduction in losses results in the output power improvement and also shifts the V-shape feature towards higher PRF.

The real power defect might be even larger than the theoretically predicted one. Technical noises, being a natural cause of energy deviations, strengthen their effect at approaching the instability zone so that the resulting

stability may become unacceptable even for the intrinsically steady-state operating point. This phenomenon is pronounced in the vicinity of the "un-saturated" lower boundary branch. In order to improve stability for given PRF, the high-Q window τ_{cd} should be set still below than the lower-branch given theoretically. This reduces the system performance even more.

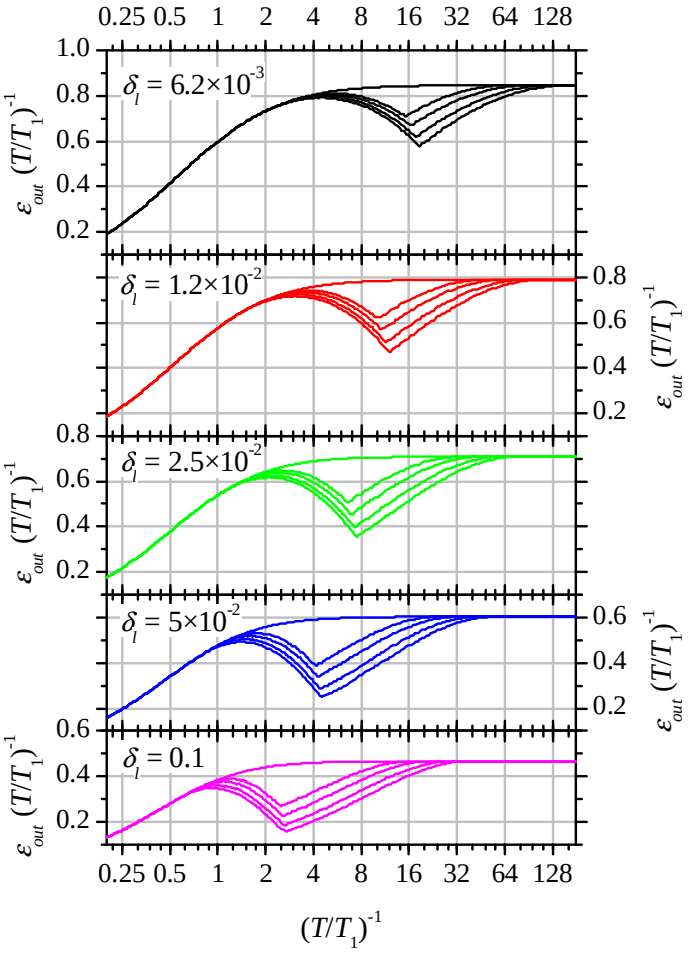

Figure 5.5. Maximum performances in stable regime. Dimensionless output power versus normalized repetition rate for different losses and initial energies. Each curve family contains power curves corresponding to ε_s=10^{-16}, 10^{-13}, 10^{-10}, 10^{-8} from bottom to top, respectively; the topmost curve represents the steady-state power reference.

Peculiarities of operation in the vicinity of the "oversaturated" upper branch are associated with the cumulative energy balance for the oscillation process, $\varepsilon_f = g_i - g_f - \varepsilon_l$. Reduction in the output energy, at dumping earlier than the

optimum moment, is a consequence of decreased extraction of the stored energy [corresponding to $(g_i - g_f)$]. On the contrary, reduction in output energy at later dumping (including the upper branch) is accompanied by increased consumption of the stored energy. This significantly shifts the balance in favor of the energy dissipated inside the cavity [corresponding to $\delta_l \ln(g_i / g_f)$ in Eq. (2.16)].

Instructive inference of regenerative amplification properties considered above is that within critical repetition rates the round-trip number takes on optimum value either near the lower or near the upper branch of the instability boundary but always on the margin of unstable operation. In general, operation at the margin of stability incurs challenges for robust operation in real systems which undergo technical noises. Even slight changes in control parameters may result in the system instability. Therefore, reliably stable operation generally requires setting the operating parameters well away from the instability border, but this in turn leads to a reduction of the system performance.

5.5. Parasitic energy dissipation

There is an important parameter related to intracavity losses which may influence performance of regenerative amplifiers indirectly: the amount of intracavity energy dissipated during the amplification stage. The accumulated over round trips fraction of intracavity energy dissipated through parasitic losses is subject to the specific operation regime. In particular, multiple passes of the already amplified optical pulse lead to substantial enhancement of energy dissipation. This, in turn, may give unacceptably high heating of intracavity components caused by the absorbed part of the dissipated power. One of the critical components in this respect can be the Pockels cell crystal. It may lose contrast under excessive heating possibly resulting in failure of the regenerative amplifier operation. This effect is especially pronounced for systems intended for high power applications. The energy defect ε_l, arisen due

to parasitic losses δ_l, can be determined for the operation cycle number k in terms of initial and final gains using Eq. (2.16) and accompanying expressions:

$$\varepsilon_l(k) = g_i(k) - g_f(k) - \varepsilon_{out}(k) = \delta_l \ln\left[\frac{g_i(k)}{g_f(k)}\right]. \qquad (4.1)$$

In case of multi-energy regime the effective lost part of the energy can be found by averaging:

$$\langle \varepsilon_l \rangle = \frac{1}{k}\sum[\varepsilon_l(k)]. \qquad (4.2)$$

The diagram of dissipated energy normalized to maximum available for extraction energy, $\langle \varepsilon_l(k) \rangle / \tilde{g}$), is presented in Figure 5.6(a). We can see that a large number of passes, typical of the upper instability boundary, substantially contribute to this parameter. The upper branch dissipated energy is about 7.5 times higher than the lower one at the repetition rate for which the system efficiencies are the same (at $T_1/T \approx 6.5$). This feature often makes operation at high round-trip number, well above τ_{cd}^{opt} point, inefficient despite obvious theoretical preference.

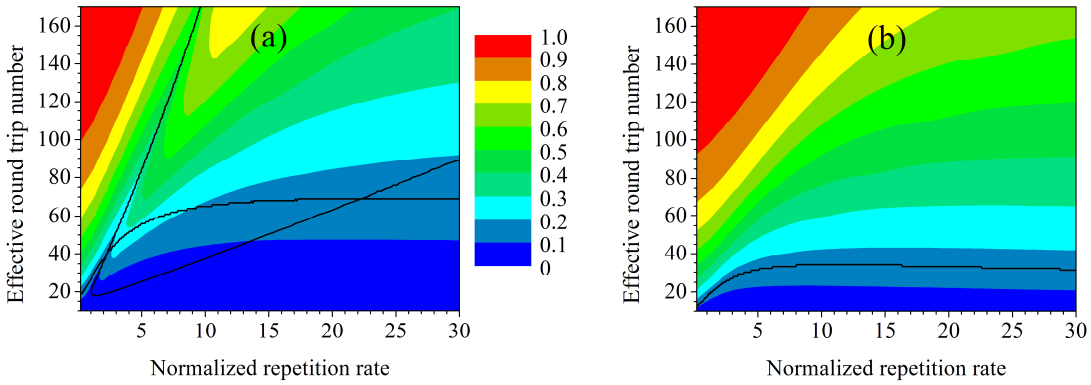

Figure 5.6. Stability diagrams (the stability boundary curve and τ_{cd}^{opt}-curves) against the background of the intracavity energy dissipation ($\langle \varepsilon_l(k) \rangle / \tilde{g}$) at δ_l=0.028 for different seed pulse energies: ε_s=7.7×10^{-7} (a) and ε_s=2.46×10^{-4} (b).

We can also mention here another advantage of the “ample” seed operation: as soon as the critical range has disappeared there is no need to operate at the

upper branch and to suffer from large intracavity energy dissipation peculiar to this regime. The diagram of dissipated energy for the ample seed pulse energy, ε_s=2.46×10^{-4} , is depicted in Figure 5.6(b).

Typical dependences of the dissipated average power on PRF for the regenerative amplifier producing the maximum stable pulse energy are shown in Figure 5.7. The power dissipation for the upper-branch operation may several times exceed the reference level corresponding to the stationary solution $\varepsilon_l^{opt}(T/T_1)^{-1}$. The thermal load of cavity optics caused by the excessive dissipated energy may be so high that the upper-branch regime becomes unfeasible. On the contrary, the lower-branch power dissipation is seen to be substantially less than the reference one.

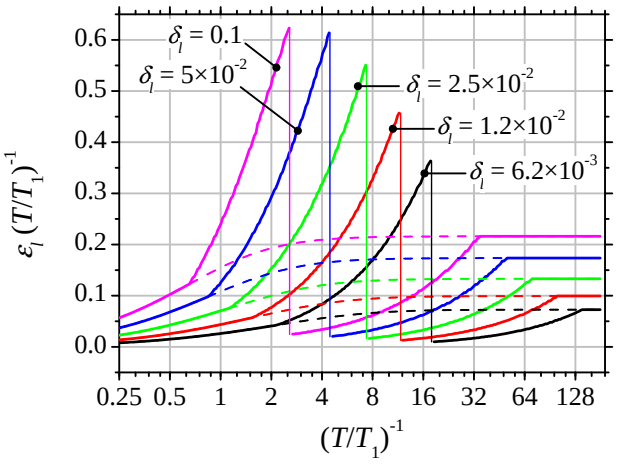

Figure 5.7. Intracavity dissipation at maximum performances in stable regime. Dimensionless dissipated average power versus PRF (solid lines) with respect to the steady-state reference curve (dash lines) for different losses at ε_s=3×10^{-15}.

5.6. Terminal level lifetime

The approach of stability diagrams is a straightforward way of regenerative amplifier optimization. However, in real systems there are specific effects which influence dynamic behavior and output parameters and they cannot be elaborated by using only approximation of simplified rate equations.

Nevertheless it is possible to understand some important contributions staying basically within the present approach.

Regenerative amplifiers are most frequently used for amplification of short (even more common term is ultrashort) optical pulses. Now we shall consider certain aspects related to regenerative amplification of such pulses. The theory described above applies to the idealized four-level system. One of the positions of that “ideality” is instant depopulation of the lower laser level (which is also called terminal level). In reality we can assume that the lower laser level is virtually unpopulated, only provided that the amplified optical pulse is much longer than the terminal-level lifetime (long pulse approximation). Otherwise, if the length of the optical pulse is much less than the terminal lifetime, then the terminal level will remain populated resulting in ”faster“ decay of population inversion (during amplification of a single pulse). Comprehensive evaluation of the terminal-level lifetime provided by Bibeau et al. [104] for different neodymium doped laser media gives actual values well exceeding 100 ps. So we can conclude that amplification of pulses shorter than 100ps virtually for all neodymium based systems is more appropriate to analyze within the short pulse approximation that is assuming negligible terminal-level depopulation during singe pulse amplification. This constrains applicability of the presently described approach. We can note in advance that the net contribution of the terminal-lifetime effect on the regenerative amplifier behavior is rather weak. It nevertheless gives some quantitative refinements to the picture presented above.

In order to elaborate regenerative amplification in the short pulse approximation we need to re-calculate the fundamental relations of final and initial gains $g_f = \hat{F}_{cd}(g_i)$. In this approximation the amplification of a single pulse was regarded as that in truly three-level gain media with initially empty ground state. After single pass amplification the ground state becomes partially populated, but by the second pass it is empty again and consequently the gain defect, which appeared due to “instant” three-levelness, is recovered. The latter

is the case since we assume the terminal-level lifetime to be much shorter than the round-trip time, T_{rt}. Typical T_{rt} value is in the range between ten and a few tens of nanoseconds, so this is good approximation for most of neodymium media (except some fluoride crystals and glasses in which the neodymium terminal lifetime is of the order of 10 ns [104]). By this means and by using a sequential procedure the basic relations $g_f = \hat{F}_{cd}(g_i)$ and corresponding output energies were determined. The subsequent procedures (evaluation of the fixed points and their stability analysis) stay unchanged for the short pulse approximation.

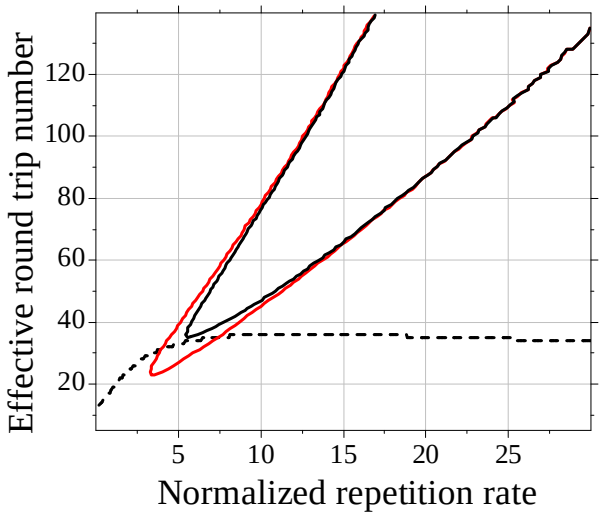

Figure 5.8. Stability diagrams for δ_l=0.028 and ε_s=1.7×10^{-4} obtained in short pulse approximation and long pulse approximation (instability zone boundaries are marked with black and red lines respectively; the common τ_{cd}^{opt}-curve is the dashed line).

It has been revealed that the influence of the terminal level appears as follows. There is a noticeable deviation between the τ_{cd}^{opt} curves at low repetition rates. However both “short pulse” and “long pulse” curves virtually coincide at the repetition rates T_1/T>1.0, indeed in the range that we are studying. The stability boundary curves practically coincide at low seed levels, although filling of the instability zone differs from that we observed earlier [e.g. in Figure 5.1(a)] towards smaller variety of regimes. These peculiarities add little in practical

essence. Therefore, we have come to nothing more than qualitative description and statement of that fact.

The only noticeable effect was observed in a regime when the seed energy was high, approaching to the ample level. The stability diagram, depicted in Figure 5.8, shows what the difference is. We can point out that the tip of the "short pulse" instability zone is somewhat shifted towards higher round-trip number and higher repetition rates. Such a shrink of the instability zone gives certain improvement of the general system stability. The ample seed pulse energy determined for short pulses is almost 1.5 times less than that found within long pulse approximation (ε_s=1.7×10^{-4} against 2.46×10^{-4}). This improvement is a rather unexpected result since terminal-level "bottleneck" in some respect hampers the ideal four-level amplification. Hence, at least partially and transitory populated terminal level does not act as additional losses as one might imagine.

5.7. High intensity features

The short pulse duration is usually accompanied by high intensities of amplified radiation. The most relevant problems related to high intensities are caused by the Kerr effect which therefore requires intent attention. This nonlinearity makes an impact on amplification process by intensity dependent refractive index change in volume of intracavity components. The effects occur in both spatial and spectral domains and commonly are described as Kerr lensing and self-phase modulation. Reduction of the Kerr effect manifestations usually implies decrease of effective optical pulse intensity which can be quantified in terms of *B* integral, in essence representing nonlinear on-axis phase shift [105]. In case of regenerative amplification multiple passes should be taken into account in order to evaluate *B* integral value accumulated during entire amplification stage. By extending the steady-state expression derived in Section 3.7 to general case we can write for the *k*-th operation cycles:

$$B(k) = B_1 \ln\left[\frac{g_i(k)}{g_f(k)}\right], \tag{4.3}$$

where B_1 is single-pass B integral calculated for the intensity which is equal to the gain media saturation fluence divided by the pulse duration (see Section 3.7 for details). The logarithm part in this formula exhibits a factor of effective impact of multiple passes. We have already met such a multiplier when the evaluated total lost part of the energy (see Eq. 4.1) and the value proportional to this factor have been depicted in Figure 5.6. We can see that operation at the upper boundary of the instability zone with short pulses is strongly unadvisable since the B integral is increased several times. The cause of that is obviously multiple passes of intense pulses peculiar to a regime behind the instability zone.

That concerns the B_1 value for fixed pulse duration, its reduction simply implies standard methods such as the mode area increase and shortening of the volume intracavity components. However, these possibilities are rather limited. Even so the thin disc geometry allows tremendous reduction of gain media length [66] but the Pockels cell still can exhibit a real challenge. Among known to date Pockels cell materials only the BBO crystal is suitable for the high average power (due to low absorption) and for high repetition rates (thanks to relatively low acoustic ringing). However, the transverse electro-optic effect, the only functional for this crystal, permits shortening of the optical pass or aperture increasing only at a limited extent until driving voltage becomes unacceptably high [54]. Thus, since the Kerr effect often restricts the capabilities of regenerative amplifiers, it is important at least to correctly select the operation regime in order to minimize its impact. We can note that operation at higher seed energy (ε_s larger than ample seed pulse energy) is beneficial in this respect too. At that condition, operation at the maximum output (τ_{cd}^{opt} curve) does not suffer from too high multiple pass factor of B integral [see Figure 5.6(b)].

Chapter 6. Experimental verification

Regenerative amplification is subject to energy instabilities at high pulse repetition rates. In this chapter experimental data which demonstrate relevance of instability effects in the Nd:YVO_4 regenerative amplifier are presented and possible techniques for performance optimization are analyzed. An increase in the seed pulse energy is demonstrated to improve amplification dynamics. Addition of a preamplifier is shown as an efficient way to achieve seed energy high enough to provide stable operation at repetition rates up to 200 kHz with the average output power near the theoretical limit.

6.1. Experimental setup

The amplification experiments were carried out in order to demonstrate basic features of amplification dynamics and to verify theoretical results presented in previous chapters. The knowledge of potential capabilities and of general limitations makes it possible to provide the best regime selection and deliberate optimization of control parameters. In a sense of practical device engineering, this means to maximize extraction of the given stored population inversion as a stable train of output pulses. We leave outside the scope of the present consideration optimization of the pump characteristics and the geometry of the optical resonator allowing higher power in TEM_{00} mode, as these do not directly relate to the amplification dynamics. The parasitic intracavity losses, although formally a governing parameter, are not an object of consideration; they should simply be reduced as much as technically possible. Since the repetition rate is usually imposed by the specifications it appears as a variable but a given parameter. There are two adjustable parameters which can be used for the system optimization – the number of round trips and the seed pulse energy.

The experimental work was performed with a system based on Nd:YVO_4 crystals, a gain medium with truly four-level nature (except terminal-level

nuances). The schematic diagram of the experimental setup which was used for investigation of regenerative amplification is shown in Figure 6.1. In essence the system consists of the seed source and the regenerative amplifier itself.

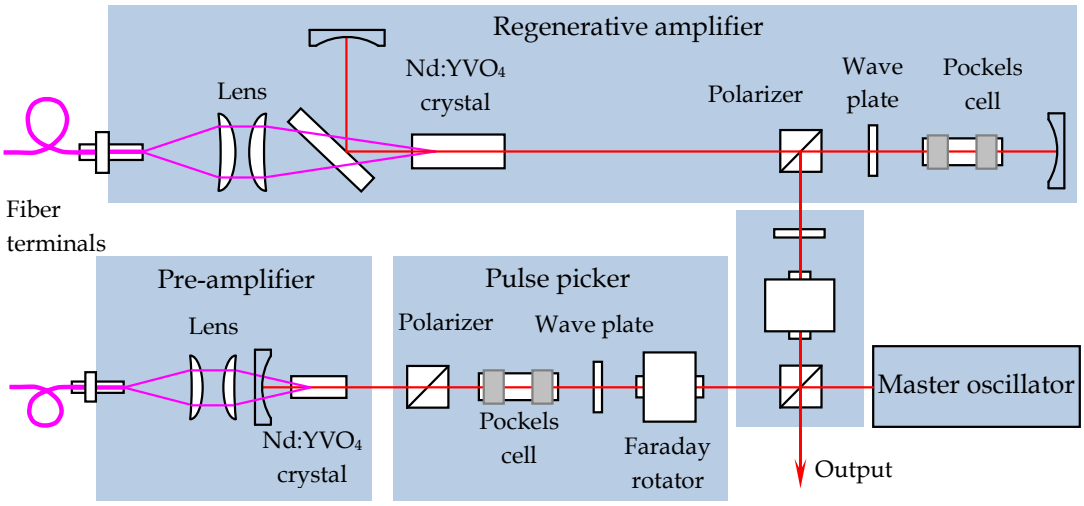

Figure 6.1. Schematic diagram of the experimental setup.

The seed pulse source for regenerative amplification experiments was based on a diode-pumped passively mode locked picosecond Nd:YVO_4 laser of moderate power. It generated a continuous pulse train with the repetition frequency of 82 MHz and the average power of 300 mW. The laser was able to produce optical pulses with duration as short as 6 ps. The short pulses were used in experiments where dynamics peculiar to high peak intensities were of interest. The initial investigations were focused on the “pure” dynamics not disturbed by optical nonlinearities. These experiments were carried out with 58 ps duration pulses obtained by installing an etalon in the oscillator cavity (the etalon narrows the bandwidth, thus widening the pulse duration).

A pulse picker was used to select pulses for further amplification and in this way to control the effective repetition frequency of the seed source. This part of the seed source system is important for high repetition rate operation, especially based on high gain laser media such as neodymium doped vanadates. If the pulse picker is not used then two negative effects caused by unwanted pulses take place. These pulses continuously pass the optical

resonator of the regenerative amplifier during pump stage and go out spatially coinciding with the useful output signal. This leads to reduced pulse contrast and to parasitic consumption of the stored energy. One can decrease the seed pulse energy and compensate for that by increasing number of round trips. This simple approach may often avoid bad influence of the unwanted seed background while operating at low repetition rates. The reduction of the seed energy, as we have already seen (theoretically), is not a good idea when turning operation to high repetition rates. In our setup the pulse picker was an electro-optic switch based on an RTP Pockels cell. Selected pulses formed an input signal for the preamplifier. The remaining pulses of the master oscillator train were directed to the fast photodiode for synchronization of electro optic components of the system including the pulse picker itself.

A double pass Nd:YVO_4 preamplifier installed behind the pulse picker was used to increase the seed pulse energy to required ample energy. High emission cross section of the Nd:YVO_4 crystal make this system efficient at relatively low input average power. Only 2 W of pumping was sufficient to achieve a gain coefficient of more than two orders of magnitude. The seed pulse energy was 3.2 nJ when pumping of the preamplifier was switched off. The energy of the pre-amplified pulse reached 1.1 μJ at 10 kHz and steadily decreased with the repetition rate to 370 nJ at 200 kHz. The calculation presented in the next section will show that the obtained energy is sufficient to ensure stable operation.

Simple estimations show that the preamplifier is a good alternative in comparison with a more straightforward seed source scheme based on a powerful master oscillator. In order to provide 370 nJ pulses the master oscillator operating in a CW mode locking regime with a reasonable repetition frequency of 50 MHz should generate the average power of 18.5 W. This way is really prodigal since the useful part of this power is much lower, e.g. only 74 mW even operating at 200 kHz. Obviously the preamplifier is a much more energy-efficient solution.

The regenerative amplifier was comprised of an optical resonator containing the gain medium (Nd:YVO_4 crystals) and an electro-optic switch. The electro-optic switch consisted of a BBO Pockels cell, a quarter-wave plate and a thin-film polarizer. The total multi-pass gain of the regenerative amplifier depends on the number of cavity round trips which is determined by the amplification-stage duration. This important parameter is easily controlled by setting the time interval during which the high voltage is applied to the Pockels cell.

The laser crystal was continuously pumped to 808 nm absorption line by the fiber coupled laser diode module with the fiber core diameter of 400 μm and the numerical aperture of 0.22. The optimal pump power, providing maximum output in TEM_{00} mode, was set to be 44 W. This optimization was performed in CW generation mode. Provided that no voltage was applied to the Pockels cell and the quarter-wave plate was adjusted for maximum output (optimal output coupling conditions), 12.5 W of average power was obtained. The output radiation was diverted from the input signal path by a standard optical circulator based on the Faraday rotator. The repetition rate of the system was limited to 200 kHz by electronics driving the electro-optic switches.

6.2. Application of stability diagrams to amplification experiments

Now we can apply the concepts developed in the theoretical part to evaluating behavior of a real system. At the beginning the basic system characteristics should be determined in order to perform reciprocal transformation of normalized parameters to dimensional ones corresponding to real operation conditions. The parameters necessary for the system characterization include the laser medium characteristics (F_{sat}, T_1), the optical resonator geometry (A_a, T_{rt}, β), the pumping properties in terms of G_0, and the loss factor l. The steady state small signal gain, imposed by the pump intensity, was found directly as the ratio of the seed energies measured right before and behind the active element of the regenerative amplifier. The parasitic intracavity losses

were derived from the specifications of the optical components. A linear optical cavity was utilized in this work that establishes a double pass through the gain media per round trip, $\beta = 2$. The emission cross section of the Nd:YVO_4 crystal (to calculate the saturation fluence) was taken from reference [107]. In order to fit the calculated PRF scale $(T/T_1)^{-1}$ to the experimental results, the gain relaxation time of slightly lower value than a commonly accepted upper-state lifetime for the Nd:YVO_4 crystal was deliberately used. This disagreement (83 µs versus 90-100 µs) perhaps appears because of lifetime quenching caused by high population inversion density, and also due to the crystal active zone temperature elevated far above the room temperature, as a result of intense pumping.

Table 6.1. Parameters used for stability diagrams calculation.

Parameter	Value
Wavelength	1064 nm
Emission cross section	11.4×10^{-19} cm^2
Gain relaxation time	83 µs
Effective mode diameter	1 mm
Steady state small signal gain	2.94
Seed pulse energies	11 pJ (low); 1.1 nJ (medium); 240 nJ (high)

It was explored amplification of three seed pulse energies differing by about two orders of magnitude: pre-amplified seed, unamplified seed and attenuated seed. This set of input signals covers the functionally important range. The value of the unamplified seed, 3.2 nJ, is of the same order of magnitude as the pulse energy of commonly used moderate power solid-state picosecond lasers. Operation with the seed energy intentionally attenuated to 32 pJ provides opportunity to evaluate typical behavior of the regenerative amplifier seeded with potentially attractive low power sources, e.g. with ultrafast laser diodes, which would substantially reduce the system size and complexity. The seed energy obtained with the pre-amplifier was expected to be high enough to reach ample level. These seed energies were measured at the output of the seed formation system. However, it was observed that during further amplification

the seed energy was not completely exploited. Mode mismatching reduces the effective seed energy. In general, it is difficult to avoid mode mismatching between a seed laser and the optical cavity of the regenerative amplifier in both spatial and spectral domains. Spectral mismatching can exist even with identical gain media because of e.g. different temperatures of laser crystals in those devices [28].

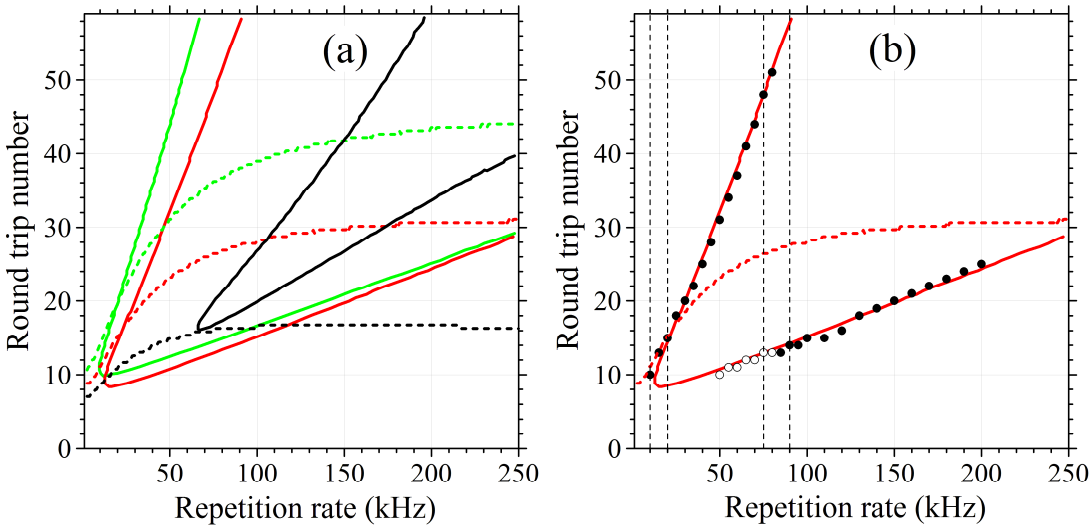

Figure 6.2. (a) Instability zone boundaries (solid lines) and τ_{cd}^{opt} curves (dotted lines) in parameter space. Black, red and green lines correspond to seed pulse energies of 240 nJ, 1.1 nJ and 11 pJ, respectively. (b) Operating point trajectories (vertical dashed lines) and measured number of optimal round trips for the pulse durations of 58 ps (solid circles) and 9 ps (open circles) with respect to stability diagram for the seed energy of 1.1 nJ.

In order to have appropriate data for theory verification the overall level of mismatching was estimated experimentally. The measured real double pass small signal gain of the whole regenerative amplifier (output/input energy ratio while the Pockels cell was disabled) was compared with “pure” steady state gain of the laser element. The effective seed value thus was determined to be about three times less than the measured one. The primary parameters of the regenerative amplifier which were used for calculations are summarized in Table 6.1.

Before proceeding to stability diagrams which describe our particular experimental conditions, we should notice that the relations between dimensional and dimensionless, normalized parameters remain unchanged as they have been introduced in Section 2.5 and Table 3.1. The stability diagrams describing amplification experiments are presented in Figure 6.2. These data were obtained in the approximation of short pulses (accounting for the terminal-level lifetime effect). As we have already known, the system capabilities are completely exploited when the τ_{cd}^{opt} curve is outside the instability region. The diagrams show that at low seed energy (11 pJ) the appropriate repetition rates should be less than 20 kHz. For the medium seed level (1.1 nJ) this range increases to 25 kHz. At higher repetition rates the τ_{cd}^{opt} curve enters the instability zone. It is important that for 240 nJ or higher seed energies the τ_{cd}^{opt} curve does not enter the instability zone in the whole range of repetition rates. So, for our laser system this energy corresponds to the ample seed value, sufficient to eliminate negative features of amplification dynamics, and thus to completely exploit the system capabilities.

6.3 Experimental bifurcation diagrams

The initial experiments were carried out with the medium seed pulse energy (the preamplifier was disabled). Various dynamic regimes, depending on a set of control parameters, were observed. As an illustration, Figure 6.3 shows oscilloscope screen shots of the output pulse train in typical single-energy and period doubling regimes.

Experimentally obtained diagrams of the average output power and pulse energy versus number of round trips demonstrating system behavior at different repetition rates are presented in Figure 6.4. The specific repetition rates were chosen to describe the most relevant cases of the regenerative amplifier dynamics in respect of the system optimization. The single-peaked dependence inherent to low repetition rates appears at 10 kHz [Figure 6.4(a)]. The average power and the pulse energy reach the maximum values

simultaneously when the round-trip number is equal to ten. At 20 kHz the situation is different [Figure 6.4(b)]. The shape of the energy curve shows that the system undergoes bifurcation in the 9–13 range of the round-trip numbers. However, in this case the period doubling does not affect the system performance because the output power reaches its maximum value in a single-energy regime. This repetition rate is still not critical.

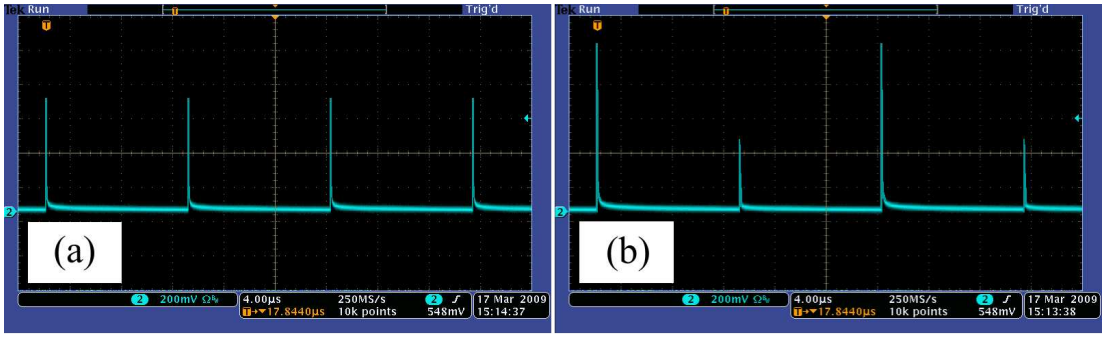

Figure 6.3. Screenshots of typical pulse trains at 90 kHz. Stable energy output and the 2*T* period doubling regime were obtained at the number of round trips equal to 14 (a) and 16 (b), respectively.

Instability effects become more pronounced at higher pulse repetition rates. The period doubling not only breaks the energy stability but also distorts the curve of the average power (as described in Section 5.1). This curve now has two explicit peaks [Figures 6.4(c) and 6.5(d)]. The first peak, corresponding to the maximum power, is located in a period doubling zone, whereas the second one is just over the instability edge. The optimal regime is obtained in the vicinity of the bifurcation point. At 75 kHz the optimal round-trip number is equal to 48. This point is close to the second power peak, on the right side of the period doubling zone [Figure 6.4(c)]. For 90 kHz repetition rate the optimal round-trip number is equal to 13 and is situated right before the first bifurcation point [Figure 6.4(d)].

The trajectories of the operating points corresponding to variation round-trip number at a constant repetition rate are presented in Figure 6.2(b). This trajectory at 10 kHz does not pass the instability zone. At 20 kHz the optimal operating point is above the instability zone. Both repetition rates 75 kHz and

90 kHz are critical – the optimal number of round trips is on the stability edge and is rather far from the point of the highest attainable power. The experimentally observed results confirm theoretical predictions that for critical repetition rates: (i) the output energy exhibits unacceptable fluctuations when the amplifier produces the highest average power, (ii) the highest stable pulse energy is reached close to the instability edge.

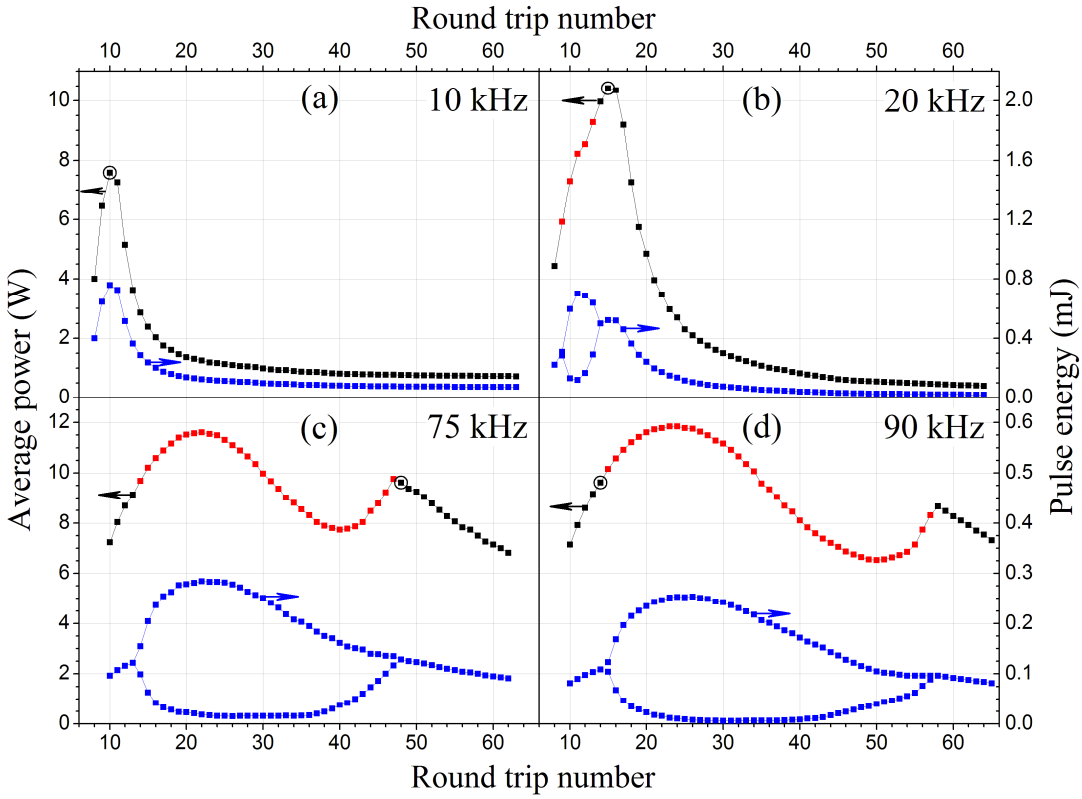

Figure 6.4. Experimental average power (black and red dots correspond to stable and unstable regimes respectively) and pulse energy (blue dots) versus number of cavity round trips for different repetition rates. The encircled points correspond to the maximum power at stable operation.

Some effects caused by nonzero terminal-level lifetime were also observed in the experiment. The presented bifurcation diagrams at 75 kHz and 90 kHz theoretically should exhibit not only $2T$ but also $4T$ regimes [as in Figure 5.1(d) of previous chapter] if the long pulse approximation is applied. The regime of $4T$ period doubling was not observed experimentally and it should not exist theoretically, provided that the contribution of the terminal-level

lifetime is taken into account. At the same time, as the theory has predicted, the terminal-level lifetime effect does not influence the system performance at such low seed level.

Real deviation from theory is observed at the lowest repetition rate (10 kHz). The output energy decays too fast behind the peak point in comparison with theoretical expectations [see Figure 5.1(b)]. This occurred because the Kerr effect influence was substantial at low repetition rates even for initial experiments performed with relatively long 58 ps pulse duration.

6.4 Performance characteristics evaluation

It has been shown in the theoretical part that variation of only round-trip number does not solve the stability problem; increase in the seed pulse energy is required in order to avoid bifurcations and corresponding instability at high repetition rates. Now we proceed to experimental verification of the seed energy influence.

System performance characteristics were compared while operating with three different seed pulse energies: ”low”, ”medium”, and ”ample”. The measurements were performed at the optimum round-trip number. The round-trip number was set for the maximum average power while maintaining stable operation for every repetition rate. The formulation of stability criteria in real experimental environments requires a certain attention. Experimental discrimination of amplification regimes to some extent suffers from uncertainty because of technical instabilities, not related to fundamental system properties. Technical noises, in essence slight modulation of governing parameters usually with random distribution, limit the system stability. The most typical of these noises are pumping source noises, seed pulse energy fluctuation, synchronization jitter, resonator disturbance by mechanical vibrations and by air flow. In our setup the technical, not disturbed by period doubling, standard deviation of the output energy was less than 0.7%. In proximity to a bifurcation point the deviation increased. The diagram of typical transition from single energy to the period doubling regime “under

magnification” of the repetition rate scale is shown in Figure 6.5; the bifurcation point looks rather as a spot than as a point. The uncertainty takes place in the range where the deviation of energy is clearly higher than the technically conditional level but where the two peaks are still not distinguishable. On the repetition rate scale this range does not exceed 1 kHz (typically the value is 0.5 kHz).

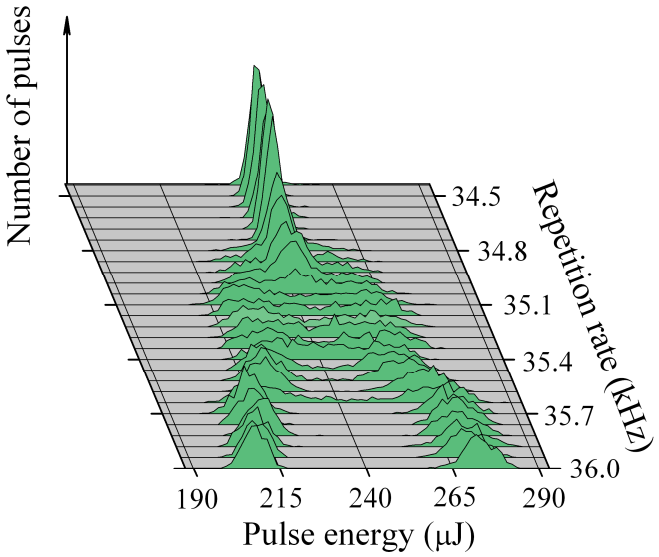

Figure 6.5. Experimental energy histogram in the vicinity of the bifurcation point.

Measurements with a sufficiently fine step are not possible in the round-trip domain (in contrast to theoretically grounded terms the real experimental round trips are discrete), and besides, the analysis of the energy histogram is a time consuming procedure. Therefore, a simple phenomenological criterion formulated for the particular setup and allowing real time measurements was used. The operation was considered stable when the standard deviation of the pulse energy did not exceed 1%. Apart from that, a special emphasis was placed on origin and spectrum of disturbing noises to be sure that they are virtually non-periodic. It was observed that even barely perceptible presence of “resonant” components (sub-harmonics of dumping frequency) in the spectrum of technical noises may tremendously enhance the influence of period doubling and can change the dynamical pattern beyond recognition. In particular the

pulse picker driving electronics had to be improved in order to eliminate seed train modulation at the frequency equal to half the system repetition rate.

Experimental dependences of the average output power versus repetition rate are presented in Figure 6.6(a). The output is virtually independent of the seed level for low repetition rates. At higher rates there is a drop in power for low and medium seed levels in compliance with theoretical notions. The most significant power decrease appears in the 80–95 kHz range, then the output power steadily grows as the repetition rate increases.

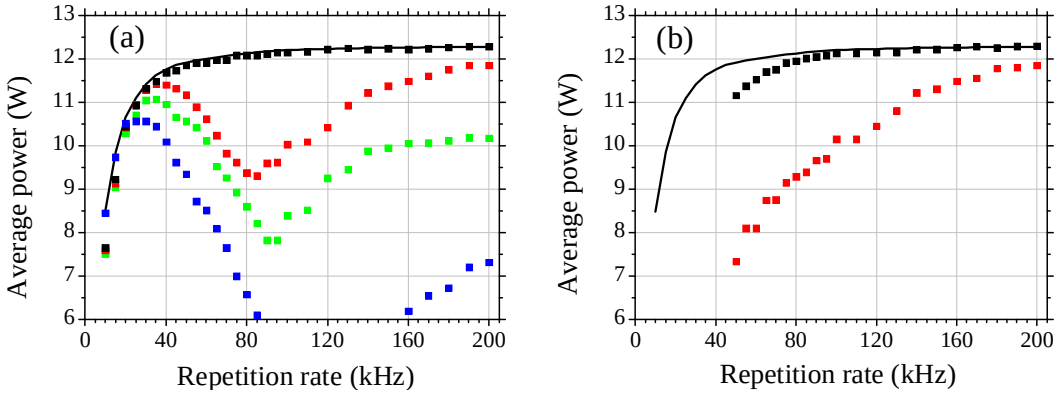

Figure 6.6. Experimental output power versus repetition rate for 58 ps (a) and 9 ps (b) pulses. Black, red and green dots correspond to measured seed pulse energies of 700 nJ, 3.2 nJ and 32 pJ, respectively. Theoretical curve of achievable power is solid line in both diagrams. Blue dots in Figure 6.6(a) are Q-switch experiment results.

Non-monotonic behavior of the power curve originates from the specific location of optimal operation points in the parameter space. Corresponding experimental data with respect to the theoretical stability diagram for the medium seed energy are presented in Figure 6.2(b). The operating points coincide with the theoretical curve of τ_{cd}^{opt} until the latter enters into the instability zone (at 25 kHz). Then operation at the upper boundary of the instability zone becomes optimal. However as the repetition rate increases the stable operating point moves further away from the τ_{cd}^{opt} position, resulting in lower output energy. Consequently, starting from 85 kHz the optimal operation

point switches to the lower boundary of the instability region. In this regime the operating point gradually comes closer to the τ_{cd}^{opt} position, and consequently, the output power steadily increases with increasing the repetition rate.

The pre-amplified seed pulse has sufficient energy to maintain stable operation at the maximum power, in accordance with the ample seed properties. The power curve obtained with the preamplifier shows no signs of downward excursion with respect to the reference curve (the curve of theoretically attainable power corresponding to τ_{cd}^{opt} round-trip number). Some slight deviation observed at low repetition rates was assumed to be caused by the Kerr effect. This nonlinearity can cause additional intensity-dependent intracavity losses (more pronounced at higher pulse energies), and so its influence is more pronounced at lower repetition rates. In order to differentiate the Kerr effect influence experiments with nanosecond pulses were performed in the same setup. The seed source was disabled so that the regenerative amplifier was transformed to a Q-switched laser with cavity dumping. Evidently this device can be regarded as a regenerative amplifier seeded by spontaneous emission getting into the lasing mode. Thus, the seed energy becomes extremely low and additionally the laser system turns to the nanosecond domain (≈15 ns output pulse length was obtained in our setup). The former gives a large drop in power at critical repetition rates, the latter gives the enhanced, with respect to the regular regenerative amplification, output energy at low repetition rate (the Kerr effect is negligible for such long pulses). The nanosecond pulse energy at low repetition rates exceeds the picosecond energy and very well agrees with the theoretical curve [Figure 6.6(a)]. This demonstrates that experimental deviations appeared because of the Kerr effect and consequently validates that the theoretical approach presented in this manuscript is wholly satisfactory.

Heating of intracavity components was not observed to affect the regenerative amplifier operation in optimal round-trip number experiments.

However, clear evidence of excessive heating was noticed during recording of bifurcation diagrams in the worse (from energy dissipation point of view) regime. The beam quality was observed to deteriorate for 90 kHz repetition rate and at round-trip numbers between 46 and 56. On the other hand the average power defect reached maximum in this range [see Figure 6.4(d)]. As we have concluded theoretically, this defect is indeed due to dissipated power, the absorbed fraction of which is heating intracavity optics.

Operations of the regenerative amplifier seeded by high and medium pulse energies were also compared for the functionally important case of shorter optical pulses. Typically about 9 ps pulse duration was obtained at the output of the amplifier seeded by the 6 ps pulse. This duration is close to the minimum value supported by the gain bandwidth of the Nd:YVO_4 crystal in high total-gain applications such as regenerative amplification. The measurements were constrained to dumping rates above 50 kHz. Nevertheless, the intensities were substantial, and the Kerr effect influence was so strong that it eventually resulted in a decrease of the output power [Figure 6.6(b)]. The average power obtained with the pre-amplified seed was slightly lower than that theoretically predicted below 80 kHz and the difference reached 6.7% at 50 kHz. However, the comparison of these characteristics with those obtained at a medium seed level shows that the benefit of the preamplifier is even more pronounced in case of shorter pulses. The difference is related to a large decrease of the average power below 85 kHz for the case of the medium seed. This is a direct consequence of inefficient operation at the upper instability boundary in the critical repetition rate range under the Kerr effect influence. Experimental optimal operation points for both 58 ps and 9 ps pulses with respect to the theoretical stability diagram are presented in Figure 6.2(b). The optimal operating points for the short pulse experiments were always settled along the less efficient lower boundary of the instability zone. Attempts to operate at the upper branch (optimum for long pulses) resulted in an even larger decrease of the output. In order to quantify this difference we can estimate the multi-pass B integral of the system (Eqs. (3.46) and (3.47) in

Section 3.7). The *B* integral calculated at the 50 kHz repetition rate gave values of 1.3 (acceptable) and 7.6 (problematic) at the transition from low to upper boundary, respectively. Thus, the high seed energy gives additional advantage at shorter pulses due to a significantly lower value of the optimal number of round trips.

The amplification experiments which were performed with the Nd:YVO_4 regenerative amplifier have shown that the developed theoretical approach accurately agrees with experimental data and can be used as guidelines for practical system design.

Conclusions

1. Complex dynamics are the inherent property of continuously pumped regenerative amplifiers operating at high pulse repetition frequencies. The operation stability is subject to the balance between the population inversion depletion in a process of amplification and its restoring provided by pumping. System dynamics can be described with adequate accuracy by a simplified space-independent laser model, which allows output characteristics (including stability features) to be represented in terms of only four dimensionless controlling parameters corresponding to the pulse repetition rate, the cavity round-trip number, the seed pulse energy, and the cavity losses.

2. Basic characteristics of the optimally coupled regenerative amplifier operating in a stable regime are derived in analytical form. They include optimum initial and final gains, the output pulse energy, the power dissipation, the multi-pass *B*-integral and the round-trip number providing optimum output coupling. The characteristics are represented as a function of the dimensionless controlling parameters times the composite coefficient containing conventional characteristics of the optical cavity, laser medium, and pumping.

3. The stable operation implies that the depletion of inversion population is precisely compensated by pumping during a single operation period and the system gets into such a stationary state (fixed point) from any initial state after finite number of periods. Unique existence of the fixed point is the fundamental property of regenerative amplification leading to the quite certain, unambiguously determined by controlling parameters, dynamics pattern. Stable operation, period doubling of various degree of repeatability and regime of deterministic chaos are peculiar to regenerative amplifiers. In order to understand the system behavior the location of stable and unstable regions was determined in space of controlling parameters. The system is stable until the repetition rate is lower than the population inversion relaxation rate. However,

beyond this point the instability zone appears and gradually expands along the axis of the round-trip number as the repetition rate increases. The instability zone does not extend beyond a certain level along the seed energy axis. This provides the possibility of system optimization by increasing the seed pulse energy.

4. Significant pulse energy fluctuations commonly take place at cavity round-trip numbers, which potentially could provide the best performance characteristics. The maximum energy in a stable regime is therefore achieved at a proximity to the instability boundary. The range of repetition frequencies, in which instabilities thus deteriorate the system performance (critical range), typically occupies 3-5 octaves, from unity to a few tens in normalized terms. Effects of instabilities permit regular in magnitude output pulses to be maintained only at the cost of a substantial decrease in the output power. Dependence of the average power on the repetition rate represents a V-shaped curve in the critical range. The most significant power drop (down to half a potentially available level) appears for low seed energies. Increase in the seed pulse energy reduces the power defect caused by instabilities that allows the system performance to reach the maximum level.

5. Diode pumped Nd:YVO_4 regenerative amplification experiments demonstrate a good agreement with theoretical inferences. In particular, increase in the seed pulse energy reduces the range of critical repetition rates and thus improves the amplifier operation especially for shorter pulse durations. Application of a preamplifier is a simple and efficient way to obtain the required seed level, which allows the system capabilities to be exploited to a full extent. Stable operation at repetition rates up to 200 kHz with the average output power close to the limit corresponding to the idealized steady-state regime was obtained.

References

1. Z. Ma, D. Li, P. Shi, P. Hu, N. Wu, and K. Du, Compact multipass Nd:YVO4 slab laser amplifier based on a hybrid resonator, JOSA B, **24** (5), 1061-1065 (2007).
2. S. Backus, J. Peatross, C. P. Huang, M. M. Murnane, and H. C. Kapteyn, Ti:sapphire amplifier producing millijoule-level, 21-fs pulses at 1 kHz, Opt. Lett., **20** (19), 2000-2002 (1995).
3. J.E. Murray, D.C. Downs, J.T. Hunt, G.L. Hermes, W.E. Warren, Off-axis multipass amplifier as a large aperture driver stage for fusion lasers, Appl. Opt., **20** (5), 826-834 (1981).
4. P. Georges, F. Estable, F. Salin, J.P. Poizat, P. Grangier and A. Brun, High-efficiency Ti:Sapphire amplifier for a cw single-mode laser, Optics Letters, **16** (3), 144-146 (1991).
5. S. Forget, F. Balembois, P. Georges and P. Devilder, A new 3D multipass amplifier based on Nd:YAG or Nd:YVO_4 crystals, Appl. Phys. B, **75** (4-5), 481-485 (2002).
6. H. Plaessmann, S.A. Ré, J.J. Alonis, D.L. Vecht and M. Grossman, Multipass diode-pumped solid-state optical amplifier, Optics Letters **18** (17), 1420-1422 (1993).
7. R. L. Fork, F. A. Beisser, and D. K. Fork, Multi-pass optical amplifier using a double confocal resonator geometry, Rev. Phys. Appl. **22** (12), 1665–1671 (1987).
8. A.M. Scott, G. Cook and A.P.G. Davies, Efficient high-gain laser amplification from a low-gain amplifier by use of self-imaging multipass geometry, Applied Optics **40** (15), 2461-2467 (2001).
9. P. Dekker, J. M. Dawes, and J. A. Piper, Characterisation of a pulsed high gain Nd:YVO4 amplifier, in *Advanced Solid State Lasers*, S. Payne and C. Pollack, eds., Vol. 1 of *OSA Trends in Optics and Photonics Series* (Optical Society of America, 1996), paper NL1.
10. G. Smith, P.C. Shardlow, M.J. Damzen, High-power near-diffraction-limited solid-state amplified spontaneous emission laser devices, Opt. Lett., **32** (13), 1911-1913 (2007).

11. G. Smith, M.J. Damzen, Spatially-selective amplified spontaneous emission source derived from an ultrahigh gain solid-state amplifier, Optics Express, **14** (8), 3318-3323 (2006).
12. Y. Ojima, K. Nawata, and T. Omatsu, Over 10-watt pico-second diffraction-limited output from a Nd:YVO4 slab amplifier with a phase conjugate mirror, Optics Express, **13** (22), 8993-8998 (2005).
13. W. Lubeigt, G. Valentine, and D. Burns Enhancement of laser performance using an intracavity deformable membrane mirror, Optics Express, **16** (15), 10943-10955 (2008).
14. M. Fermann, A. Galvanauskas and G. Sucha *Ultrafast Lasers: Technology and Applications*, (Marcel Dekker, New York, 2002).
15. H. Liu, C. Gao, J. Tao, W. Zhao, and Y. Wang, Compact tunable high power picosecond source based on Yb-doped fiber amplification of gain switch laser diode. Optics Express, **16** (11), 7888-7893 (2008).
16. Y. Jeong, J. Sahu, D. Payne, and J. Nilsson, Ytterbium-doped large-core fiber laser with 1.36 kW continuous-wave output power, Optics Express, **12** (25), 6088-6092 (2004).
17. R. Paschotta, J. Nilsson, A.C. Tropper, and D.C. Hanna, Ytterbium-doped fiber amplifiers, IEEE Journal of Quantum Electronics, **33** (7), 1049-1056 (1997).
18. P.K. Mukhopadhyay, K. Ozgoren, I.L. Budunoglu, and O. Ilday, All-fiber low-noise high-power femtosecond Yb-fiber amplifier system seeded by an all-normal dispersion fiber oscillator, IEEE Journal of Selected Topics in Quantum Electronics, **15** (1), 145-152 (2009).
19. J. Limpert, T. Schreiber, T. Clausnitzer, K. Zöllner, H.-J. Fuchs, E.-B. Kley, H. Zellmer, and A. Tünnermann, High-power femtosecond Yb-doped fiber amplifier, Optics Express, **10** (14), 628-638 (2002)
20. F. Röser, T. Eidam, J. Rothhardt, O. Schmidt, D. Schimpf, J. Limpert, and A. Tünnermann, Millijoule pulse energy high repetition rate femtosecond fiber chirped-pulse amplification system, Opt. Lett., **32** (12), 3495-3497 (2007).
21. E.M. Dianov, M.E. Likhachev, and S. Fevrier, Solid-core photonic bandgap fiber for high-power fiber lasers, IEEE J. of Selected Topics in Quantum Electronics, **15** (1), 20-29 (2009)

22. J.R. Marciante, Gain filtering for single-spatial-mode operation og large-mode-area fiber amplifiers, IEEE J. of Selected Topics in Quantum Electronics, **15** (1), 30-36 (2009)
23. F. Poli, A. Cucinotta, D. Passaro, S. Selleri, J. Laegsgaard, and J. Broeng, Single-mode regime in large-mode-area rear-earth-doped rod-type PCFs, IEEE J. of Selected Topics in Quantum Electronics, **15** (1), 54-60 (2009)
24. A.V. Smith, B.T. Do, G.R. Hadley, R.L. Farrow, Optical damage limits to pulse energy from fibers, IEEE J. of Selected Topics in Quantum Electronics, **15** (1), 153-158 (2009)
25. J. Kleinbauer, D. Eckert, S. Weiler, D. Sutter, 80 W ultrafast CPA-free disk laser, *Proc. SPIE*, **6871**, 68711B (2008)
26. W. Koechner, *Solid-State Laser Engineering*, (Springer, USA, 2006).
27. P.J. Delfyett, A. Yusim, S. Grantham, S. Gee, K. Gabel, M. Richardson, G. Alphonse, and J. Connolly, Ultrafast semiconductor laser-diode-seeded Cr:LiSAF regenerative amplifier system, Applied Optics, **36** (15), 3375-3380 (1997).
28. J. Murray and W. Lowdermilk, Nd:YAG regenerative amplifier, J. Appl. Phys. **51** (7), 3548-3555 (1980).
29. V. Magni, Resonators for solid-state lasers with large-volume fundamental mode and high alignment stability, Applied Optics, **25** (1), 107-118 (1986).
30. X.D. Wang, P. Basseras, R.J. Dwayne Miller, J. Sweetser, and I.A. Walmsley, Regenerative pulse amplification in the 10-kHz range, Optics Letters, **15** (15), 839-841 (1990).
31. L. Turi and T. Juhasz, High-power longitudinally end-diode-pumped Nd:YLF regenerative amplifier, Optics Letters **20** (2), 154-156 (1995).
32. M. Delaigue, I. Manek-Hönninger, C. Hönninger, A. Courjaud, and E. Mottay, 1 mJ, Multi-kHz, Sub-500 fs Diode-Pumped Ytterbium Laser Amplifier, in CLEO/QELS Conference, *OSA Technical Digest Series* (CD) (Optical Society of America, 2007), paper CMT2.
33. X. Ribeyre, L. Videau, A. Migus, R. Mercier, and M. Mullot, Nd:glass diode-pumped regenerative amplifier, multimillijoule short-pulse chirped-pulse-amplifier laser, Opt. Lett., **28** (15), 1374-1376 (2003).

34. P. Deb, K.C. Gupta, and J. Fuloria, Nd:glass regenerative amplifier with increased bandwidth and high output energy for chirped pulse amplification systems, Appl. Opt. **49** (10), 1698-1706 (2010).

35. S. Ito, T. Nakajyo, T. Yanagida, F. Sakai, A. Endo, and K. Torizuka, Diode-pumped, chirped-pulse Yb:S-FAP regenerative amplifier for laser-Compton X-ray generation, Optics Communications, **259** (2), 812–815 (2006).

36. T. Nakanishi, Y. Takeuchi, A. Yoshida, J. Kawanaka, R. Yasuhara, T. Kawashima, and H. Kan, Milli-Joules, Kilo-Hertz Regenerative Amplifier Using Total-Reflection Active-Mirror with Cryogenic Yb:YAG, in Advanced Solid-State Photonics, *OSA Technical Digest Series* (CD) (Optical Society of America, 2010), paper AWB27.

37. K.H. Hong, J.T. Gopinath, D. Rand, A.M. Siddiqui, S.W. Huang, E. Li, B.J. Eggleton, J.D. Hybl, T.Y. Fan, and F.X. Kärtner, High-energy, kHz-repetition-rate, ps cryogenic Yb:YAG chirped-pulse amplifier, Opt. Lett. **35** (11), 1752-1754 (2010).

38. A. Giesen, H. Hügel, A. Voss, K. Wittig, U. Brauch and H. Opower, Scalable concept for diode-pumped high-power solid-state lasers, Applied Physics B, **58** (5), 365-372 (1994)

39. R. Paschotta, J. Speiser, and A. Giesen, Comment on 'Surface loss limit of the power scaling of a thin-disk laser', J. Opt. Soc. Am. B, **24** (10), 2658-2658 (2007).

40. T. Metzger, A. Schwarz, C. Teisset, D. Sutter, A. Killi, R. Kienberger, and F. Krausz, High-repetition-rate picosecond pump laser based on a Yb:YAG disk amplifier for optical parametric amplification, Opt. Lett. **34** (14), 2123-2125 (2009).

41. D. Strickland and G. Mourou, Compression of amplified chirped optical pulses, Opt. Comm., **56** (3), 219-221 (1985).

42. G. Mourou and D. Umstadter, Development and Applications of Compact High-Intensity Lasers, Phys. Fluids B, **4** (7), 2317-2325 (1992).

43. M. Siebold, J. Hein, M. Hornung, S. Podleska, M. Kaluza, S. Bock, and R. Sauerbrey, Diode-pumped lasers for ultra-high peak power. Appl. Phys. B, **90** (3-4), 431-437 (2008).

44. A. Dubietis, G. Jonušauskas, and A. Piskarskas, Powerful femtosecond pulse generation by chirped and stretched pulse parametric amplification in BBO crystal, Opt. Commun., **88** (4-6), 437-440 (1992).

45. A. Dubietis, R. Butkus, A.P. Piskarskas, Trends in Chirped Pulse Optical Parametric Amplification, IEEE J. Sel. Top. Quantum Electron. **12** (2), 163-172 (2006).

46. N. Ishii, C.Y. Teisset, T. Fuji, A. Baltuska, and F. Krausz, Seeding of an eleven femtosecond amplifier and its Nd picosecond pump laser from a single broadband Ti:sapphire oscillator, IEEE J. Sel. Top. Quantum Electron., **12** (2), 173-180 (2006).

47. C. Y. Teisset, N. Ishii, T. Fuji, T. Metzger, S. Köhler, R. Holzwarth, A. Baltuška, A. M. Zheltikov, and F. Krausz, Soliton-based pump-seed synchronization for few-cycle OPCPA, Optics Express, **13** (17), 6550-6557 (2005).

48. J. Meijer, K. Dub, A. Gillner, D. Hoffmann, V. Kovalenko, T. Masuzawa, A. Ostendorf, R. Poprawe, and W. Schulz, Laser machining by short and ultrashort pulses, state of the art and new opportunities in the age of the photons, CIRP Annals - Manufacturing Technology, **51** (2), 531-550 (2002).

49. M. Gifford and K.J. Weingarten, Diode-pumped Nd:YLF regenerative amplifier, Optics Letters, **17** (24), 1788-1790 (1992).

50. T. Norris, Femtosecond pulse amplification at 250 kHz with a Ti:sapphire regenerative amplifier and application to continuum generation, Opt. Lett., **17** (14), 1009-1011 (1992).

51. G.D. Goodno, Z. Guo, R.J.D. Miller, I.J. Miller, J.W. Montgomery, S.R. Adhav, and R.S. Adhav, Investigation of β-BaB_2O_4 as a Q-switch for high power applications, Appl. Phys. Lett. **66** (13), 1575 (1995).

52. M. Hornung, M. Siebold, J. Hein, R. Sauerbrey, and G. Hollemann, High-Average Power Diode-Pumped Amplification of Picosecond-Pulses, in *Advanced Solid-State Photonics, Technical Diges*t (Optical Society of America, 2005), paper MF2.

53. M. Siebold, M. Hornung, J. Hein, G. Paunescu, R. Sauerbrey, T. Bergmann, and G. Hollemann, A high-average-power diode-pumped Nd:YVO_4

regenerative laser amplifier for picosecond-pulses. Applied Physics B, **78** (3-4), 287-290 (2004).

54. D. Nickel, C. Stolzenburg, A. Bevertt, A. Geisen, J. Haüssermann, F. Butze, and M. Leitner, 200 kHz electro-optic switch for ultrafast laser systems. Rev. Sci. Instrum., **76** (3), 033111-033111/7 (2005).
55. G. Raciukaitis, M. Grishin, R. Danielius, J. Pocius, L. Giniūnas, High repetition rate ps- and fs- DPSS lasers for micromachining, International Congress on Applications of Lasers & Electro- Optics, ICALEO 2006, *Congress Proceedings* (in CD), **99**, Paper M1001, (Laser Institute of America, 2006).
56. Information from web product catalogue: http://www.ekspla.com/
57. Information from web catalogue: http://www.bme-bergmann.de/
58. P. F. Moulton, Spectroscopic and laser characteristics of Ti:Al_2O_3, J. Opt. Soc. Am. B **3** (1) 125-133 (1986).
59. B. Walker, C. Toth, D. Fittinghoff, T. Guo, D. Kim, C. Rose-Petruck, J. Squier, K. Yamakawa, K. Wilson, and B. Barty, A 50 EW/cm^2 Ti:sapphire laser system for studying relativistic light-matter interactions, Opt. Express, **5** (10), 196-202 (1999).
60. I. Matsushima, H Yashiro, and T. Tomie, 10 kHz 40 W Ti:sapphire regenerative ring amplifier, Opt. Lett., **31** (13), 2066-2068 (2006).
61. S. Biswal, J. Itatani, J. Nees, and G. Mourou, Efficient energy extraction below the saturation fluence in a low-gain low-loss regenerative chirped-pulse amplifier, IEEE J. Sel. Top. Quantum Electron., **4** (2), 421-425 (1998).
62. J. Kawanaka, K. Yamakawa, H. Nishioka, and K. Ueda, 30-mJ, diode-pumped, chirped-pulse Yb:YLF regenerative amplifier, Opt. Lett., **28** (21), 2121-2123 (2003).
63. D. S. Sumida and T. Y. Fan, Emission spectra and fluorescence lifetime measurements of Yb:YAG as a function of temperature, in *Advanced Solid State Lasers*, T. Y. Fan and B. Chai, Eds. (OSA, Washington, D.C., 1994), pp. 100–102.
64. A. Pugžlys, G. Andriukaitis, A. Baltuška, L. Su, J. Xu, H. Li, R. Li, W. Lai, P. Phua, A. Marcinkevičius, M. Fermann, L. Giniūnas, R. Danielius, and S.

Ališauskas, Multi-mJ, 200-fs, CW-pumped, cryogenically cooled, Yb,Na:CaF_2 amplifier, Opt. Lett., **34** (13), 2075-2077 (2009).

65. H.W. Bruesselbach, D. S. Sumida, R. A. Reeder, and R.W. Byren, Low heat high-power scaling using InGaAs-diode-pumped Yb:YAG lasers, IEEE J. Sel. Topics of Quantum Electron., **3** (2), 105–116 (1997).
66. J. Speiser and A. Giesen, Scaling of thin disk pulse amplifiers. Proc. SPIE, **6871**, 68710J (2008)
67. A. Giesen and J. Speiser, Fifteen years of work on thin-disk lasers: results and scaling laws, IEEE J. Sel. Topics Quantum Electron. **13** (3), 598-609 (2007).
68. H. Sayinc, U. Buenting, D. Wandt, J. Neumann, and D. Kracht, Ultrafast high power Yb:KLuW regenerative amplifier. Opt. Express, **17** (17), 15068-15071 (2009).
69. Information from web product catalogue: http://www.trumpf-laser.com; model TruMicro 5050.
70. J. Kleinbauer, R. Knappe, and R. Wallenstein, 13-W picosecond Nd:$GdVO_4$ regenerative amplifier with 200-kHz repetition rate, Appl. Phys. B, **81** (2-3), 163-166 (2005).
71. D. Clubley, A. Bell, and G. Friel, High average power Nd:YVO based picosecond regenerative amplifier, *Proc. SPIE*, **6871**, 68711D (2008).
72. F. Tavella, A. Marcinkevicius, and F. Krausz, Investigation of the superfluorescence and signal amplification in an ultrabroadband multiterawatt optical parametric chirped pulse amplifier system, New Journal of Physics, **8** (219), 1-11 (2006).
73. S. Witte, R.Th. Zinkstok, W. Hogervorst, and K.S.E. Eikema, Generation of few-cycle terawatt light pulses using optical parametric chirped pulse amplification, Optics Express, **13** (13), 4903-4908 (2005).
74. S. Witte, R.Th. Zinkstok, A.L. Wolf, W. Hogervorst, W. Ubachs, and K.S.E. Eikema, A source of 2 terawatt, 2.7 cycle laser pulses based on noncollinear optical parametric chirped pulse amplification, Optics Express, **14** (18), 8168-8177 (2006).
75. A. E. Siegman, *Lasers* (University Science Books, 1986).

76. W. Lowdermilk and J. Murray, The multipass amplifier: theory and numerical analysis, J. Appl. Phys., **51** (5), 2436-2444 (1980).
77. L.M. Frantz and J.S. Nodvik, Theory of pulse propagation in a laser amplifier, J. of Appl. Phys. **34** (6), 2346-2349 (1963).
78. L. McDonagh, R. Wallenstein and R. Knappe, 47 W, 6 ns constant pulse duration, high-repetition-rate cavity-dumped Q-switched TEM_{00} Nd:YVO_4 oscillator, Opt. Lett. **31** (22), 3303-3305 (2006)
79. M. Ebrahimzadeh, G. J. Hall, and A. I. Ferguson, Picosecond infrared optical parametric generation in KTP using a diode-laser-pumped solid-state laser, Optics Letters, **16** (22), 1744-1746 (1991).
80. J. J. Degnan, Theory of the Optimally Coupled Q-Switched Laser, IEEE J. Quantum Electron. **25** (2), 214-220 (1989).
81. J. J. Zayhowski and P. L. Kelley, Optimization of Q-Switched Lasers, IEEE J. Quantum Electron., **27** (9), 2220-2225 (1991).
82. A. Hofer, Th. Graf, W. Lüthy, and H.P. Weber, Fully analytical simulation of Q-switched lasers, Laser Phys. Lett., **1** (6), 282-284 (2004).
83. R. B. Chesler, M. A. Karr, and J. E. Geusic, An Experimental and Theoretical Study of High Repetition Rate Q-Switched Nd: YAlG Lasers, Proc. of the IEEE **58** (12), 1899-1913 (1970).
84. J. Liu, B. Ozugus, J. Erhard, A. Ding, H. Weber and X. Meng, Diode-pumped cw and Q-switched Nd:$GdVO_4$ laser operating at 1.34 μm, Opt. and Quantum Electron. **35** (4), 811-824 (2003).
85. D. B. Coyle, D. V. Guarra and R. B. Kay, An interactive numerical model of diode-pumped, Q-switched/cavity-dumped lasers, J. Phys. D: Appl. Phys. **28** (3), 452-462 (1995).
86. H. Haken, Analogy between higher instabilities in fluids and lasers, Physics Letters A, **53** (1), 77-78 (1975).
87. E. Lorenz, Deterministic nonperiodic flow, Journal of the Atmospheric Sciences, **20** (2), 130-141 (1963).
88. F. Arecchi, R. Meucci, G. Puccioni, and J. Tredicce, Experimental evidence of subharmonic bifurcations, multistability, and turbulence in a Q-switched gas laser, Phys. Rev. Lett., **49** (17), 1217-1220 (1982).

89. D. Tang, S. Ng, L. Qin, and X. Meng, Deterministic chaos in a diode-pumped Nd:YAG laser passively Q switched by a Cr^{4+} YAG crystal, Opt. Lett., **28** (5), 325-327 (2003).

90. M.D. Wei, Modeling a passively Q-Switched Nd:YVO_4 laser with an application to spatio-temporal instability, Jpn. J. Appl. Phys., **49** (7), 2701-2705 (2010).

91. M. Kovalsky, A. Hnilo, Chaos in the pulse spacing of passive Q-switched all-solid-state lasers, Optics Letters, **35** (20), 3498-3500 (2010).

92. S. Valling, T. Fordell, and A. Lindberg, Experimental and numerical intensity time series of an optically injected solid state laser, Opt. Commun., **254** (4-6), 282-289, (2005).

93. J. Liu, V. Petrov, U. Griebner, F. Noack, H. Zhang, J. Wang, and M. Jiang, Optical bistability in the operation of a continuous-wave diode-pumped Yb:$LuVO_4$ laser, Opt. Express **14** (25), 12183-12187 (2006).

94. J. Dörring, A. Killi, U. Morgner, A. Lang, M. Lederer, and D. Kopf, Period doubling and deterministic chaos in continuously pumped regenerative amplifiers, Opt. Express, **12** (8), 1759-1768 (2004).

95. D. Müller, A. Giesen, and H. Hügel, Picosecond thin-disk regenerative amplifier. *Proceedings of SPIE*, **5120**, 281-286 (2003).

96. U. Buenting, H. Sayinc, D. Wandt, U. Morgner, and D. Kracht, Regenerative thin disk amplifier with combined gain spectra producing 500 μJ sub 200 fs pulses, Opt. Express, **17** (10), 8046-8050 (2009).

97. L. A. Eyres, J. J. Morehead, J. Gregg, D. J. Richard and W. Grossman, Advances in High power Harmonic Generation: Q-Switched Lasers with Electronically Adjustable Pulse Width, *Proc. SPIE* **6100**, 349-358 (2006).

98. O. Svelto, *Principles of Lasers* (Plenum Press, 1998)

99. L.W. Casperson, Laser power calculations: sources of error, Applied Optics, **19** (3), 422-434 (1980).

100. K. T. Alligood, T. D. Sauer, and J. A. Yorke, *Chaos. An Introduction to Dynamical Systems*, (Springer, 1996).

101. I. Ross, G. New, and P. Bates, Contrast limitation due to pump noise in an optical parametric chirped pulse amplification system, Optics Communications, **273** (2), 510-514 (2007).
102. C. Liu, T. Riesbeck, X. Wang, J. Ge, Z. Xiang, J. Chen, and H. Eichler, Influence of spherical aberrations on the performance of dynamically stable resonators, Optics Communications, **281** (20), 5222–5228 (2008).
103. D. Stučinskas, R. Antipenkov, A. Varanavičius, M. Grishin, J. Kodz, A. Melnikaitis, and A. Vanagas, Thermal lens compensation in high average power diode pumped Nd:YVO_4 laser using aspheric optical element, Lithuanian Journal of Physics, **49** (4), 433-438 (2009).
104. C. Bibeau, S. Payne, and H. Powell, Direct measurements of the terminal laser level lifetime in neodymium-doped crystals and glasses, J. Opt. Soc. Am. B, **12** (10), 1981-1992 (1995).
105. D. Brawn, *High Peak Power Nd:Glass Laser Systems*, (Springer-Verlag, New-York, 1981).
106. J. Speiser, and A. Giesen, Scaling of thin disk pulse amplifiers, *Proc. SPIE*, **6871**, 68710J (2008).
107. R. Peterson, H. Jenssen, and A. Cassanho, Investigation of the spectroscopic properties of Nd:YVO_4, in: *Proc. OSA TOPS, Advanced Solid-State Lasers*, M.E. Fermann and L.R. Marshall, (Ed.), **68**, 294-298 (2002).